The Development of a Three-Degree-of-Freedom Vibration Control System Test Facility

by

Travis Lee Hein

Submitted to the Department of Mechanical Engineering
in partial fulfillment of the requirements for the degree of

Bachelor of Science and Master of Science in Mechanical Engineering

at the

MASSACHUSETTS INSTITUTE OF TECHNOLOGY

May 1994

Author . . . .
Department of Mechanical Engineering
May 6, 1994

Certified by. . . . .
Jamie W. Burnside
Company Supervisor
Thesis Supervisor

Certified by. . . . .
James K. Roberge
Professor of Electrical Engineering
Thesis Supervisor

Certified by. . . . .
David L. Trumper
Professor of Mechanical Engineering
Thesis Supervisor
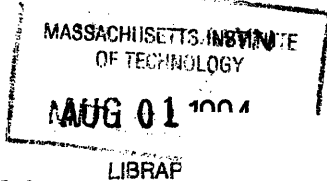
Accepted by . . . .
Ain A. Sonin
Chairman, Departmental Committee on Graduate Students

The Development of a Three-Degree-of-Freedom Vibration Control System Test Facility

by

Travis Lee Hein

Submitted to the Department of Mechanical Engineering
on May 6, 1994, in partial fulfillment of the
requirements for the degree of
Bachelor of Science and Master of Science in Mechanical Engineering

Abstract

In this thesis, I developed a test facility which simulates the operational vibration of aircraft and spacecraft in three degrees-of-freedom: one linear and two angular degrees-of-freedom over a frequency range of 10 to 200 Hz. The purpose of the test facility is to evaluate the performance of control algorithms designed to actively reject a disturbance environment created by the facility.

Three electrodynamic shakers coupled to a common payload mounting platform provided this disturbance environment. The main focus of this project was upon the mechanical design and finite element analysis of the components which couple the three actuators to the mounting platform. Specially-designed flexures were utilized instead of conventional ball-and-socket joints to eliminate friction from the system. A center post composed of a linear bearing, suspension system, and another flexure system was designed and fabricated to improve the vibrational performance of the system.

A frequency domain, feed-forward controller was used to control the output of the shakers, to ensure a payload mounted on the platform will be subjected to the desired power spectral density profiles specified by the user.

The controller was found to be able to track the three degrees-of-freedom to within ± 1 dB. The main limitation to the accuracy of the system was determined to be the ability of the controller to record accurate transfer functions of the three controlled degrees-of-freedom. The mechanical characteristics of the facility do not limit the current controller tracking abilities. Furthermore, the mechanical design of the test facility allow the operational frequency range to be increased to approximately 400 Hz.

Thesis Supervisor: Jamie W. Burnside
Title: Company Supervisor

Thesis Supervisor: James K. Roberge

Title: Professor of Electrical Engineering

Thesis Supervisor: David L. Trumper
Title: Professor of Mechanical Engineering

Acknowledgments

Contents

List of Figures

7

8

List of Tables

Chapter 1

Introduction

This chapter provides a general introduction for the three degree-of-freedom vibration test facility developed at Lincoln Laboratory. This includes the motivating factors behind the development, an overview of the components of the test facility, and a description of the performance specifications.

1.1 Motivation for Control Systems Test Facility

Air-borne electronic packages, such as delicate optical guidance equipment, require control systems to actively reject disturbances which result from operational flight conditions. The vibration environment for equipment installed in jet aircraft (except engine-mounted) stems from four principal mechanisms [8]

    a. Engine noise impinging on aircraft structure

    b. Turbulent aerodynamic flow along external aircraft structures

    c. Pressure pulse impingement due to repetitive firing of guns

    d. Airframe structural motions due to maneuvers, aerodynamic buffet, landing, taxi, etc.

This test facility was designed to simulate this last source of vibration.

Testing control system performance is vital to the success of the equipment, yet testing under actual disturbance conditions can require a large investment in time and money. Air-borne and space-based electronic packages simply cannot be tested

under actual disturbances; the cost and difficulty of a test flight or launch creates the need for simulation of the disturbance. Vibration data from test flights can be used to establish the typical background vibration which disturbs the controlled plant. Simulation of these vibrational conditions utilizing this data becomes vital to control system performance evaluation.

Computer simulation has become an invaluable tool toward the testing of the dynamic performance of control designs. There are two areas of computer modeling which offer the capability of testing control designs: finite element (FE) modeling programs such as MSC/Nastran; and Matlab/Simulink. The FE programs excel in determining the dynamic behavior of complex mechanical systems and in simulating vibrations, but lack the capability to evaluate complex control systems. The strengths of Matlab/Simulink are exactly opposite; it can evaluate control systems with flexibility and ease, but it does not offer accurate dynamic analysis of complex systems, nor does it provide a flexible disturbance environment.

Finite element models offer one major advantage: close approximations of continuous systems which provide a much higher level of accuracy than lumped parameter models. Since computation time is very short, several thousand degrees of freedom can be assigned in a reasonable finite element model. Finite element programs can provide dynamic evaluations of very complex structures. These programs are capable of determining natural frequencies, mode shapes, and responses to random vibration inputs. With this technique, simulation of vibrational flight conditions can be performed very easily. The desired power spectral density (PSD) curve for acceleration is defined by the user and applied to a section of the model. Using the FE method, a control engineer can even determine the dynamic performance of a simple control law. Complex multi-input multi-output control systems, however, cannot be evaluated. A finite element test facility could be created, although it would be severely limited in its control law performance capabilities.

Matlab/Simulink, on the other hand, offers an extremely useful tool for evaluating control laws. Multi-input multi-output control schemes can be implemented and altered relatively easily in block diagram or state-space form. A control test facility

12

built in Matlab would offer versatile control design, but the plant dynamics would be based on lumped parameter models which represent ideal models of dynamic system behavior. Also, the simulation of complex three degree-of-freedom vibrational disturbance environments is not possible within Matlab. A Matlab test facility could be created as well, but it would not be capable of simulating the desired disturbances or accurately predicting complex dynamic behavior.

A more accurate method of evaluating the performance of control law design involves a combining the strengths of the previous methods: applying known disturbances directly to the controlled plant. Since the hardware itself is tested, the dynamic behavior of the system is not idealized. This ensures that the response is accurate and reliable. If actual disturbance conditions can be simulated accurately, this method provides the best prediction of control law performance.

The majority of vibration experienced by equipment in operational service has been determined by analysis to be composed of a wide range of frequencies in various combinations of intensity. Random vibration effectively simulates this broadband disturbance in a test situation [8]. Unfortunately, alterations to control laws using this testing method may be difficult and time consuming if the hardware electronics must be altered with each control law alteration in the case of an analog control system or if code must be manually rewritten using a digital control system.

1.2   Overview of Control Systems Test Facility

With these concepts in mind, the Advanced Control Concepts Evaluation Laboratory (ACCEL) was proposed to provide a disturbance environment in order to facilitate control law design and development. ACCEL was the original concept of several members of the Control Systems Engineering Group at Lincoln Laboratory including Jamie Burnside, Anthony Hotz, and Robert Gilgen. ACCEL allows systems to be subjected to three degree-of-freedom mechanical vibrations (two angular and one translational). Three electrodynamic shakers are coupled to a platform which transforms three linear motions, with phase shift, to desired rotation and translation

13
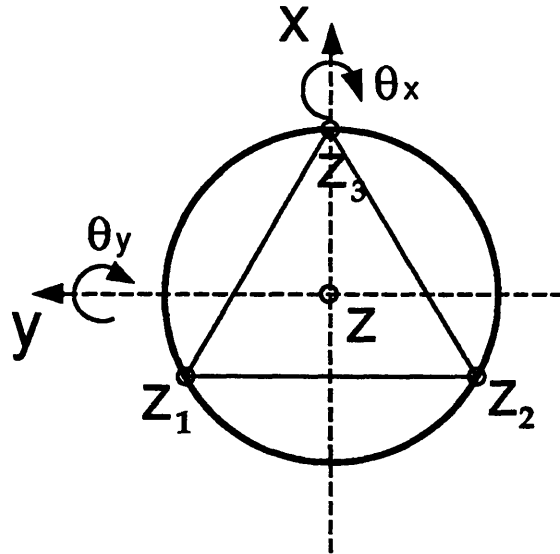
Figure 1-1: Disturbance and Shaker Axes

In addition, ACCEL offers a flexible means of control law implementation with a programmable signal processing chip, the SPROC DSP chip. This chip, with four parallel processors for high-speed real-time processing, will serve as a programmable controller which can handle single-input single-output as well as multi-input multi-output systems.

A block diagram of the system appears in Figure 1-3. The three independent shakers are controlled by the I*star computer, which allows the user to input a power spectral density (PSD) curve of the desired acceleration over the disturbance frequency range in each degree of freedom. I*star is capable of generating control spectra for three independent axes to yield desired output power spectral densities. This
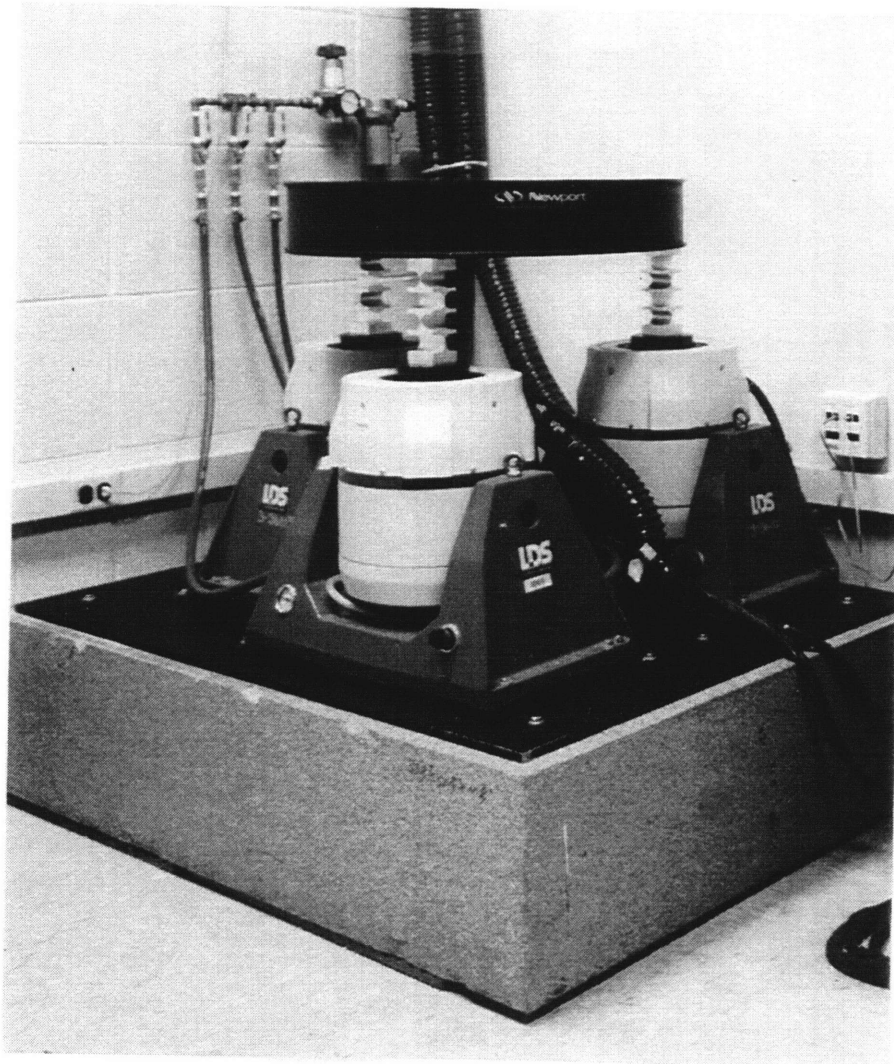
Figure 1-2: Photograph Depicting Shaker Configuration

flexibility allows the ACCEL system to create a wide variety of disturbance environments. The I*star computer also acts as a frequency domain controller; it performs a plant inversion to achieve the desired PSD disturbance levels. It calculates the correct input to the system by inverting the plant transfer function which is in memory and multiplying it by the desired output, specified by the user.

The I*star computer creates control signals in the disturbance axes (θ_x, θ_y, and Z). Since the disturbance axes do not match the shaker axes, a coordinate transformation is necessary to convert a command from the former axes to the latter. This

coordinate transformation was developed by Ramona Tung of the Control Systems Engineering Group at Lincoln Laboratory. It basically multiplies the three inputs by a 3X3 transformation matrix utilizing analog circuitry. The outputs from the coordinate transformation are then fed to the power amplifiers and then to the actuators. The actuators provide the desired disturbance accelerations to the controlled plant, the payload.

The test payload is mounted to a platform which is attached to the three shakers using three mechanical flexure mounts. These flexures allow the platform to rotate in θ_x and θ_y. A center post with another flexure system couples the center of the platform to ground in order to restrain the remaining three degrees-of-freedom.

Three accelerometers, one mounted above each shaker, provide the feedback for the system. These signals, however, are in the shaker force axes. Consequently, a reverse coordinate transformation is performed in order to observe the response of the system in the three disturbance axes. This reverse coordinate transformation is the inverse of the previous coordinate transformation matrix. These signals are sent back to the I*star computer as feedback to update the plant transfer function in memory.

Control laws to be tested using ACCEL can be defined in the familiar Matlab/Simulab programming environment in either state-space or block diagram form. The completed design can then be compiled into executable SPROC code and downloaded to the chip's memory. The SPROCboard, which houses the SPROC chip, allows the chip to interface with the plant being tested. The performance of the control system can then be evaluated. Alterations to the control system can be performed quickly in Matlab and downloaded to the SPROC chip. This portion of the test facility was not developed within the scope of this thesis project.

1.3 Performance Specifications of Test Facility

The performance of the control test facility can be measured by several factors. The system bandwidth, disturbance rejection, stability, maximum angular deflection, maximum angular and linear acceleration, and maximum payload mass represent the
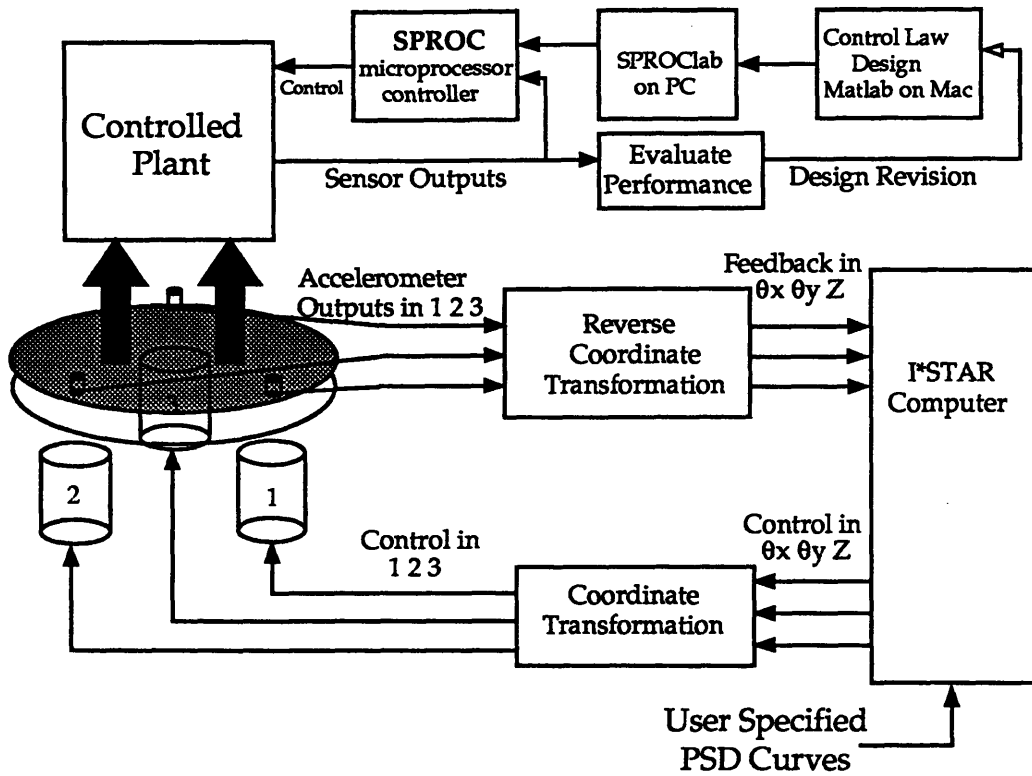
Figure 1-3: Block Diagram of ACCEL

most important of these factors. Table 1.1 summarizes the performance goals for this project. The maximum accelerations listed are based on bare-table calculations.

Table 1.1: Performace Specifications of Project

Parameter	Units	Value
Frequency Operation Range	Hz	10 to 100
Max Angular Displacement (θ_x & θ_y)	mrad	± 11.8
Max Linear Displacement	inches	$\pm .125$
Max Payload weight	lb	100
Max Angular Acceleration, θ_x	rad/sec^2	241.3
Max Angular Acceleration, θ_y	rad/sec^2	278.7
Max Translational acceleration	g	6.5

Chapter 2

Literature Review

This chapter outlines prior research projects which were helpful in the development of the three degree-of-freedom vibration test facility. This research includes two beam steering mirror projects developed at Lincoln Laboratory, and a three degree-of-freedom vibration test facility developed for the Syminex Company.

2.1 Beam Steering Mirror Projects

Much of the research performed on beam steering mirrors is applicable to the development of this test facility. The two projects discussed involve mirrors which, like the mounting platform in this project, can rotate in two degrees-of-freedom. In the case of the steering mirrors, the controlled output are angular positions, whereas angular and linear accelerations are the controlled outputs for the vibration test facility. Two distinct approaches will be evident in the following projects. The large aperture mirror incorporates critical damping to allow operation through the undesired modes, leaving the natural frequency unchanged. The small aperture mirror utilizes stiffeners which raise the natural frequencies of the undesired modes well above the closed loop bandwidth, as well as employing damping for part of the system.

Large Steering Mirror

In an effort to demonstrate the feasibility of producing a high performance steering mirror in the 2-4m class, Lincoln Laboratory developed a 2m aperture steering mirror
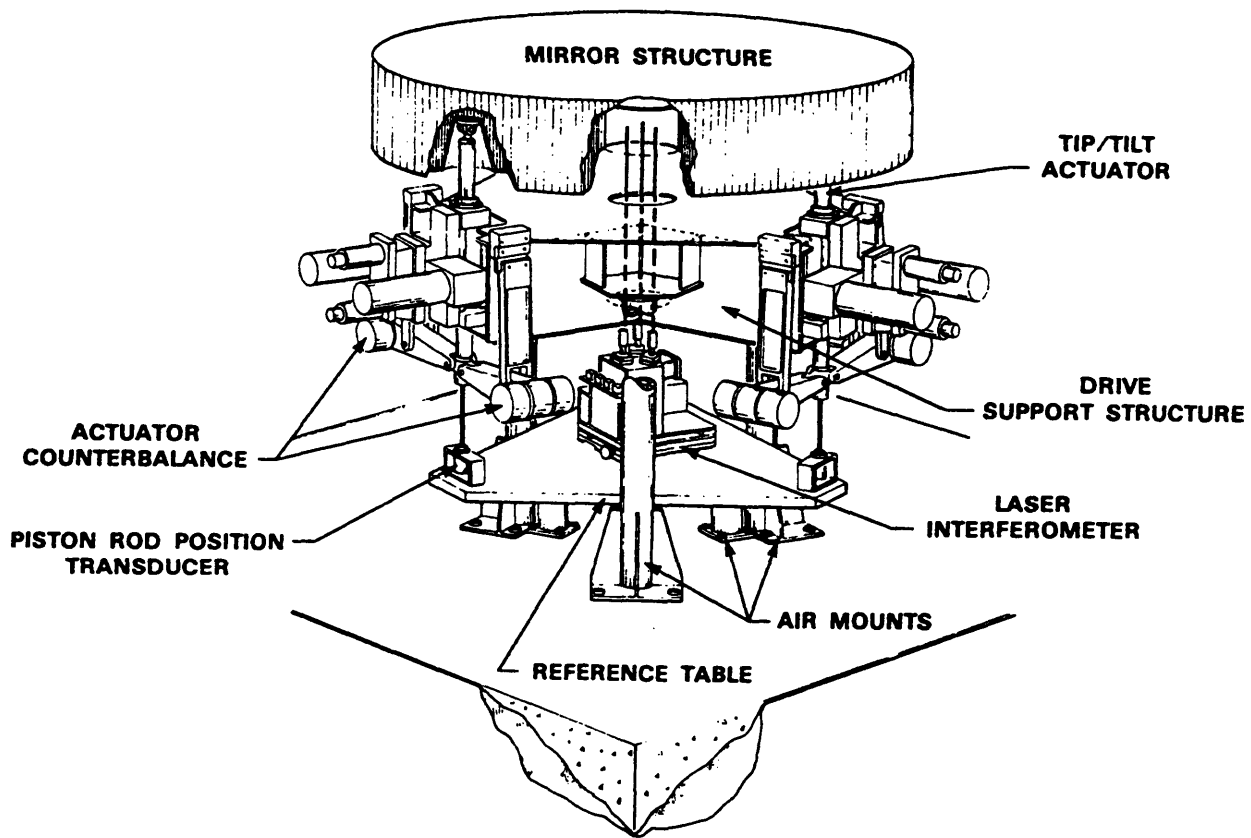
Figure 2-1: 2m Aperture Beam Steering Mirror

[3]. This mirror consists of an 85 inch diameter by 14 inch deep aluminum honeycomb sandwich fabricated by Parsons of California. Upon delivery, the structure weighed 300 lb and possessed a freely supported natural frequency of 334 Hz. The mirror was designed to rotate in two degrees-of-freedom with a maximum angular displacement of ±7.5 degrees. It is supported and driven by three hydraulic actuators spaced 120 degrees apart as shown in Figure 2-1.

The general approach for this project involves critically damping the undesired lateral mode of the mirror system. The actuators are coupled to the mirror using flexible strut dampers and ball joints set into conical frustrum inserts to ensure the center of each ball is located at the transverse center of the structure. Figure 2-2 depicts the strut damper arrangement.

STRUT DAMPER
ASSEMBLY

SPRING WASHER

UPPER SEAL

SPHERE

HOUSING

LOWER SEAL

HOLLOW ROD

STRUT

HYDRAULIC
CYLINDER
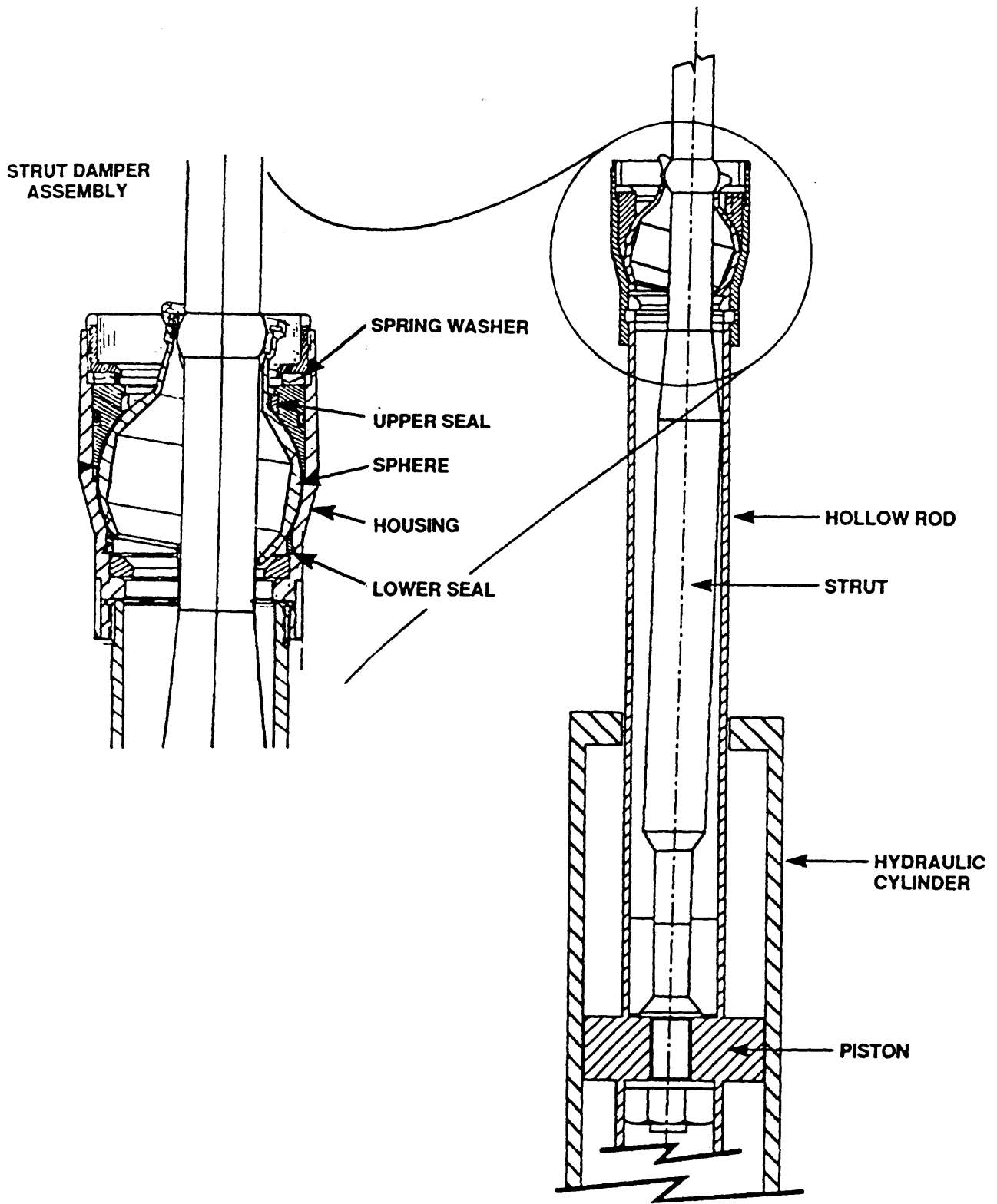
PISTON

Figure 2-2: Flexible Piston for Beam Steering Mirror

The strut damper is a viscous damper acting horizontally between the strut and the hollow piston rods. This damper provides near critical damping to a low natural frequency: a lightly damped lateral rigid body mode of the mirror structure on the struts. The damping forces are obtained from the shearing action of a 0.15 mm thick film of silicone fluid of 600,000 cst viscosity. The shearing action occurs when the mirror rotates through an angle, forcing the struts to sway laterally.

High Bandwidth Steering Mirror (HBSM)

In an effort to produce a small-aperture two axis steering mirror with a closed loop bandwidth of 10 KHz, the HBSM project was developed by Gregory Loney at Lincoln Laboratory [6]. The mirror aperture is only 18 mm with maximum angular displacements of only 20 mrad. The mirror is driven by four magnetic voice coil actuators. Figure 2-3 shows an exploded view of the HBSM design.

Much of the design work focused upon constraining the mirror to prevent motion of the mirror axially, laterally, and torsionally. The degrees-of-freedom which are not actuated were stiffened using an axial flexure and a flexure ring. The system was stiffened to raise the natural frequencies of the modes which couple into the desired mirror motions. The bipod legs of the flexure ring are long low section modulus reed offering little bending stiffness and high axial stiffness. The flexure ring constrains motion coplanar to the mirror and allows rotational compliance about an axis perpendicular to the mirror normal. This bipod design also resists torsion about the long axis of the axial flexure. The vibrational modes of the bipod legs which compose the flexure ring were additionally damped with a layer of viscoelastic material in order to reduce the coupling between the bipod leg modes and mirror rotation.

This approach was successful in achieving a 10 KHz closed-loop bandwidth, with no significant coupling modes below 20 KHz (the coupling modes of the bipod legs which appear below 10 KHz were well damped).

MAIN HOUSING

SENSOR ASSEMBLY

MOUNTING BLOCK

FLEXURE RING

END CAP

ACTUATOR

SPACER

AXIAL FLEXURE

EPOXY-RIVETED LEAF

MOTOR CONNECTOR

LOCATING PIN

MIRROR

SENSOR PLATE ASSY

BASE SUPPORT

WIRE PLATE

CLAMP RING

RISER

SENSOR ELECTRONICS
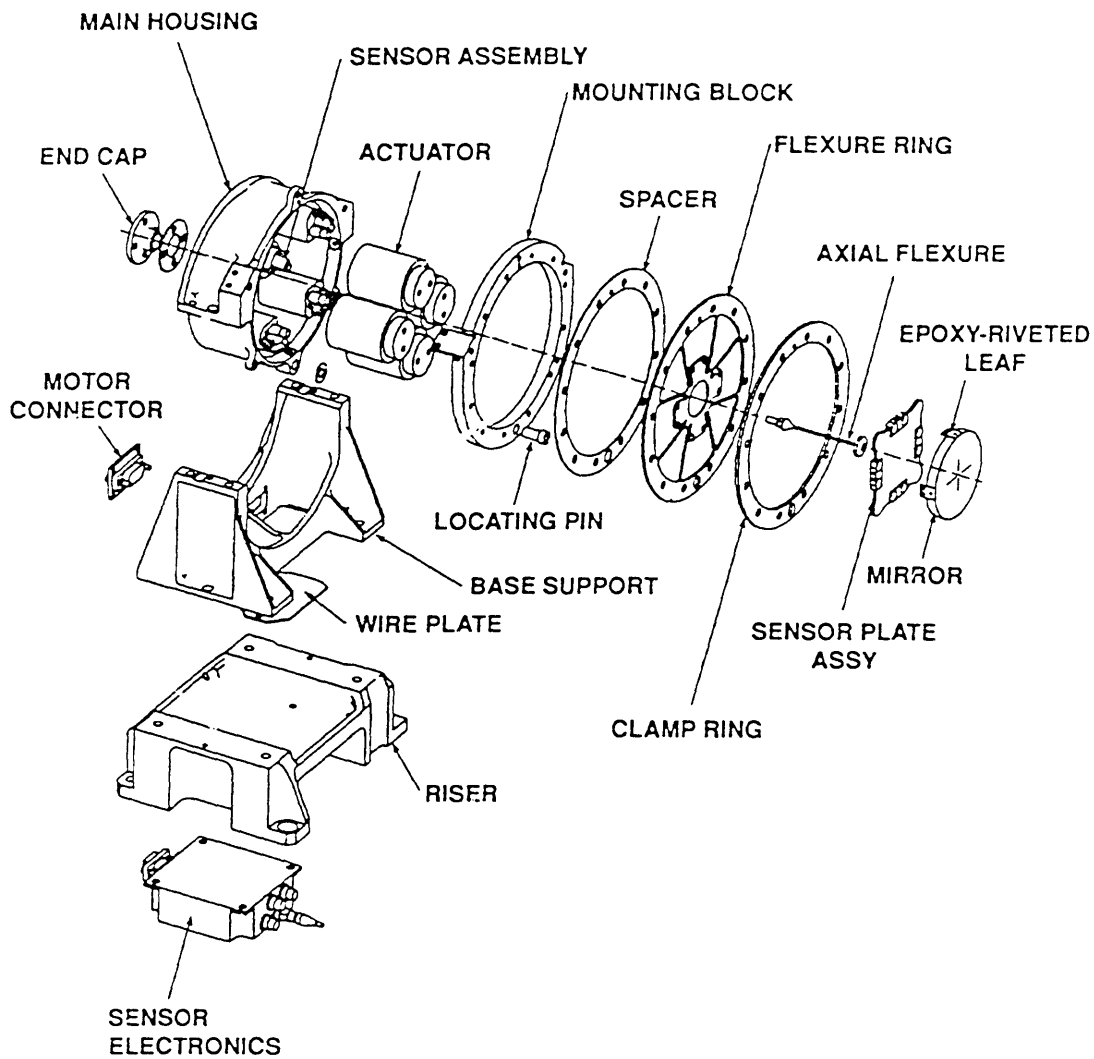
Figure 2-3: Exploded View of HBSM

2.2 Syminex Three Degree-of-Freedom Shaker System

A three degree-of-freedom vibration test facility has been developed by Christophe Touzeau and Stephan Antalovsky for Syminex [14]. The test facility aided in developing a helicopter-borne weapon system involving an optical sight fixed on a supporting mast above the rotor. The test facility has been designed to accelerate a payload of up to 300 lbs at distinct frequencies which represent the harmonics of the helicopter motion below 100 Hz, as well as provide random noise in the 100-200 Hz frequency range. The vibration environment includes:

1. Two orthogonal rotations at ω, $n\omega$, and $2n\omega$, maximum ± 5.1 degrees

2. Vertical translation at $n\omega$

where ω is the angular speed of the rotor, and n is the number of blades of the helicopter.

A diagram of the test facility which incorporates three electrodynamic, water-cooled shakers from Ling Dynamic Systems (LDS Model 954LS) is shown in Figure 2-4. The baseplate is accelerated in two orthogonal angular degrees-of-freedom, pitch and roll, and in one linear degree-of-freedom, Z. Feedback was accomplished using one linear accelerometer for Z and two angular accelerometers for the pitch and roll.

The shakers are coupled to a triangular baseplate using three hydrostatic double ball joints. Double ball joints must be used in order to allow the baseplate to rotate through an angle (single ball joints would over-constrain the system). The payload to be tested is mounted to the tip of a mast which is attached rigidly to the baseplate.

The first tests conducted in January 1992 successfully reproduced a number of flight conditions, showing the capability of the system to correctly simulate the complex real vibration environment. The control accuracy and repeatability of the proved to be good, with typical accuracies of ± 0.2 dB on amplitudes, ± 1 degree on phases and ± 1 degree on directions of movement [14].

The system performance, however, was limited by the heavily loaded parts, the ball-and-socket bearings and the roller bearing guides, used to allow the fixture to

TESTED
ITEM

SUPPORTING
MAST

VERTICAL ROLLER
BEARING GUIDES

BASEPLATE

BALL-AND-SOCKET
JOINT

HYDROSTATIC
DOUBLE
BALL JOINT

ELECTRODYNAMIC
EXCITER

LOAD DISCHARGER
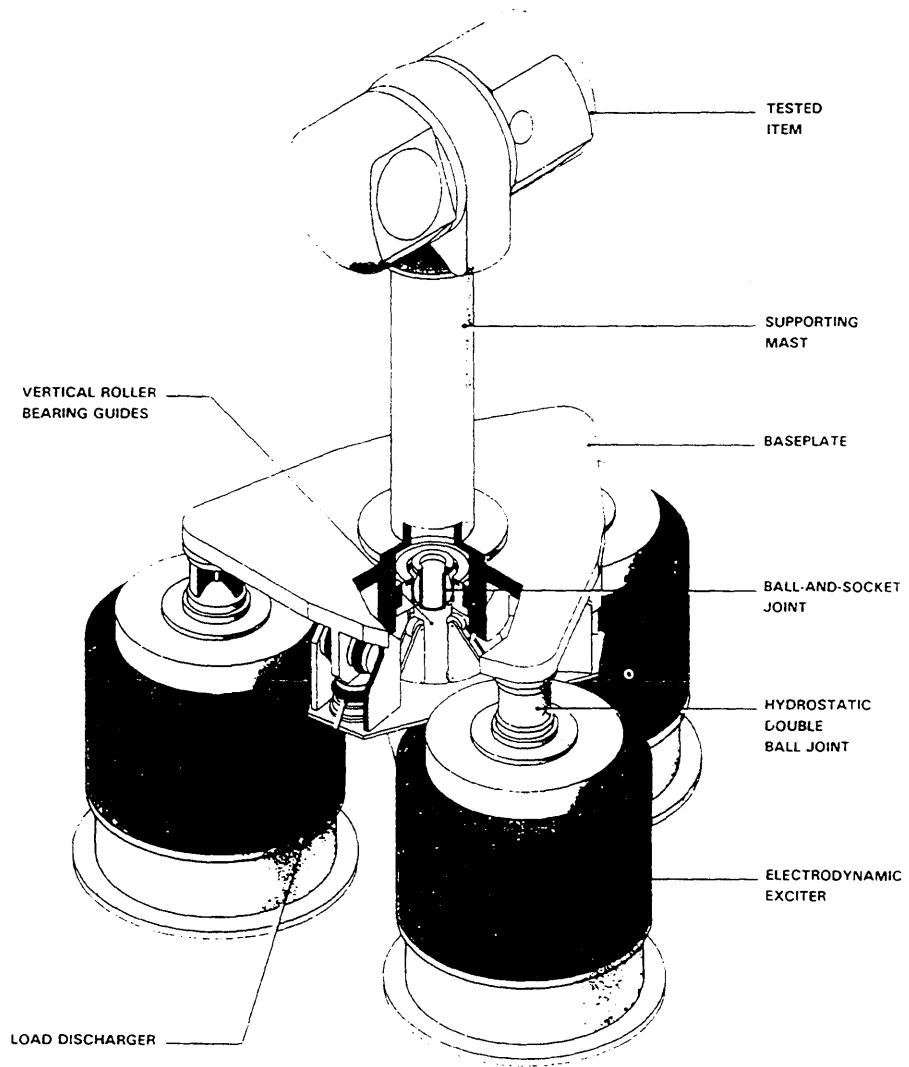
Figure 2-4: Diagram of Syminex 3 DOF Shaker System

rotate and translate. Undesired sine tones which produced errors in payload motion were detected. These problems were the result of the nonlinear behavior of the fixture, and particularly its bearing elements. [2].

Consequently, the development of the vibration test facility at Lincoln Laboratory sought to avoid a bearing system such as the one utilized in the Syminex project, thus circumventing the nonlinearities which are introduced into the system performance.

2.3   Laser Line-of-Sight Control

Jeffrey Ludwig of the Control Systems Engineering Group at Lincoln Laboratory developed a control system to stabilize a space-based laser communications system [7]. A beam steering mirror mounted to a platform was used to focus a laser beam on a detector. The control system was necessary to keep the beam fixed on the detector despite the presence of platform disturbances in one angular degree-of-freedom in a frequency range of 0-50 Hz. The platform disturbances in this project were applied using one electrodynamic shaker in an arrangement shown in Figure 2-5

The project attempted to constrain the platform motion to pure rotation about one axis. Three identical right angle flexures hinges were designed to accomplish this goal. One hinge couples the platform to the disturbance actuator, while the other two serve to establish a fixed pivot point directly under the mirror. A sketch of the right angle flexure is shown in Figure 2-6

These flexure hinges possess a low rotational stiffness about one axis, but retain relatively high stiffnesses in the five other degrees-of-freedom. More importantly, the flexures do not introduce nonlinearities into the system; they act as pure torsional springs within their elastic range. This represents a significant improvement over an alternative bearing configuration.

The success of this configuration was limited by the mounting posts which ideally should serve as a fixed point of attachment for two right-angle flexures. These posts in reality act as cantilever beams and allow the platform to displace vertically, as well as rotate. The first structural resonance of these mounting posts appeared at
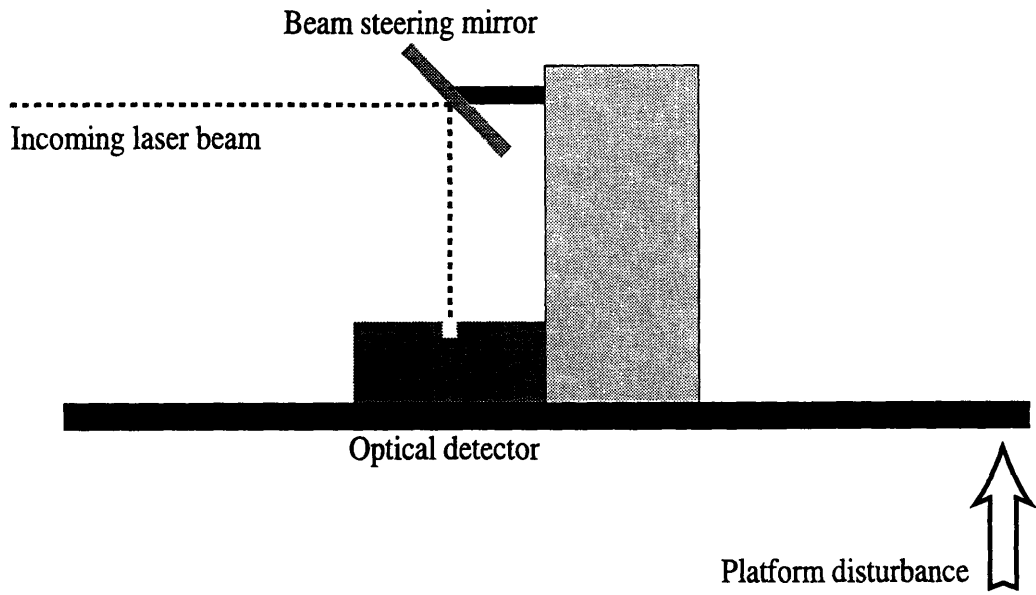
Figure 2-5: Diagram of Single Degree-of-Freedom Line-of-Sight Experiment
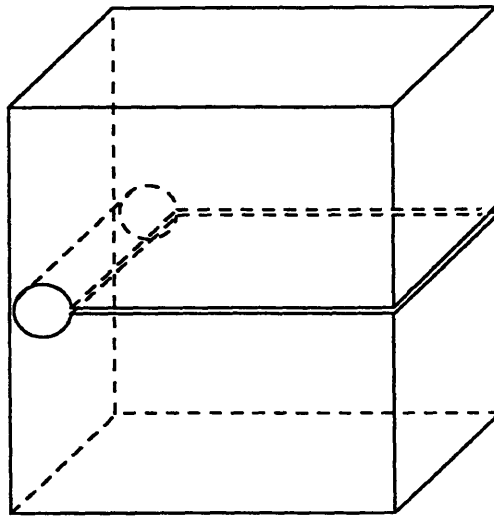
Figure 2-6: Sketch of Right Angle Flexure Hinge

approximately 20 Hz. This vertical motion produced an equivalent error observed on the quad cell detector, causing the measured disturbance rejection of the system to be higher in the area of the post resonances.

The research presented was extremely useful in the development of the test facility. This research allowed me to focus upon the areas of design which would be most crucial to successful completion of the project. The following chapter introduces these critical issues as they relate to the vibration test facility.

Chapter 3

Fundamental Issues

This chapter serves as an introduction to the fundamental issues faced during the development of the controls test facility. The dynamics of a six degree-of-freedom model are examined. The dynamics discussion leads to a section which treats the problems of vibrational modes which couple into the actuated degrees-of-freedom of the system. Finally, several basic control issues are discussed.

3.1   Six Degree-of-Freedom Model

An examination of the dynamics of a six degree-of-freedom model aids in predicting the vibrational performance of the system. The purpose of these calculations is to determine the approximate mode shapes for the system. This model will demonstrate that the eigenvectors exhibit coupled motion between several degrees-of-freedom.

Figure 3-1 depicts the model evaluated. Several views are shown in this figure in order to clearly depict the location of the springs attached to the mounting platform. The model consists of the mounting platform, which has a mass m, rotational inertia J in θ_x and θ_y, and rotational inertia J' in θ_z. Translational stiffnesses in X, Y, and Z, and rotational stiffnesses in θ_x, θ_y, and θ_z represent the mechanical structures (the flexures and center post) which offer stiffness to the vibrational platform. The model is evaluated with the following assumptions:

a. The platform is completely rigid

b. The platform experiences small angular motion

c. The dynamic effect of the payload is negligible

The platform is not completely rigid at frequencies above 600 Hz, however, this model is developed to study resonances below this frequency. Also, while the payload will greatly influence the dynamics of the system, this model is intended to determine the dynamic behavior of the unloaded system.
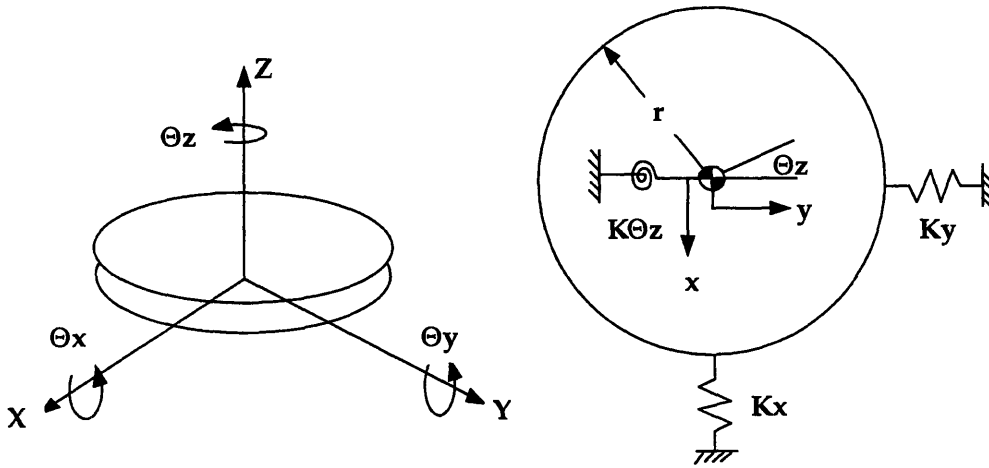
Figure 3-1 a. Mounting Platform   Figure 3-1 b. X-Y Plane View of Model
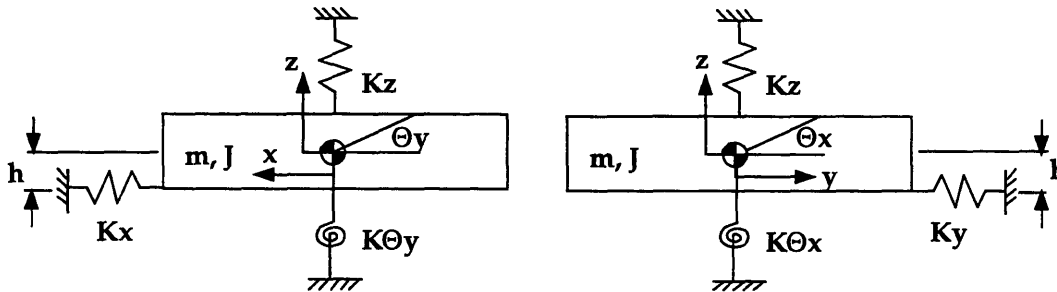
Figure 3-1 c. X-Z Plane View of Model   Figure 3-1 d. Y-Z Plane View of Model

Figure 3-1: Six Degree-of-Freedom Model

The generalized coordinates for the platform in the model consist of the three controlled degrees-of-freedom, θ_x, θ_y, and Z, and in the three uncontrolled degrees-

of-freedom, X, Y, and θ_z.

$$\zeta = X, Y, Z, \theta_x, \theta_y, \theta_z \tag{3.1}$$

The equations of motion are determined using the Lagrangian approach. The terms for the kinetic energy, T^*, and the potential energy, V are:

$$T^* = \frac{1}{2}m\dot{x}^2 + \frac{1}{2}m\dot{y}^2 + \frac{1}{2}m\dot{z}^2 + \frac{1}{2}J\dot{\theta}_x{}^2 + \frac{1}{2}J\dot{\theta}_y{}^2 + \frac{1}{2}J'\dot{\theta}_z{}^2 \tag{3.2}$$

$$V = \frac{1}{2}k_z z^2 + \frac{1}{2}k_x(x+h-r\theta_z)^2 + \frac{1}{2}k_y(y-h\theta_x-r\theta_z)^2 + \frac{1}{2}k_{\theta_x}\theta_x^2 + \frac{1}{2}k_{\theta_y}\theta_y^2 + \frac{1}{2}k_{\theta_z}\theta_z^2 \tag{3.3}$$

The Lagrangian is

$$\mathcal{L} = T^* - V. \tag{3.4}$$

Lagrange's equations are

$$\frac{d}{dt}(\frac{\partial \mathcal{L}}{\partial \dot{\zeta}_i}) - \frac{\partial \mathcal{L}}{\partial \zeta_i} = \Xi_i \quad i = 1 \; to \; i = 6, \tag{3.5}$$

where Ξ_i is the generalized force. The resulting equations of motion for the system take the following form:

$$\left[\; M \; \right]\left\{ \ddot{x} \right\} + \left[\; C \; \right]\left\{ \dot{x} \right\} + \left[\; K \; \right]\left\{ x \right\} = \left\{ F \right\},$$

where [M] is the 6X6 mass matrix, [C] is the 6X6 damping matrix, [K] is the 6X6 stiffness matrix, $\{x\}$ is the 6X1 column vector representing the generalized coordinates, and $\{F\}$ is the 6X1 column vector representing the generalized forces. The damping of the system is small and can therefore be neglected in order to simplify calculations. The mass and stiffness matrices are as follows:

31

$$
\begin{bmatrix} & M & \end{bmatrix} = \begin{bmatrix} m & & & & & \\ & m & & & & \\ & & m & & & \\ & & & J & & \\ & & & & J & \\ & & & & & J' \end{bmatrix},
$$

and

$$
\begin{bmatrix} & K & \end{bmatrix} = \begin{bmatrix} k_x & & & & k_x h & -k_x r \\ & k_y & & -k_y h & & -k_y r \\ & & k_z & & & \\ & -k_y h & & k_{\theta_x} + k_y h^2 & & k_y h r \\ k_x h & & & & k_{\theta_y} + k_x h^2 & -k_x h r \\ -k_x r & -k_y r & & k_y h r & -k_x h r & k_{\theta_z} + k_y r^2 + k_x r^2 \end{bmatrix}.
$$

In order to determine the eigenvectors for the system, we first assume that the solutions to the differential equations take the form:

$$
\{x(t)\} = \begin{Bmatrix} u_1 \\ u_2 \\ u_3 \\ u_4 \\ u_5 \\ u_6 \end{Bmatrix} e^{iwt}
$$

and thus

$$\{\ddot{x}(t)\} = -\omega^2 \begin{Bmatrix} u_1 \\ u_2 \\ u_3 \\ u_4 \\ u_5 \\ u_6 \end{Bmatrix} e^{i\omega t}.$$

Substituting this into the above equations of motion yields:

$$\begin{bmatrix} & & \\ & K - \omega^2 M & \\ & & \end{bmatrix} \begin{Bmatrix} v_i \end{Bmatrix} = \begin{Bmatrix} F \end{Bmatrix}.$$

In order to calculate the natural frequencies and mode shapes, $\{F\}$ is set to 0. The determinant of the above matrix gives the undamped natural frequencies of the system. The corresponding mode shapes can be determined by plugging in the natural frequencies and solving for the six column vectors, $\{v_i\}$ which satisfy the above equation when $\{F\} = 0$.

The most important conclusion drawn from this model concerns the form of the eigenvectors. Several of the eigenvectors for the system are coupled between several degrees-of-freedom. The eigenvectors for the system are shown below. The asterisks represent nonzero terms of the vectors.

$$v_1 = \begin{bmatrix} * \\ \\ \\ \\ * \\ * \end{bmatrix} \quad v_2 = \begin{bmatrix} \\ * \\ * \\ \\ \\ * \end{bmatrix} \quad v_3 = \begin{bmatrix} \\ \\ * \\ \\ \\ \end{bmatrix} \quad v_4 = \begin{bmatrix} \\ * \\ \\ * \\ \\ * \end{bmatrix} \quad v_5 = \begin{bmatrix} * \\ \\ \\ \\ * \\ * \end{bmatrix} \quad v_6 = \begin{bmatrix} * \\ * \\ \\ * \\ * \\ * \end{bmatrix}$$

These eigenvectors point to a problem which involves mode shapes which exhibit

motion in desired and undesired degrees-of-freedom. The three actuators control θ_x, θ_y, and Z. Motions in X, Y, and θ_z are observable but uncontrollable. Consequently, any mode shape which involves motion in the undesired degrees-of-freedom will be uncontrolled. For example, at the first resonance of the model, the table will be translating in X, and rotating in θ_y, and θ_z, but will only be controlled in θ_y. The undesired motion in X and θ_z presents a serious problem. The coupling in the eigenvectors cannot be avoided, so the approach followed basically involves maximizing the stiffnesses of the system in X, Y, and θ_z in order to raise the resonances above the desired frequency range of operation. This topic is covered in depth in Chapter 4.

The model also yields the 6X6 transfer function matrix:

$$\begin{bmatrix} K - \omega^2 M \end{bmatrix} \begin{Bmatrix} x \end{Bmatrix} = \begin{Bmatrix} F \end{Bmatrix}.$$

Premultiplying by the inverse of the previous matrix yields:

$$\begin{Bmatrix} x \end{Bmatrix} = \begin{bmatrix} K - \omega^2 M \end{bmatrix}^{-1} \begin{Bmatrix} F \end{Bmatrix} = \begin{bmatrix} H \end{bmatrix} \begin{Bmatrix} F \end{Bmatrix},$$

where

$$\begin{bmatrix} H \end{bmatrix} = \begin{bmatrix} H_{xf_x} & H_{xf_y} & H_{xf_z} & H_{xf_{\theta_x}} & H_{xf_{\theta_y}} & H_{xf_{\theta_z}} \\ H_{yf_x} & H_{yf_y} & H_{yf_z} & H_{yf_{\theta_x}} & H_{yf_{\theta_y}} & H_{yf_{\theta_z}} \\ H_{zf_x} & H_{zf_y} & H_{zf_z} & H_{zf_{\theta_x}} & H_{zf_{\theta_y}} & H_{zf_{\theta_z}} \\ H_{\theta_x f_x} & H_{\theta_x f_y} & H_{\theta_x f_z} & H_{\theta_x f_{\theta_x}} & H_{\theta_x f_{\theta_y}} & H_{\theta_y f_{\theta_z}} \\ H_{\theta_y f_x} & H_{\theta_y f_y} & H_{\theta_y f_z} & H_{\theta_y f_{\theta_x}} & H_{\theta_y f_{\theta_y}} & H_{\theta_y f_{\theta_z}} \\ H_{\theta_z f_x} & H_{\theta_z f_y} & H_{\theta_z f_z} & H_{\theta_z f_{\theta_x}} & H_{\theta_z f_{\theta_y}} & H_{\theta_z f_{\theta_z}} \end{bmatrix} = \begin{bmatrix} * & & & & * & * \\ & * & & * & & * \\ & & * & & & \\ & * & & * & & * \\ * & & & & * & * \\ * & * & & * & * & * \end{bmatrix}.$$

Each element in the matrix H represents the single-input single-output transfer func-

tion between the output displacement of the first subscript and the input force of the second subscript. Notice that several of the terms are zero; the elements in boldface and the asterisks again represent the nonzero terms of the matrix.

3.2 Vibrational Coupling

As the block diagram in Figure 1-3 shows, there are two distinct control loops. The user defined control loop which employs the SPROC processing chip, and the control loop about the shaker system which includes the I*star computer. The control system design that will be discussed refers to the latter system composed of the three shakers, the vibrational platform, the flexure mounts and the other mechanical structures attached to the system. In essence, this project is concerned with applying the desired vibrational disturbance to the payload.

The system has a built-in frequency domain controller, the I*star computer, which performs a plant inversion to achieve the desired disturbance. A low-level random noise signal is applied to the system as a pretest and the response is measured in θ_x, θ_y, and Z. Three transfer functions are then calculated: $H_{\ddot{\theta}_x f_{\theta_x}}$, $H_{\ddot{\theta}_y f_{\theta_y}}$, and $H_{\ddot{z}f_z}$. Using the desired output and the transfer function, the I*star controller computes a suitable input to the system. The I*star has two important design performance characteristics. First, it represents an open-loop feed-forward control design; it is not a traditional closed loop system. Secondly, it controls three single-input single output systems; it considers the three actuated degrees-of-freedom as completely uncoupled systems.

Additional time-domain control may be necessary in order to compensate for the coupling which can result from two different sources: coupling between the actuated degrees-of-freedom and coupling caused by the mechanical components of the system. The following sections will elaborate on these sources of coupling.

35

3.2.1 Coupling Between Actuated Degrees-of-Freedom

The first source of coupling exists between the three actuated degrees-of-freedom for example, driving the system in θ_x will result in small motion in θ_y. The previous model demonstrates that the actuated degrees-of-freedom are not coupled, but coupling will exist due to imperfections in the mechanical components of the system or small errors in the coordinate transformation circuit. Consider the 6X6 matrix of transfer functions developed in the previous section:

$$
\begin{Bmatrix} x \\ y \\ z \\ \theta_x \\ \theta_y \\ \theta_z \end{Bmatrix} =
\begin{bmatrix}
H_{Xf_X} & 0 & 0 & 0 & H_{Xf_{\theta_Y}} & H_{Xf_{\theta_Z}} \\
0 & H_{Yf_Y} & 0 & H_{Yf_{\theta_X}} & 0 & H_{Yf_{\theta_Z}} \\
0 & 0 & \mathbf{H_{Zf_Z}} & 0 & 0 & 0 \\
0 & H_{\theta_X f_Y} & 0 & \mathbf{H_{\theta_X f_{\theta_X}}} & 0 & H_{\theta_X f_{\theta_Z}} \\
H_{\theta_Y f_X} & 0 & 0 & 0 & \mathbf{H_{\theta_Y f_{\theta_Y}}} & H_{\theta_Y f_{\theta_Z}} \\
H_{\theta_Z f_X} & H_{\theta_Z f_Y} & 0 & H_{\theta_Z f_{\theta_X}} & H_{\theta_Z f_{\theta_Y}} & H_{\theta_Z f_{\theta_Z}}
\end{bmatrix}
\begin{Bmatrix} F_x \\ F_y \\ F_z \\ F_{\theta_x} \\ F_{\theta_y} \\ F_{\theta_z} \end{Bmatrix}.
$$

Now examine the smaller 3X3 matrix of transfer functions which includes only the actuated degrees-of-freedom:

$$
\begin{Bmatrix} \ddot{z} \\ \ddot{\theta}_x \\ \ddot{\theta}_y \end{Bmatrix} =
\begin{bmatrix}
\mathbf{H_{\ddot{z}f_Z}} & H_{\ddot{z}f_{\theta_x}} & H_{\ddot{z}f_{\theta_y}} \\
H_{\ddot{\theta}_x f_z} & \mathbf{H_{\ddot{\theta}_x f_{\theta_X}}} & H_{\ddot{\theta}_x f_{\theta_y}} \\
H_{\ddot{\theta}_y f_z} & H_{\ddot{\theta}_y f_{\theta_x}} & \mathbf{H_{\ddot{\theta}_y f_{\theta_y}}}
\end{bmatrix}
\begin{Bmatrix} F_z \\ F_{\theta_x} \\ F_{\theta_y} \end{Bmatrix}.
$$

The I*star controller treats the actuated degrees-of-freedom as three independent single-input single-output systems. It calculates only the three transfer functions (the diagonals of the matrix). The off-diagonal terms are nonexistent, according to the model. These off-diagonal terms which represent coupling between the actuated degrees-of-freedom, however, may be significant. Since the I*star computes a transfer function between the input of one degree-of-freedom and the output from the same degree-of-freedom, eg. $\mathbf{H_{\ddot{\theta}_x f_{\theta_x}}}$, any coupling causes the output to be changed. The I*star computer will sense this coupling, but it will appear as 'artificial resonances' in the three transfer functions. Take, for example, the coupling between θ_y and θ_x. This

coupling will be observed by the I*star computer, but it will attribute the output motion to only the θ_x input. The correct transfer function will not be calculated in this case.

3.2.2 Coupling Caused by Mechanical Components of System

The second source of coupling is a result of the vibrational characteristics of the mechanical components of the system. The mechanical components, such as the flexures and the mounting platform, have their own vibrational modes which change the vibrational characteristics of the entire system. The previous model shows that the system has mode shapes which exhibit motion in both desired (θ_x, θ_y, and Z) and undesired (θ_z, X, and Y) degrees-of-freedom. Motions in X, Y, and θ_z will couple into the three actuated degrees of freedom. The extent to which these motions will couple into the desired degrees-of-freedom depends on the design of these mechanical components. These components are the main limitation to high bandwidth performance. Consequently, the most in-depth research and testing focused upon the mechanical components of the system: the flexures and the center post.

3.3 Control Issues

Several approaches can be taken to deal with the control aspect of this design problem, but it is important to note that the success of any control system used in the test facility is severely limited by the mechanical design. There are three areas of possible solutions to the problem:

Without the I*star computer in the loop:

a. closing three single-input single-output loops about each actuated degree-of-freedom

With the I*star computer in the loop:

b. utilizing an additional decentralized control which involves single-input single-output loops about each shaker

c. running the system with the I*star computer as the only controller

It is important to note that depending upon the performance of the open-loop system, a feedback control system may not be beneficial. The system is open-loop stable, so a control system is not necessarily required. However, achieving stability is not a sufficient design goal for a control system. Three other important design factors include stability robustness, and noise and disturbance rejection.

The final choice for the system controller consisted of the I*star computer as the sole controller. This controller was shown to produce adequate results.

3.3.1 Three Single-Input Single-Output Loops About Each DOF

The coupling resonances introduced by the mechanical components of the system severely limit high bandwidth performance. These coupling resonances are difficult to compensate by electronic means, as described in the HBSM research [6]. By way of illustration, examine the magnitude and phase plots of an ideal transfer function (ratio of acceleration output and voltage input) shown below in Figure 3-2.

This transfer function was chosen to resemble the transfer function of a single degree-of-freedom of the actual system. The system consists of two zeros and four poles. The first critically damped resonance at 20 Hz drops the phase from -180 degrees to -360 degrees (the simulation has offset the phase by -360 degrees). The second underdamped resonance at 600 Hz drops the phase an additional 180 degrees. This ideal system exhibits no coupling resonances; there is a -40 dB/dec rolloff after the second pair of poles.

The general closed loop feedback system block diagram containing disturbance is shown in Figure 3-3 [12]. The system has three inputs: r(s), the command or reference input, d(s), the disturbance, and n(s), the measurement noise which is introduced via sensors. The sensor noise can usually be modeled as uniformly distributed in frequency (white noise). The output of the closed loop system is:
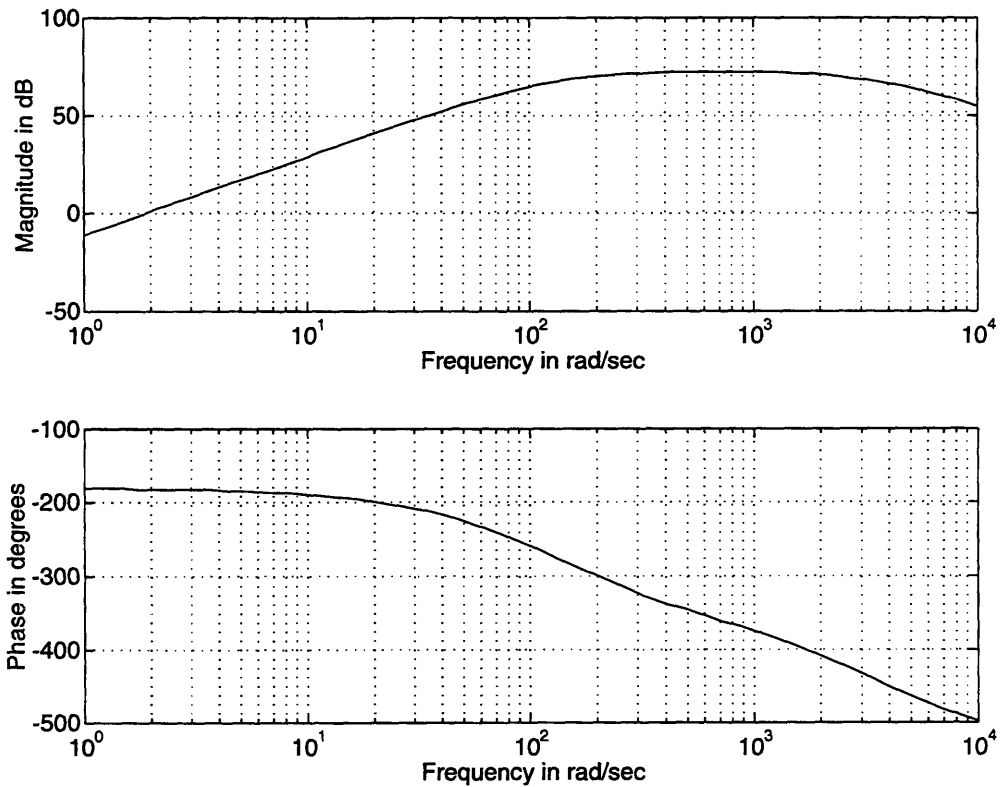
Figure 3-2: Ideal Transfer Function

$$y(s) = \frac{KG(s)}{1 + KG(s)} r(s) + \frac{1}{1 + KG(s)} d(s) - \frac{KG(s)}{1 + KG(s)} n(s). \qquad (3.6)$$

Since the system is open-loop stable, the main goal of a feedback control system in this case is to enhance the system with disturbance and noise rejection properties.

The second term in the above equation represents the disturbance effect in the system. In order to reduce the effect of d(s), the loop gain KG(s) must be kept large in regions where d(s) is large. Assuming that the disturbances will be low frequency, the controller will be designed to raise the loop gain in the low frequency range of the open loop transfer function. The block diagram for this controller is shown in Figure 3-4. There are three single-input single-output loops about each degree-of-freedom.

The ideal transfer function (as shown in Figure 3-2) has very poor disturbance

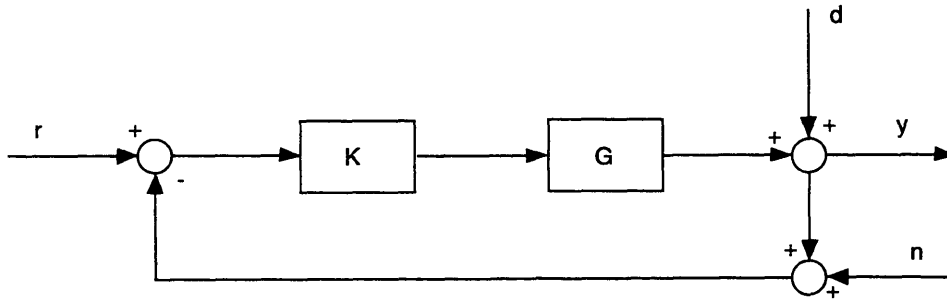Figure 3-3: General Closed Loop Block Diagram Including Disturbance and Measurement Noise Inputs

rejection abilities because its loop gain rolls off at low frequencies. Consequently, the low frequency response of the system must be altered. Two lag compensators are added to the system (two poles at .159 Hz and two zeros at 10 Hz), along with an integrator at .159Hz. This raises the loop gain at low frequencies, thus attenuating $d(s)$. The lag compensator, however, does produce a phase drop in the system, but this drop is far enough removed from the crossover frequency to not affect the stability of the system.

The third term in the above equation represents the noise effect in the system. In order to suppress the noise, the loop gain must be kept small in regions where $n(s)$ is large and tight command-following is not required. Thus, the compensated system should roll off at high frequencies. The pure integrator term ensures that the system will sufficiently attenuate high frequency noise by decreasing the slope of the transfer function.

Finally, a gain is chosen to produce the desired crossover frequency of 200 Hz. The compensated system has a phase margin of 59.0 degrees. The compensation design process followed is outlined [Roberge]. The block diagram of the compensated system is shown in Figure 3-5 and the compensated open-loop transfer function is shown in Figure 3-6.
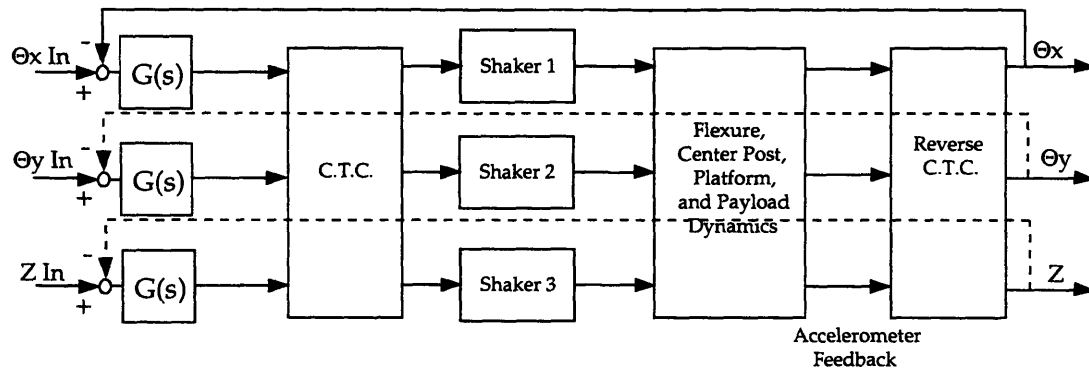
Figure 3-4: Closed Loop Block Diagram of Single-Input Single-Output Control Scheme

In reality, however, the transfer functions exhibit coupling modes which appear as spikes in the phase and magnitude plots. This problem was encountered in the HBSM project [6]. These coupling modes limit the bandwidth of the system. As the bandwidth of the system increases, these modes cause the servo loop to become unstable. The resonances appear as spikes in magnitude and phase at frequencies above the crossover frequency. If these resonances are not attenuated properly, they may push the magnitude above 0 dB, causing instability. To ensure stability, the first coupling resonance must be roughly a factor of 4 greater than the cross over frequency. There is a tradeoff between stability and disturbance rejection on one hand, and bandwidth on the other.

The same system, however, operated open-loop without compensation has a much greater bandwidth, retains stability (since the system is open-loop stable), but does not possess any enhanced disturbance or noise rejection properties. The open-loop system can be operated at a frequency just below the first coupling resonance, thus increasing the frequency operation range.

In conclusion, feedback would unnecessarily limit the bandwidth of the compensated system if the transfer functions are well-behaved. In this case, the I*star controller will provide sufficient control. The system transfer functions are well-behaved if they are stable, smooth, and show no coupling between actuated degrees-of-freedom

Zref

K

$\dfrac{s+62.8}{s+1}$

$\dfrac{s+62.8}{s+1}$

$\dfrac{1}{s+1}$

$\dfrac{1}{s^2+251s+15791}$

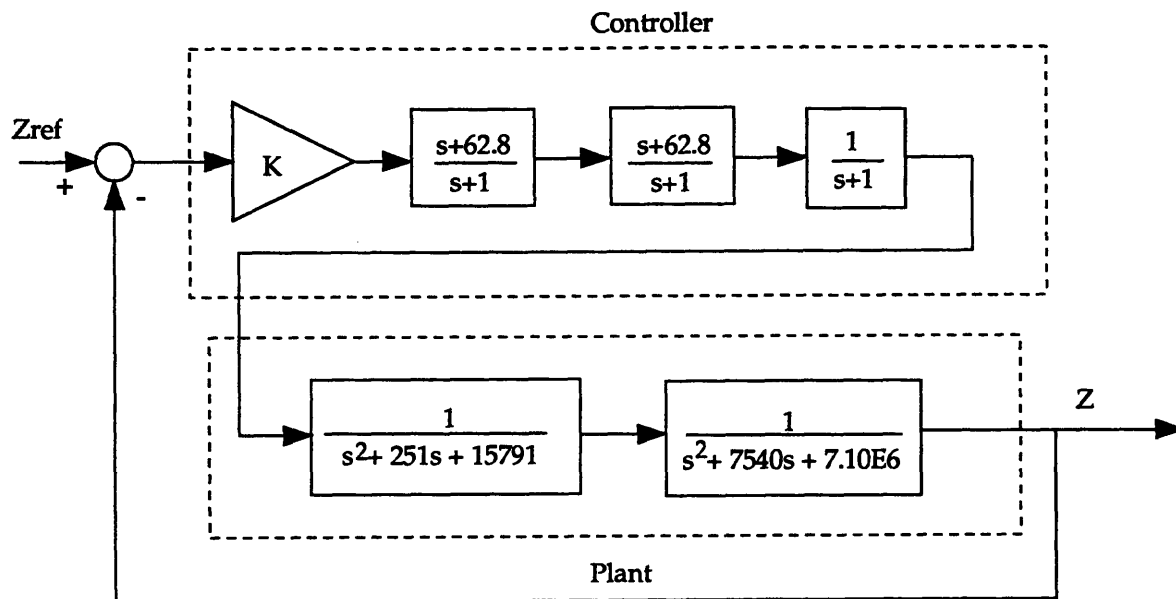$\dfrac{1}{s^2+7540s+7.10E6}$

Z

Plant

Figure 3-5: Compensated Closed Loop Block Diagram

over the desired frequency range. Strangely enough, a feedback control system may not improve system performance.

3.3.2 I*star Controller Alone

The I*star controller represents a feed-forward controller which utilizes estimates of the plant transfer function in order to shape the input to achieve the desired output. Figure 3-7 shows a block diagram of the control system.

A closed-loop feedback controller is not required because the system is open-loop stable, but it would provide the system with disturbance rejection which the I*star controller cannot. The I*star controller, using plant inversion, does not perform well near undamped resonances or in regions which exhibit the first form of coupling mentioned: coupling between actuated degrees of freedom. However, the I*star performs well in other areas. It has the benefit of allowing the system to be operated at higher frequencies than a closed loop system.
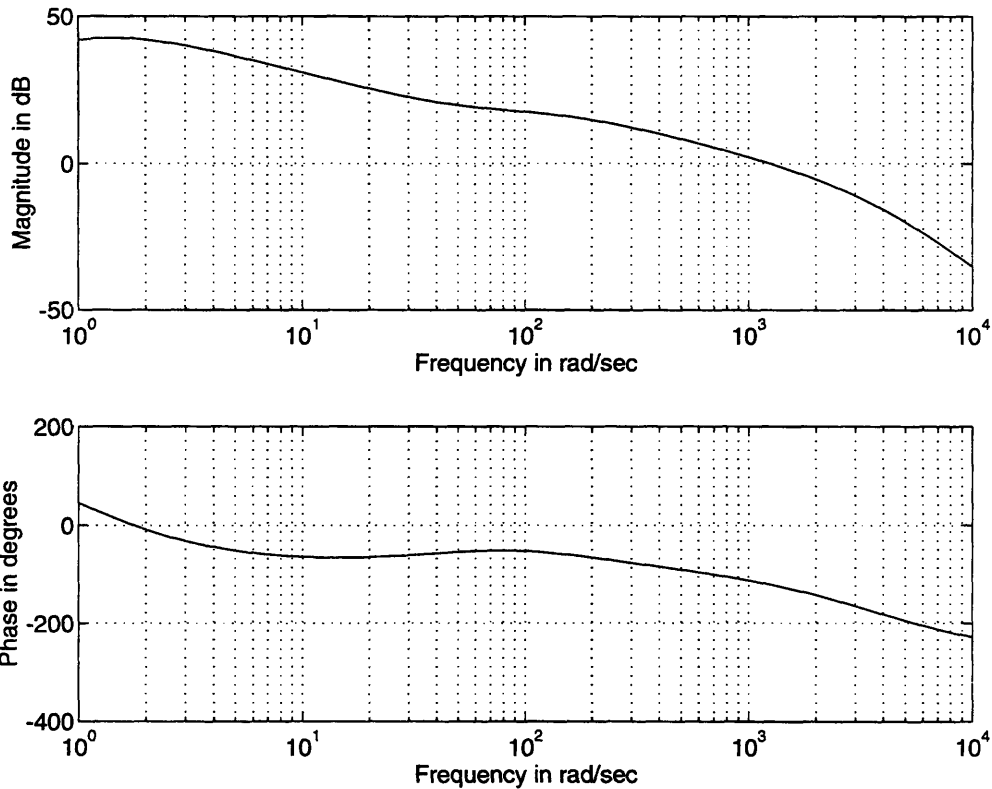
Figure 3-6: Compensated Ideal Transfer Function

3.3.3 Three Single-Input Single-Output Loops About Each Shaker

Three single-input single-output loops about each shaker could be utilized in addition to the I*star controller to give the system disturbance and noise rejection properties, as the single loops about each degree-of-freedom could but without sacrificing bandwidth. A block diagram for this control scheme is shown in Figure 3-8.

The benefit of placing the control loops about the shakers lies in a larger possible bandwidth. The feedback for the control loop would be provided by an additional set of accelerometers, one directly on the mounting plate of each shaker. The goal of this approach is to control a transfer function which has resonances which are of lower frequencies than those of the entire flexure/platform system. For example, the

43
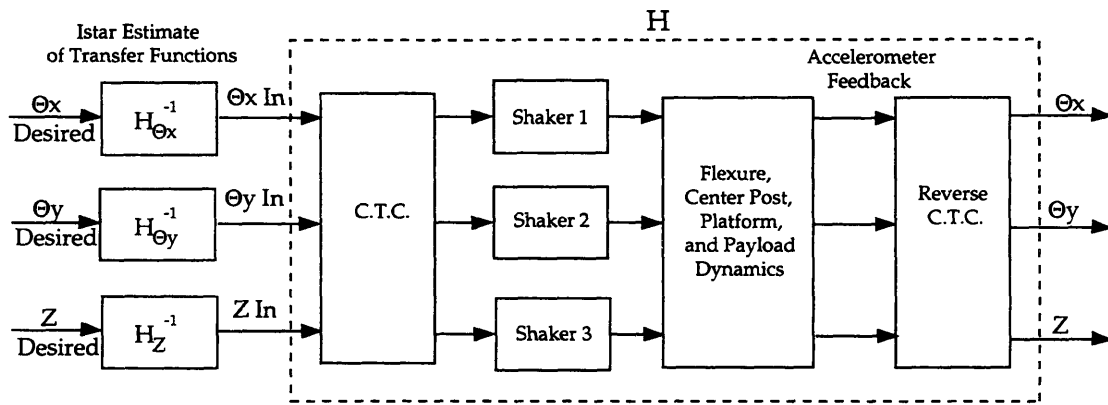
Figure 3-7: I*star Controller Block Diagram
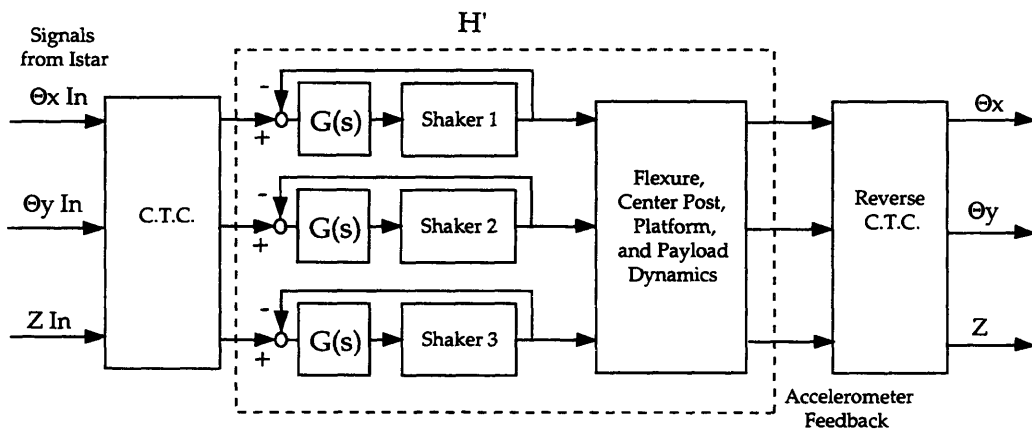
Figure 3-8: Three SISO Loops About Each Shaker

flexure/platform system will exhibit natural frequencies below 600 Hz, but the shakers are limited by the resonance of the armature which occurs at 4850 Hz. The placement of the accelerometers attempts to ensure the resonances introduced by the flexures and the mounting platform will not appear in the controlled transfer function. This allows the cross over frequency of the controlled system to be placed higher than the previous single-input single-output design, while still giving the system disturbance and noise rejection properties.

This approach is limited by the influence of the dynamics of the flexures and platform. A simple two degree-of-freedom model shown in Figure 3-9 illustrates this

point. The mass m_1 represents the armature of a single shaker, k_1 the axial stiffness of a single shaker, c_2 the damping of the flexures, m_2 the mass of the platform, and k_2 the stiffness of the flexures.
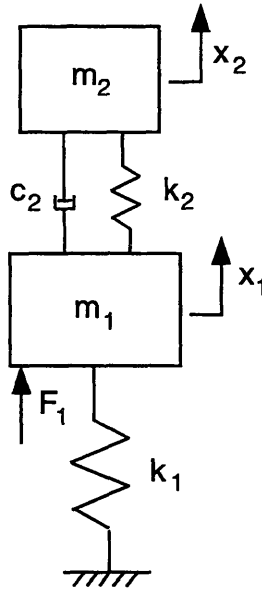
Figure 3-9: Two Degree-of-Freedom Model

The transfer function relating the displacement of m_1 to an input force, F_1, applied to m_1 is:

$$H_{X1F1} = \frac{(k_2 + m_2 s^2) + sc_2}{[(k_1 + m_1 s^2)(k_2 + m_2 s^2) + m_2 k_2 s^2] + sc_2[(m_1 + m_2)s^2 + k_2]} \quad (3.7)$$

The acceleration of the armature is dependent upon the dynamics of the flexure/platform combination. Consequently, the success of this approach relies upon attenuating the effect of the dynamics of the flexures/platform combination.

Chapter 4

Component Characterization and Design

In this chapter, the main components of the three-degree-of-freedom vibration test facility are described, along with the performance specifications which drove the design. The performance of the components is judged primarily upon their frequency response characteristics. The vibrational behavior of mechanical components, in particular, the location of the natural frequencies introduced by the components is examined closely.

The components discussed in this chapter include the coordinate transformation circuit, the electrodynamic shakers, the vibrational mounting platform, the four-axis flexures, the center post, and the accelerometers used to provide feedback for the system.

4.1   Coordinate Transformation Circuit

The coordinate transformation circuit was developed and built by Ramona Tung of the Control Systems Engineering Group at Lincoln Laboratory. This circuit transforms the disturbance axes (θ_x, θ_y, and Z) into the shaker axes (1, 2, and 3) by converting the desired rotation and translation into three linear motions with different phases. The force axes of the three shakers do not align with the disturbance axes θ_x, θ_y, and Z (as shown in Figure 1.1). Consequently, a coordinate transformation is

required to allow the user to create a vibrational environment using the disturbance axes. The feedback for the system is accomplished through the use of three linear accelerometers positioned on the vibrational platform directly above each shaker. These signals are aligned with the force axes of the shakers, so a reverse coordinate transformation is necessary to feed back the correct signals. This reverse transformation matrix is the inverse of the transformation matrix. By assuming the disturbance axes are aligned with the principal axes, the center of gravity of the assembly is at the geometric center of the platform, and that the platform is perfectly rigid, the 3X3 matrix which relates the actuator axes and the disturbance axes is easily derived from geometry and rigid body mechanics [15]. See Appendix A for discussion. The transformation matrix is shown below:

$$
\begin{bmatrix} \ddot{Z}_1 \\ \ddot{Z}_2 \\ \ddot{Z}_3 \end{bmatrix} = \begin{bmatrix} & & \\ & \mathbf{M} & \\ & & \end{bmatrix} \begin{bmatrix} \ddot{\theta}_x \\ \ddot{\theta}_y \\ \ddot{Z} \end{bmatrix} = \begin{bmatrix} 0.264 & 0.152 & 1.0 \\ -0.264 & 0.152 & 1.0 \\ 0.0 & -0.305 & 1.0 \end{bmatrix} \begin{bmatrix} \ddot{\theta}_x \\ \ddot{\theta}_y \\ \ddot{Z} \end{bmatrix}. \quad (4.1)
$$

Where the column vector composed of $\ddot{Z}_1$, $\ddot{Z}_2$, and $\ddot{Z}_3$ represents the control inputs in the shaker force axes, and the column vector composed of $\ddot{\theta}_x$, $\ddot{\theta}_y$ and $\ddot{Z}$ represents the control inputs in the disturbance axes. Again, the reverse coordinate transformation, which converts the accelerometer outputs in the shaker axes to the disturbance axes is simply the inverse of the transformation matrix, M^{-1}:

$$
\begin{bmatrix} \ddot{\theta}_x \\ \ddot{\theta}_y \\ \ddot{Z} \end{bmatrix} = \begin{bmatrix} & & \\ & \mathbf{M}^{-1} & \\ & & \end{bmatrix} \begin{bmatrix} \ddot{Z}_1 \\ \ddot{Z}_2 \\ \ddot{Z}_3 \end{bmatrix} = \begin{bmatrix} 1.894 & -1.894 & 0.0 \\ 1.094 & 1.094 & -2.187 \\ 0.333 & 0.333 & 0.333 \end{bmatrix} \begin{bmatrix} \ddot{Z}_1 \\ \ddot{Z}_2 \\ \ddot{Z}_3 \end{bmatrix}, \quad (4.2)
$$

where the column vector composed of $\ddot{Z}_1$, $\ddot{Z}_2$, and $\ddot{Z}_3$ represents the accelerometer outputs in the shaker force axes, and the column vector composed of $\ddot{\theta}_x$, $\ddot{\theta}_y$ and $\ddot{Z}$ represents the accelerometer output in the disturbance axes.

4.2 Electrodynamic Shakers

The electrodynamic shakers used in the test facility are model V556 purchased from Ling Dynamic Systems. The theory of operation is very simple. Each shaker houses a wire coil which is attached to the moving element of the shaker, the armature. A magnetic field is produced by an electromagnet within each shaker. When current is applied to the coil in the magnetic field, a force F proportional to the current I and the magnetic flux intensity B, is produced which accelerates a component mounted to the surface plate of the shaker:

$$F = BIl \tag{4.3}$$

where l is the length of coil. By applying a sinusoidal current to the shaker, the armature translates vertically, thus accelerating the payload in one linear degree-of-freedom. The current is supplied to the shaker by a power amplifier which converts an input voltage to an output current. The armature features a light weight, rugged magnesium frame which ensures a high natural frequency. In order to ensure linear motion of the armature, each shaker is equipped with a suspension system. A cross-section of one of the electrodynamic shakers used in the test facility is shown in Figure 4-1.

Table 4.1 describes the various performance characteristics of each shaker [4]. The high cross-axial (lateral) and rotational stiffnesses of the shaker are provided by four low mass suspension rollers running on flexures and a central linear bearing system. The polypropylene flexures attached to the rollers bend as the armature translates vertically. The suspension rollers are preloaded to ensure that no chatter will occur during operation. Two rubber shear mounts also link the armature to the shaker housing. These mounts provide the axial stiffness and, more importantly, damping to the vertical motion of the shaker. The lower guidance system for the armature features a linear ball bearing with nylon balls. The linear bearing is produced by Ransom, Hoffman, and Pollard of England.

The bare-table electromagnetic shaker has two natural frequencies: one associated
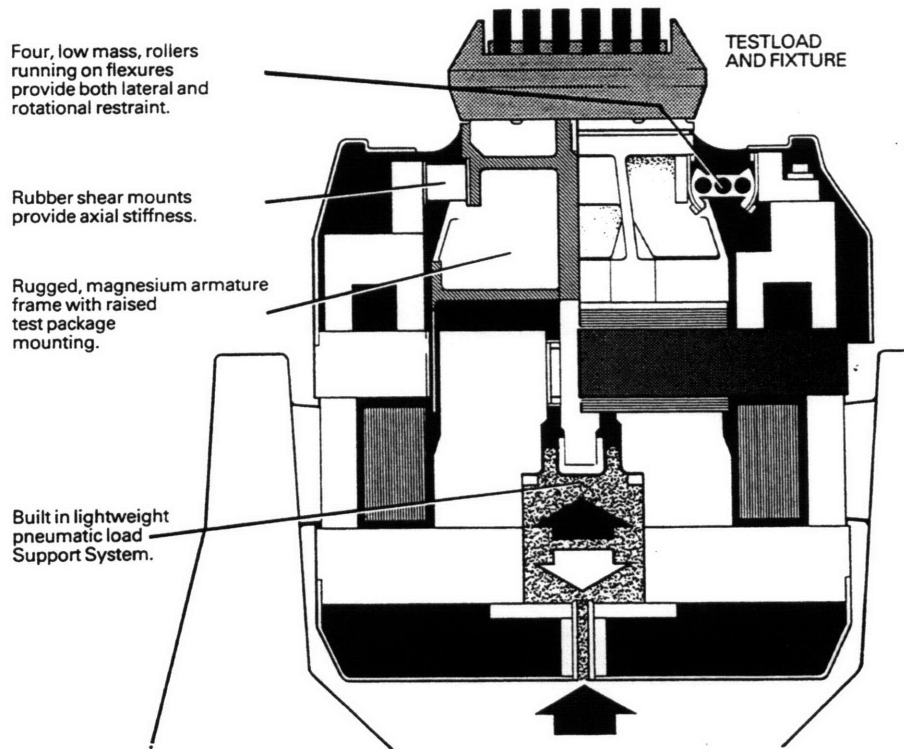
48

Four, low mass, rollers running on flexures provide both lateral and rotational restraint.

TESTLOAD AND FIXTURE

Rubber shear mounts provide axial stiffness.

Rugged, magnesium armature frame with raised test package mounting.

Built in lightweight pneumatic load Support System.

Figure 4-1: Cross Section of LDS Model V556 Vibration Generator

Table 4.1: Shaker Performance

Parameter	Units	Value
Frequency Operation Range	Hz	5 to 6300
Random Force (rms)	lbf	80
First Armature Resonance	Hz	4850
Max Payload Weight	lbf	55
Max Rated Travel	inches	$\pm.50$
Cross-Axial Stiffness	lbf/in	1300
Axial Stiffness	lbf/in	90
Rotational Stiffness	lbf/in	72,000
Max Input Current	amps	30

with the mass of the armature on the shear mounts and the other associated with the armature itself. The performance of a single shaker is characterized by these two natural frequencies, one at the low end of the frequency operating range, and one at the high end. Figure 4-2 shows the magnitude and phase plots of the transfer function of a bare shaker (the ratio of the output acceleration and the input voltage) plotted over a frequency range of 1 to 2000 Hz. The first natural frequency, which occurs at approximately 50 Hz, is well damped. The phase drops from 180 degrees to 0 degrees as a result of this resonance. This represents the natural frequency of the mass of the armature translating on the axial stiffness provided by the shear mounts. This resonance is well damped in order to allow the shaker to be operated through this range. The higher resonance appears at 4850 Hz, and is lightly damped. The phase drops an additional 180 degrees to -180 degrees. This represents the natural frequency of the armature itself. This lightly damped resonance allows the user to operate the shaker just below the natural frequency and not see the effects of the resonance. If this resonance were better damped, the phase drop would appear at a lower frequency, thus lowering the effective operation range.

The shaker has three distinct operating ranges. At low frequencies (5-20 Hz), the shaker is displacement limited. The stiffness term dominates in the equations of motion when the driving frequency, ω, is less than first natural frequency, ω_n. At higher frequencies (20-100 Hz), the shaker is velocity limited. The damping term dominates in this range when ω is roughly equal to ω_n. In the highest frequency range (100-4850Hz), the shaker is acceleration limited. The mass term dominates when ω is greater than ω_n [4].

A photograph of the three shakers is shown in Figure 4-3. The shakers are mounted so that the shaker force axes form the corners of an equilateral triangle. Each shaker is equipped with an inflatable air bladder which supports static loading. The pressurized bladder offsets the applied load to a shaker to ensure the armature remains at its mean position. When the armature is located at its mean position, full rated travel is possible. Each shaker is connected to an in-house 100 psi air supply line - the small diameter hoses in Figure 4-3 - in order to achieve full rated travel with various
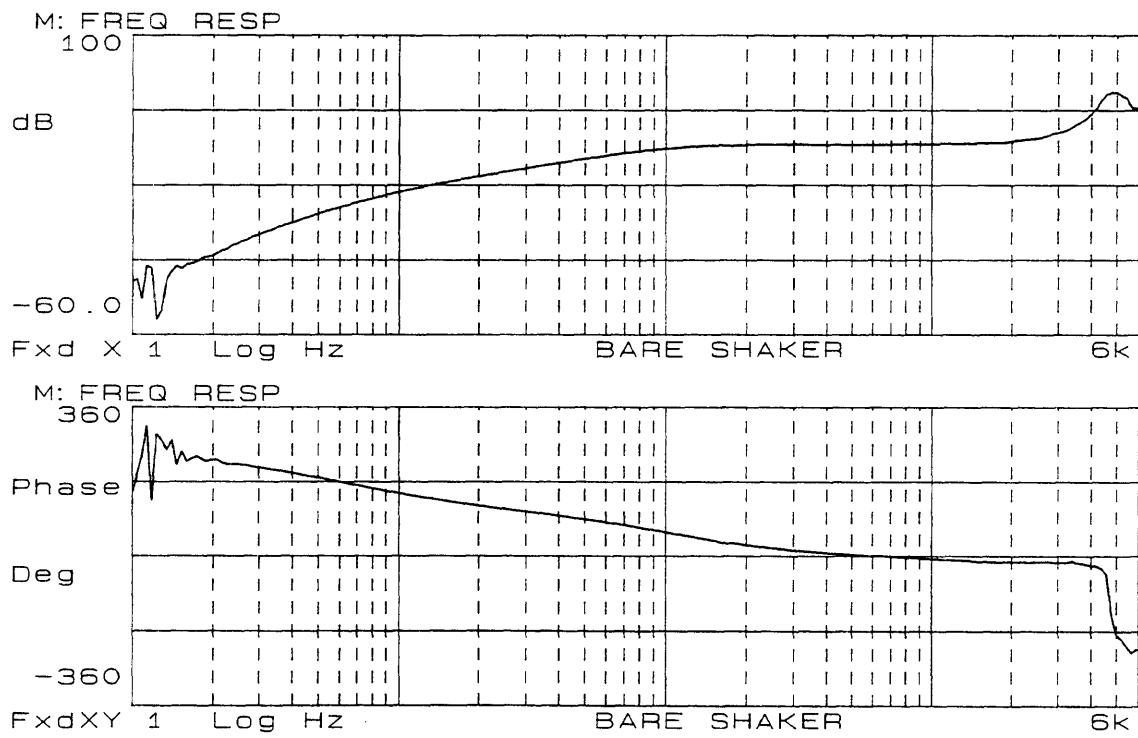
50

M: FREQ RESP

Figure 4-2: Bare Shaker Transfer Function

payloads.

Each shaker is also equipped with a blower which cools the shaker during operation. Three large diameter hoses can be seen leading to the ceiling in Figure 4-3. These hoses lead to blowers, which are located in a soundproof box mounted above the lab. The blowers actually pull air through the vents in each of the shaker housings cooling the system during operation.

The three shakers are mounted upon a 3/4" aluminum plate which is attached to a large granite slab resting on a rubber pad. The granite slab ensures that the force delivered by the shakers will not be sufficient to move the aluminum plate relative to the floor.

Each shaker has a field power supply and a power amplifier, Ling Dynamics FPS 1000 and PA 1000, respectively shown in Figure 4-3. The power amplifiers convert the input voltage signal to a current signal which is sent to each shaker. The power amplifiers also monitor the signal which is sent to the shakers and shut down if a spike is encountered, a blower is not operating, or the output exceeds a user-defined current limit.

One very troublesome problem was encountered with one of the power amplifiers: it unnecessarily inverts an input voltage. This was clearly observed when a single degree-of-freedom was driven. One shaker was 180 degrees out of phase. This was remedied by inverting the output of the coordinate transformation which lead to that power amplifier.

4.3 Vibrational Mounting Platform

The mounting platform, custom-made by the Newport Company, features an aluminum honeycomb structure supported between two aluminum plates. The upper plate has threaded mounting holes evenly spaced 1 inch apart. The circular platform is 26 inches in diameter, 4 inches thick, and weighs 36.9 lbs. The platform is attached to the three flexures at three points spaced 120 degrees apart at a radius of 12 inches. These flexures are aligned with each shaker axis. The center of the plat-
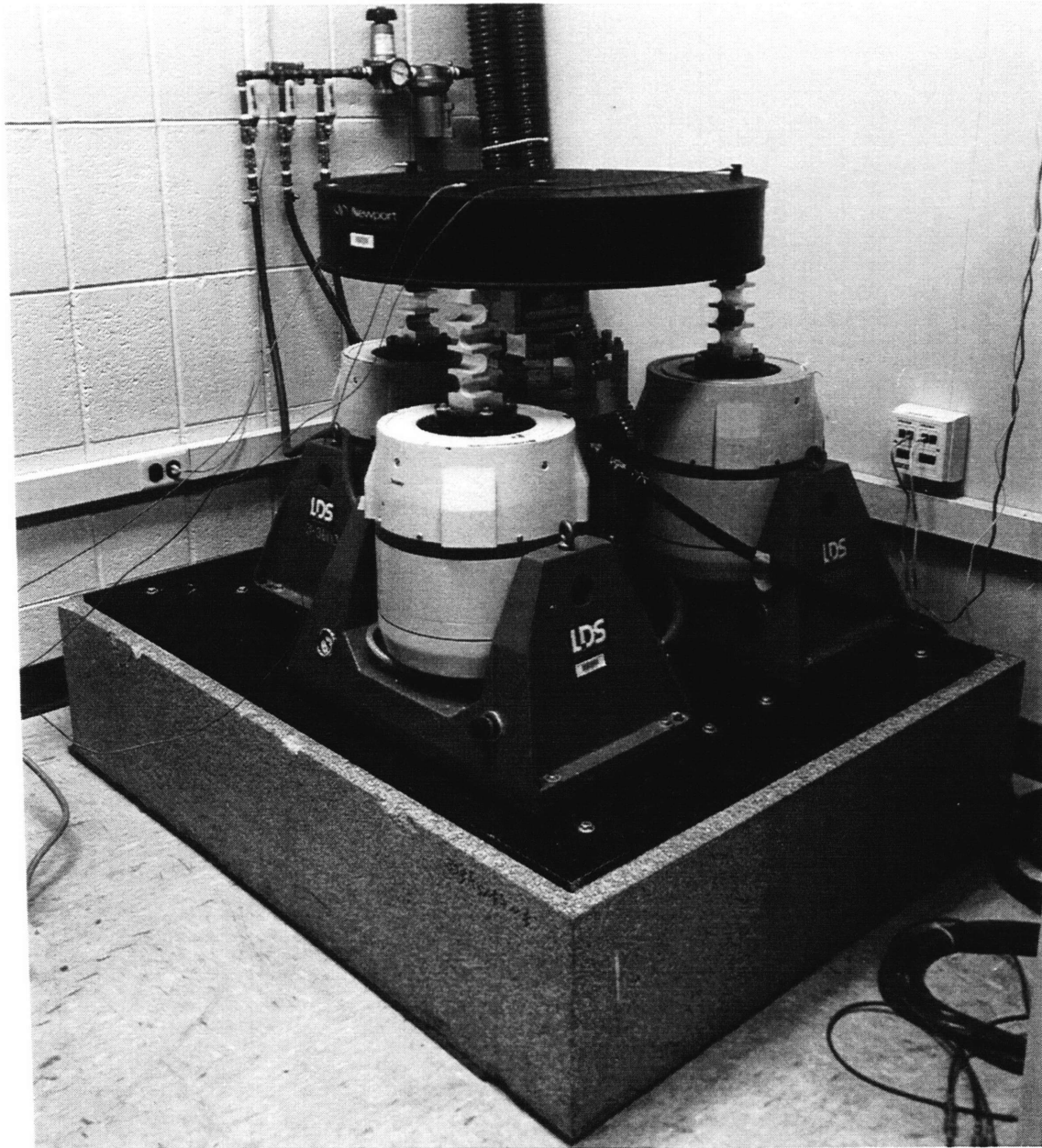
Figure 4-3: Shaker Assembly

form is also attached to the granite slab by a post with another flexure combination. The platform was chosen to have a good stiffness to weight ratio in order to ensure that vibrational modes in the platform are well above the frequency range of interest. A modal survey conducted by Ramona Tung identified the platform fundamental free-free resonant frequency at 900 Hz [15]. Experimental testing, however, with the platform constrained at three points by the flexures, shows platform resonances appearing at approximately 600 Hz. I believe this lower resonance is due to the different constraints placed upon the platform.

4.4 Four-Axis Flexures

4.4.1 Design Goals

The vibrational mounting platform must be mechanically coupled to the three actuators. The platform must be free to translate in the Z direction and, more importantly, rotate in θ_x and θ_y. Also, in order to ensure that the payload will not be subjected to undesired motions in X, Y, and θ_z, the platform should be constrained in these directions. Consequently, one main goal for the coupling mechanism design consists of permitting the three desired degrees-of-freedom and constraining the three undesired degrees-of-freedom.

Another design goal involves the elimination of friction in the coupling mechanisms. The previous work performed on the Syminex three degree-of-freedom shaker system showed nonlinearities in system performance introduced by the bearing and ball joint systems used. The friction of the coupling mechanism proved to be very undesirable.

The mechanical coupling devices must also be able accomodate for the longer distance between the shaker axes as the platform rotates. Figure 4-4 illustrates this geometric constraint. L_1 is the distance between the shaker axes before the table rotates through θ_x and L_2 is the distance after the table rotates. The shaker suspension system which support each armature is extremely stiff laterally (1300 lbf/in). Slight
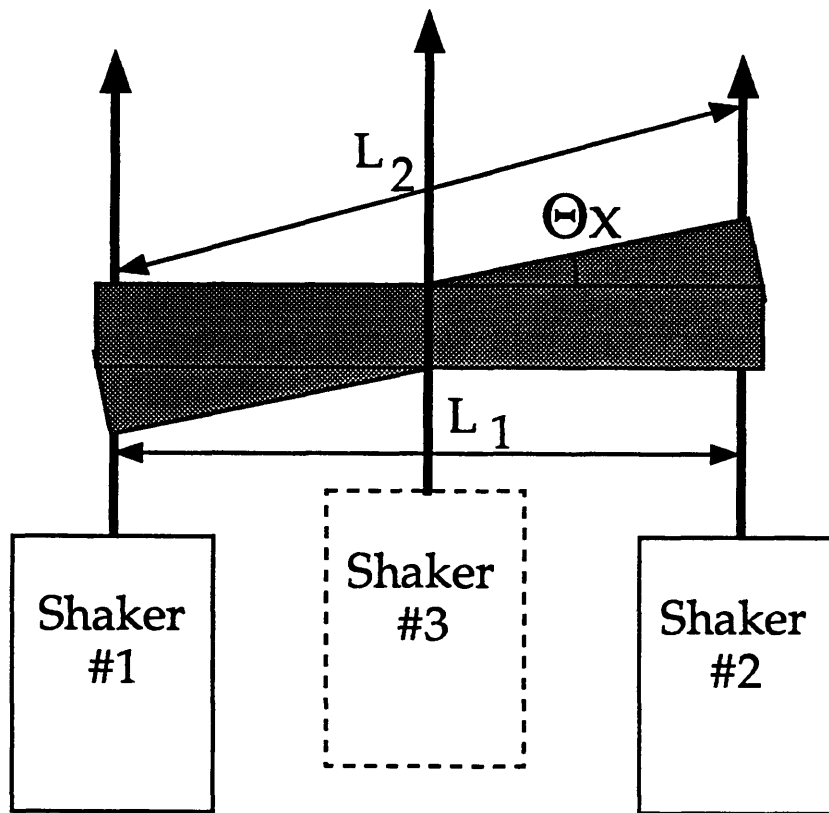
Figure 4-4: Platform Rotation

lateral displacement will cause the shakers to lock in place if the armature is forced to rotate. The mechanical coupling devices must therefore be able to accomodate the longer distance L_2 to prevent this.

This same problem was encountered in the development of the Syminex shaker system. In that case, three hydrostatic double ball joints were used to couple the baseplate to the shakers. Single ball joints would not allow the rotation to occur.

4.4.2   Design of Flexures

A drawing of a general single-axis flexure with critical dimensions is shown in Figure 4-5 [10]. This type of flexure design is commonly used as a means of mounting high-resolution optical elements. The flexure mounts isolate the optical elements from
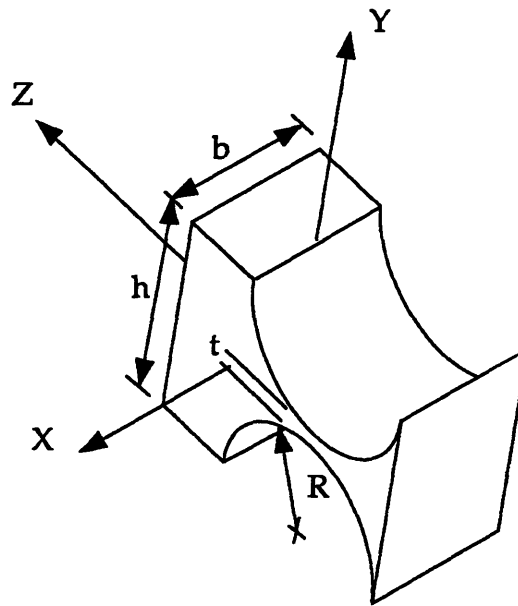
Figure 4-5: Drawing of Single-Axis Flexure

mechanical and thermal effects of the support system [17]. In this application, the flexures serve as pivot bearings. Properly-designed flexures can provide up to twenty degrees of rotation with no static friction, low hysteresis, and no lubricant required [18].

The final design of the flexure coupling system is shown in Figure 4-6, and a fully detailed drawing is included in Appendix B. The flexures are composed of four very narrow sections which are .050 inches at the thinnest section. A single-axis flexure allows rotation in one angular degree-of-freedom, whereas these *four*-axis flexures allow rotation about four axes. The end result is rotation about two orthogonal angular degrees-of-freedom. The four-axis (not two-axis) design was necessary to allow for the greater distance between the shaker axes as the platform rotates as previously described. This flexure design was chosen because it eliminates friction entirely; the thin strip of aluminum acts as a torsional spring within its linear range of elasticity.

Each single-axis flexure was fabricated by milling one face of a block of 6061-T6
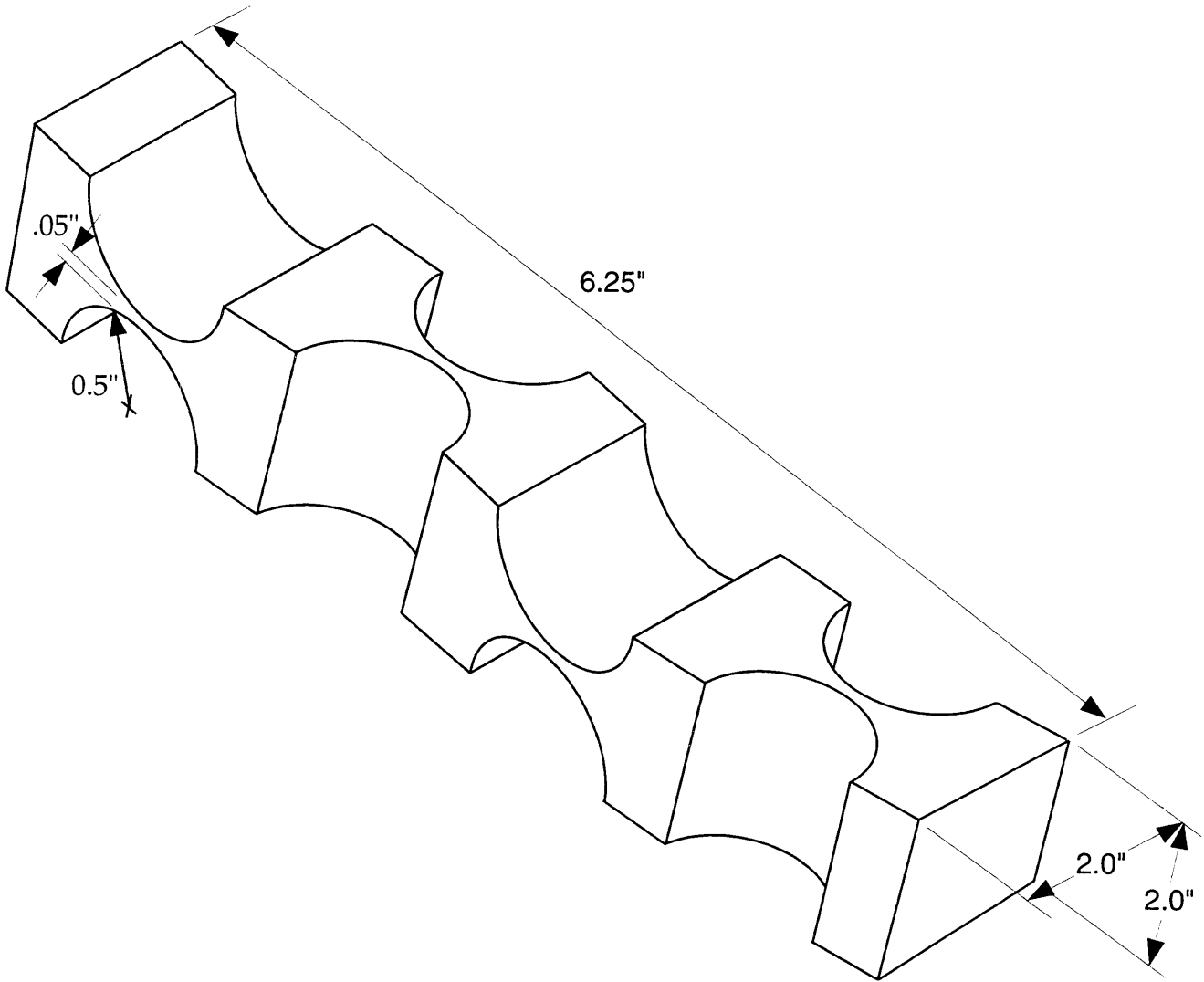
56

Figure 4-6: Drawing of Four-Axis Flexure

aluminum. The space created by the material removal was then supported with a cylinder of the same radius to allow milling of the opposite face. This process was repeated three times to create one four-axis flexure.

This design features a high axial stiffness and extremely low rotational stiffnesses in θ_x and θ_y. The intent of this design is to place the natural frequencies for the modes dominated by motion in θ_x and θ_y below 10 Hz (the lower bound of the frequency operation range) and all other natural frequencies above 100 Hz (the upper bound of the frequency operation range). The design has one major drawback: the flexure/platform system has low stiffness in the X, Y, and θ_z directions. These low stiffnesses are significant because they place the natural frequencies which exhibit motion in X, Y, and θ_Z within the desired frequency operation range. In order to account for this deficiency, additional stiffness is added to the system through a post which attaches to the center of the platform. This technique is discussed fully in the following section.

Fundamental Rocking Modes

The exact expression for the rotational stiffness of a single-axis flexure is unwieldy, but the exact expression can be closely approximated using the dimensions shown in Figure 4-5 without appreciable loss of accuracy to:

$$\frac{M_x}{\alpha_x} \approx \frac{2Ebt^{5/2}}{9\pi R^{1/2}} \tag{4.4}$$

where E is the Young's Modulus of the material, R is the radius of the narrow section, b is the depth of the narrow section, t is the thickness of the flexure at its narrowest point, α_x is the angular displacement of the compliant rotational degree-of-freedom and M_x is the moment applied to produce the angular displacement [10]. Two assumptions are required: $t/2R \ll h/2R$ and $t/2R \ll 1$. This equation holds only for a right circular hinge, which is defined by h, the width of the flexure face, in the equality:

$$h = 2R + t \tag{4.5}$$

58

The four-axis flexure can be considered as four single-axis flexures stacked upon each other. Each single-axis aluminum flexure with R of 0.5 inches, b of 2 inches, and t of 0.05 inches was designed to have rotational stiffnesses of 19.5 in-lbf/degree. In order to determine the rough location of the natural frequencies of the combined platform/flexure system, this rotational stiffness was used in a simple model consisting of the rotational inertia of the platform, J, on a torsional spring, $3k_{torsional}$ (for three flexures in parallel). The corresponding natural frequency for this system takes the form:

$$f_n = \frac{1}{2\pi}\sqrt{\frac{k_{torsional}g}{J}} \qquad (4.6)$$

where g is gravity and J is given by:

$$J = \frac{W}{12}(3r^2 + d^2) \qquad (4.7)$$

The weight of the platform, W, is 36.9 lbf, the radius of the platform, r, is 13 inches, and the thickness of the platform, d, is 4.5 inches. The natural frequency for the rocking mode of this system is 4.55 Hz. The mode shape of the actual system which is dominated by motion in θ_x will appear at approximately this frequency. This analysis will also hold for the mode shape dominated by motion in θ_y. The mode shapes do not consist entirely of pure rotation as this simple mass/spring model suggests, but are comprised of motion in many degrees-of-freedom, as shown by the more detailed model in Chapter 3.

The design goal of the flexures is to allow rotation in θ_x and θ_y to occur by giving the system very low stiffness in the θ_x and θ_y directions. The natural frequencies for these simplified rocking modes are consequently extremely low frequency. They occur below the desirable frequency operation range (10-100 Hz).

Fundamental Piston Mode

An expression for the fundamental piston mode (displacement purely in Z) for a single-axis flexure can be derived from the axial stiffness which is approximated by [10]:

$$k_{axial} = \frac{F_z}{\Delta_z} \approx \frac{Eb}{[\pi(R/t)^{1/2} - 2.57]} \qquad (4.8)$$

where F_z is a force in the Z direction and Δ_z is the resulting linear displacement. The axial stiffness of a single axis flexure with the same dimensions as the last case is $2.7 X 10^6$ lbf/in. The corresponding piston mode natural frequency for a simple model consisting of three four axis flexures $3k_{axial}/4$ (three springs in parallel each composed of four springs in series) attached to a weight W representing the mounting platform follows the equation:

$$f_n = \frac{1}{2\pi}\sqrt{\frac{k_{EQ}g}{W}} \qquad (4.9)$$

$f_n = 745$ Hz. This piston mode natural frequency is well above the desired frequency operation range.

Fundamental Shearing Mode

The fundamental shearing mode for a single axis flexure can be determined from the stiffness which is approximated by the following equation:

$$k_{lateral} = \frac{F_x}{\Delta_x} = \frac{F_y}{\Delta_y} \approx \frac{Gb}{[\pi(R/t)^{1/2} - 2.57]} \qquad (4.10)$$

Where G is the Shear Modulus (G = $3.8 X 10^6$ for Aluminum 6061). A single flexure possesses a shearing stiffness of $1.03 X 10^6$ lbf/in. The fundamental shearing mode in both X and Y for a system consisting of three four axis flexures ($3k_{lateral}/4$) and a weight representing the platform appears at 458.5 Hz. The system should exhibit a mode which will be dominated by shearing motion at this frequency. This natural frequency lies well outside the desired operation range.

Maximum Stress

The maximum stress developed in the flexures occurs as the platform rotates through an angle of ±48 mrad, which corresponds to maximum stroke of the shakers (±.5 in). The expression for the stress seen by the flexures is:

$$\sigma = \frac{Et}{2L}\theta \qquad (4.11)$$

where E is the Young's Modulus of the material, t is the thickness of the flexure at the narrowest point, θ is the angular displacement, and L is defined as the effective length of the flexure [7]. The maximum stress was calculated to be 60,000 psi. In order to lower this value well below the yield strength of aluminum (40,000 psi), the maximum angle was decreased to ±12 mrad which lowered the maximum stress t0 15,000 psi. It is important to note that the maximum rotation will occur only at low frequencies, 5-20 Hz. In this frequency range, the shakers are displacement limited. At higher frequencies, the shakers will not reach their full rated travel (in these ranges, the shakers are velocity and acceleration limited).

Fatigue Life Data

The flexures bend by design as the platform rotates through an angle and therefore possess a finite fatigue life. A suitable fatigue life was determined using the calculation for the maximum stress and a fatigue life curve. The maximum angular displacement has been limited to ±12 mrad in order to achieve a suitable fatigue life for the flexures. The maximum stress developed in the flexures is 15,000 psi. It has been proven empirically that 6061-T6 aluminum can undergo $4X10^8$ cycles of this stress level before yielding occurs [9]. In order to provide a reasonable estimate of the fatigue life, the highest operation frequency, 100 Hz, is used in the calculation. Again, the maximum stress will only be present in the 5-20 Hz range. The system can operate for 1,111 hours ($4X10^6$ seconds) at full stroke before failure will occur. New flexures should be fabricated after six months of operation.

4.4.3 Finite Element Model

A finite element model of the system was developed using the modeling program Patran and analyzed by the evaluation program MSC/Nastran. The model contains a total of 5300 nodes. Each four-axis flexure is composed of 1500 solid elements. The platform is modelled as 96 plate elements specified as composites. The composite

Table 4.2: Finite Element Model: Natural Frequencies and Mode Shapes

Mode Number	Natural Frequency (in Hz)	Mode Shape
1	8.20	X and θ_y (combined rocking/lateral)
2	8.49	Z (first piston mode)
3	8.96	Y and θ_x (combined rocking/lateral)
4	26.83	θ_z (torsional)
2	385.53	Z (second piston mode)

plate properties are used to correctly model the aluminum honeycomb sandwich of the platform. This model includes three pure spring elements, one below each flexure which characterize the axial stiffness of the shaker suspensions (the shear mounts). These springs have a stiffness of 90 lbf/in in only one degree-of-freedom: Z. The model is constrained by using several single point constraints on select nodes on the bottom face of each four-axis flexure. These constraints allow motion only in Z and prohibit motion in X, Y, θ_x, θ_y, and θ_z. This accurately simulates the motion allowed by the shaker actuators. Figure 4-7 depicts the finite element model developed.

The model was first subjected to an acceleration load equal to gravity in the Z direction in order to ensure the model was accurate in estimating the weight of the system and the elements were connected properly. The model returned a weight of 36.6 lbs.

An eigenvalue analysis was then performed over a frequency range of 0 to 1000 Hz. This dynamic analysis determined the natural frequencies and mode shapes for the system. Table 4.2 summarizes the results of the dynamic analysis returned by Nastran.

Modes 1 and 3 represent the coupled lateral and angular modes described in Chapter 3. Mode 1 consists of lateral displacement in Y and rotation about the X axis. The lateral motion dominates this mode shape, as seen in Figure 4-8. The actual displacements of the mode shapes are exaggerated by the post-processor, Patran, in order to allow easy observation of the mode shape. Mode 3 represents a similar mode shape with combinations of displacement in X and rotation about the Y axis. Again,
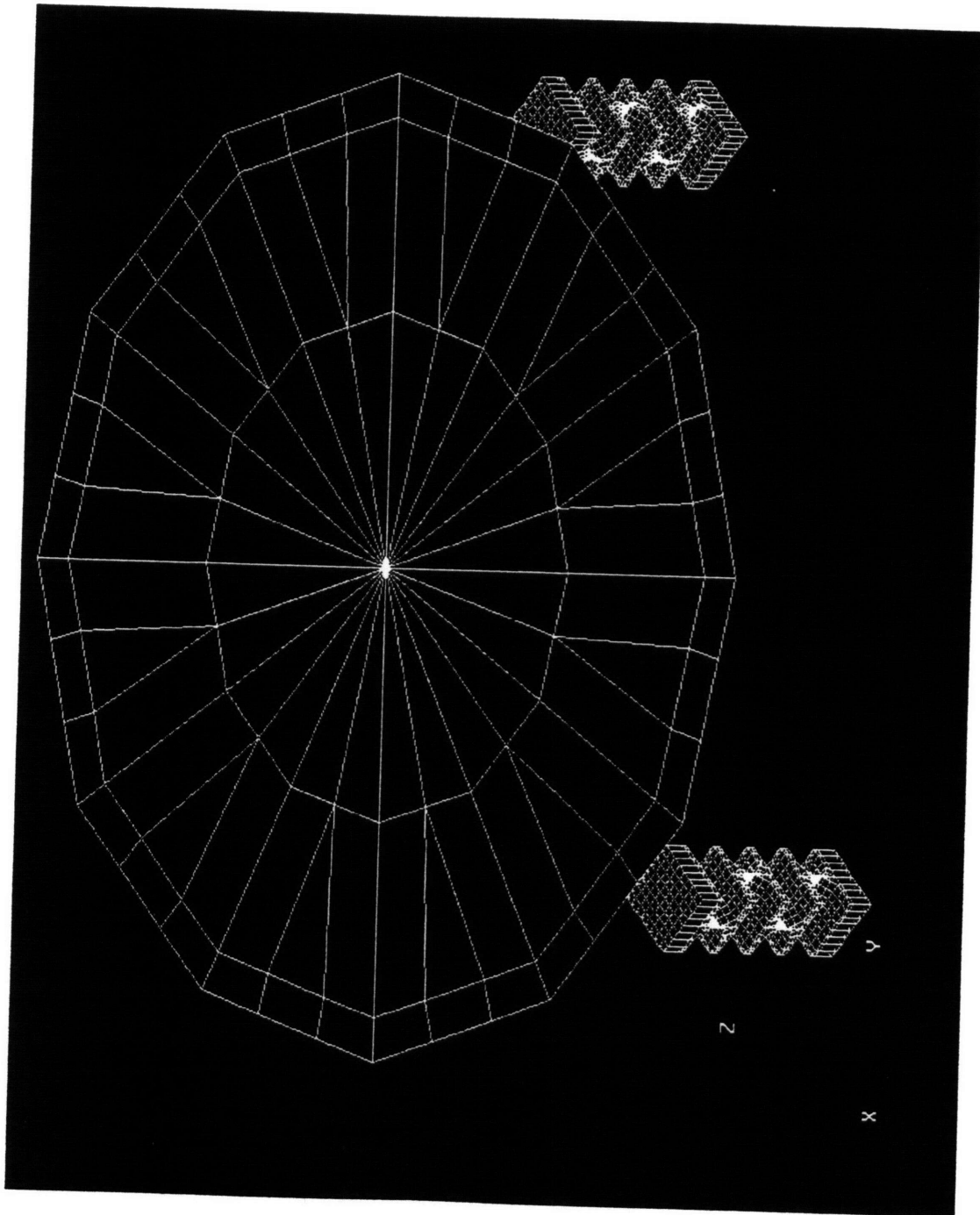
Figure 4-7: Finite Element Model of Flexures and Platform

the lateral motion dominates this mode shape, as seen in Figure 4-10. Although these modes will be uncontrolled, it will not pose a problem because they occur below the desired frequency operation range. Mode 2 represents the first piston mode of the system. The mass of the platform and flexures translates purely in the Z direction on the 90 lbf/in spring elements which model the shear mounts of the shakers. Figure 4-9 depicts this mode shape. Mode 4 (see Figure 4-11) exhibits torsional motion; the platform rotates about the Z axis. This mode shape will be a problem because the corresponding natural frequency lies within the desired operating frequency range. Finally, mode 5 shown in Figure 4-12 is another piston mode of the system. The platform translates in the Z direction, this time compressing the four-axis flexures. This mode also shows the vibrational platform is no longer completely rigid at these frequencies.
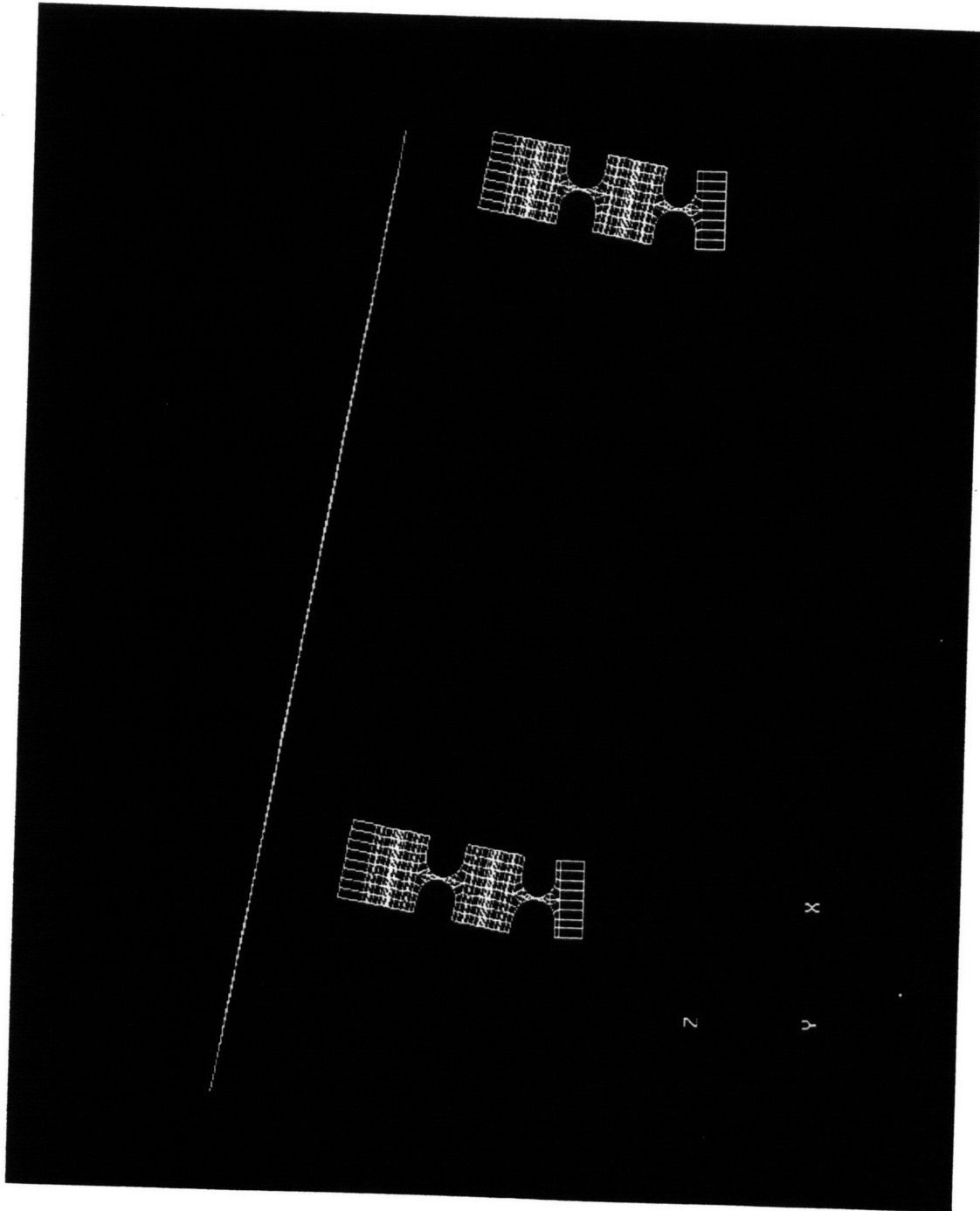
Figure 4-8: Mode 1 - 8.20 Hz
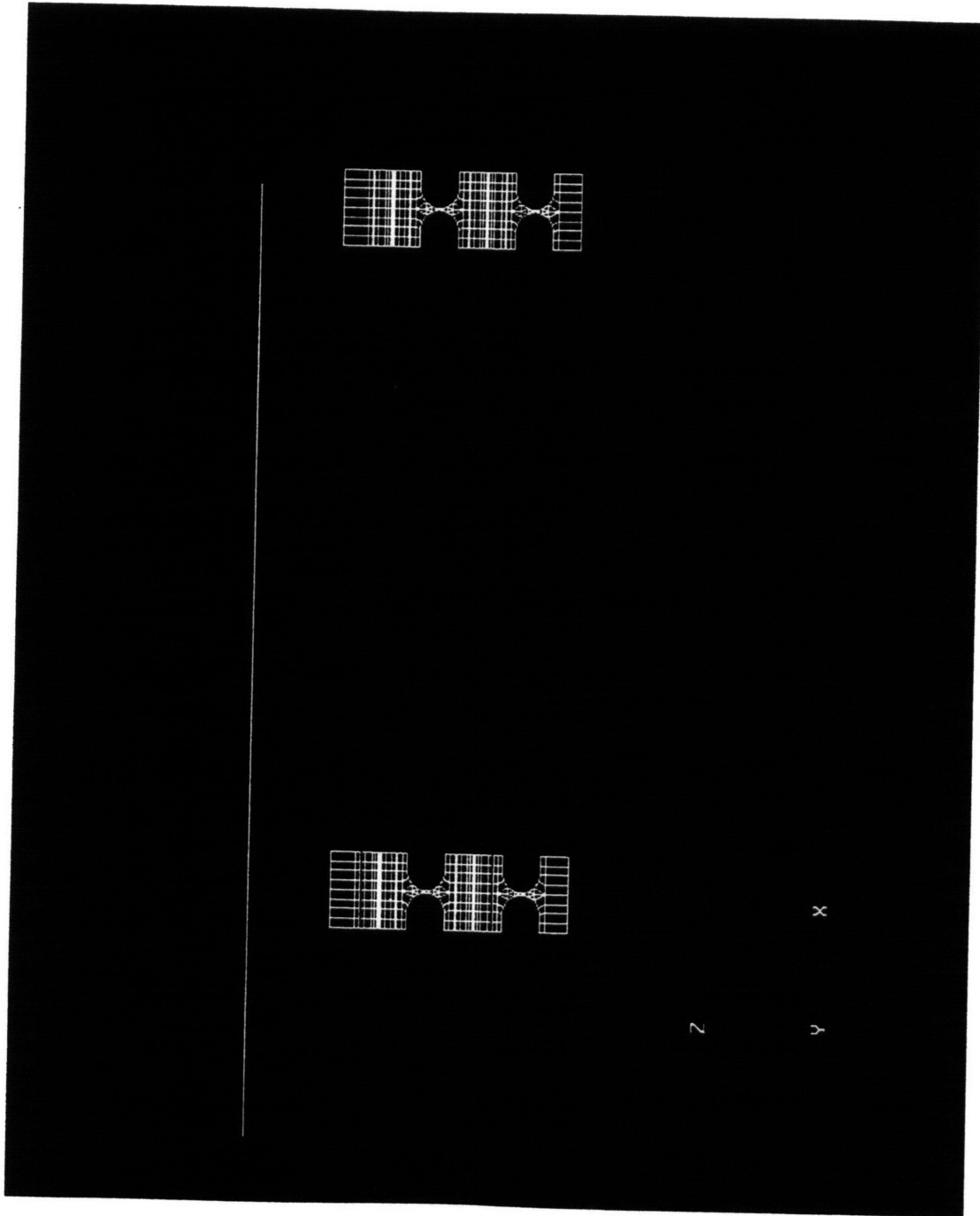
Figure 4-9: Mode 2 - 8.49 Hz
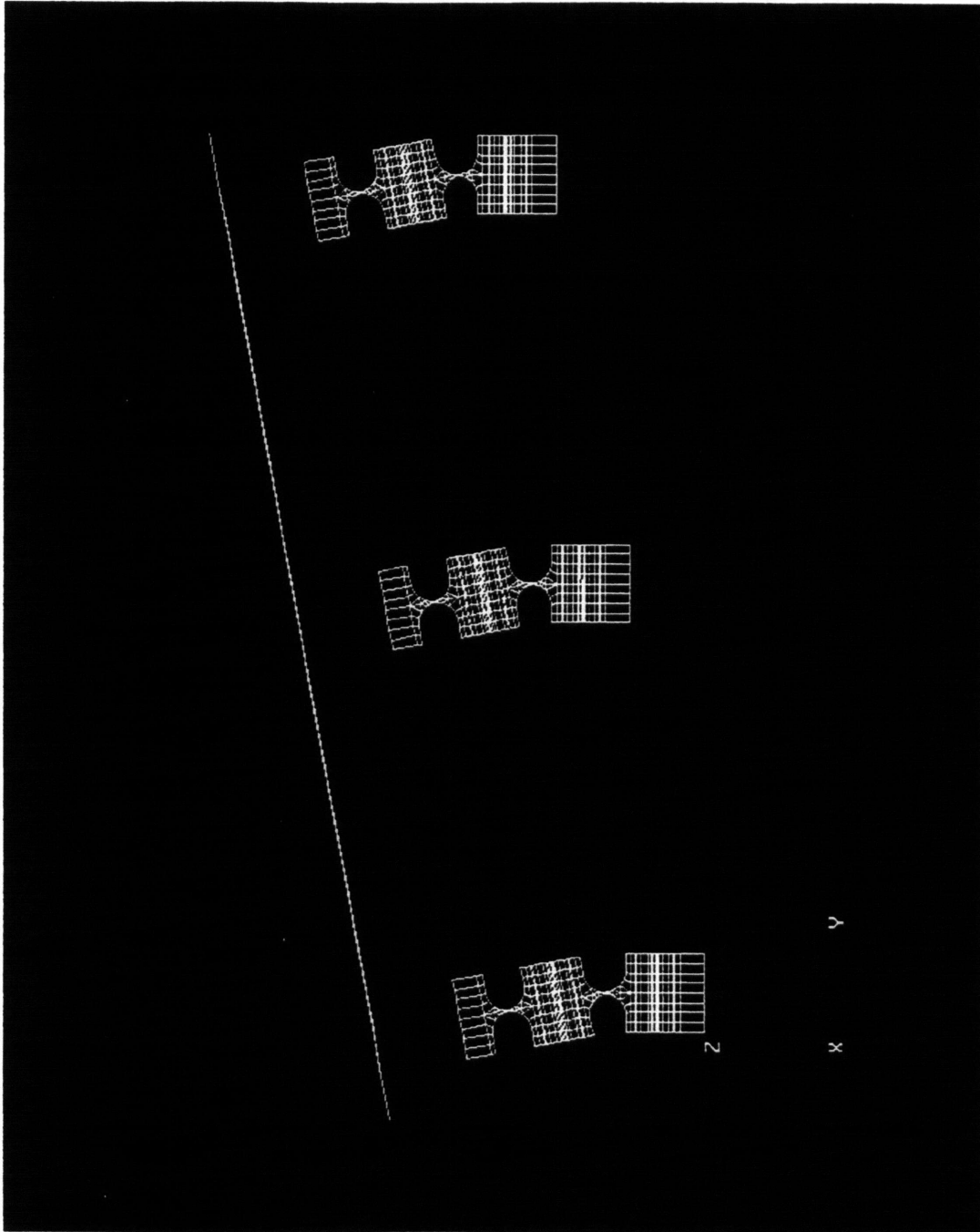
Figure 4-10: Mode 3 - 8.96 Hz
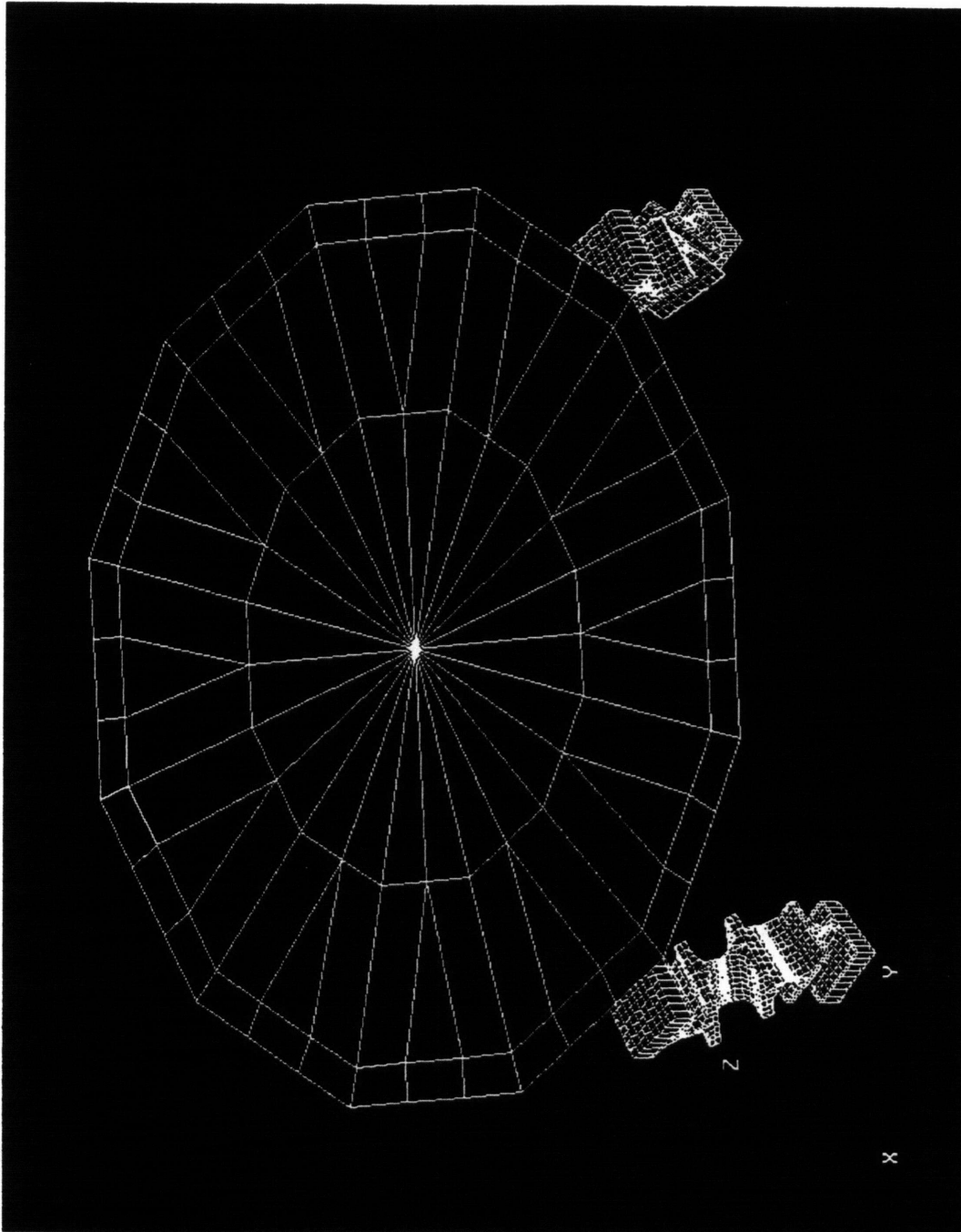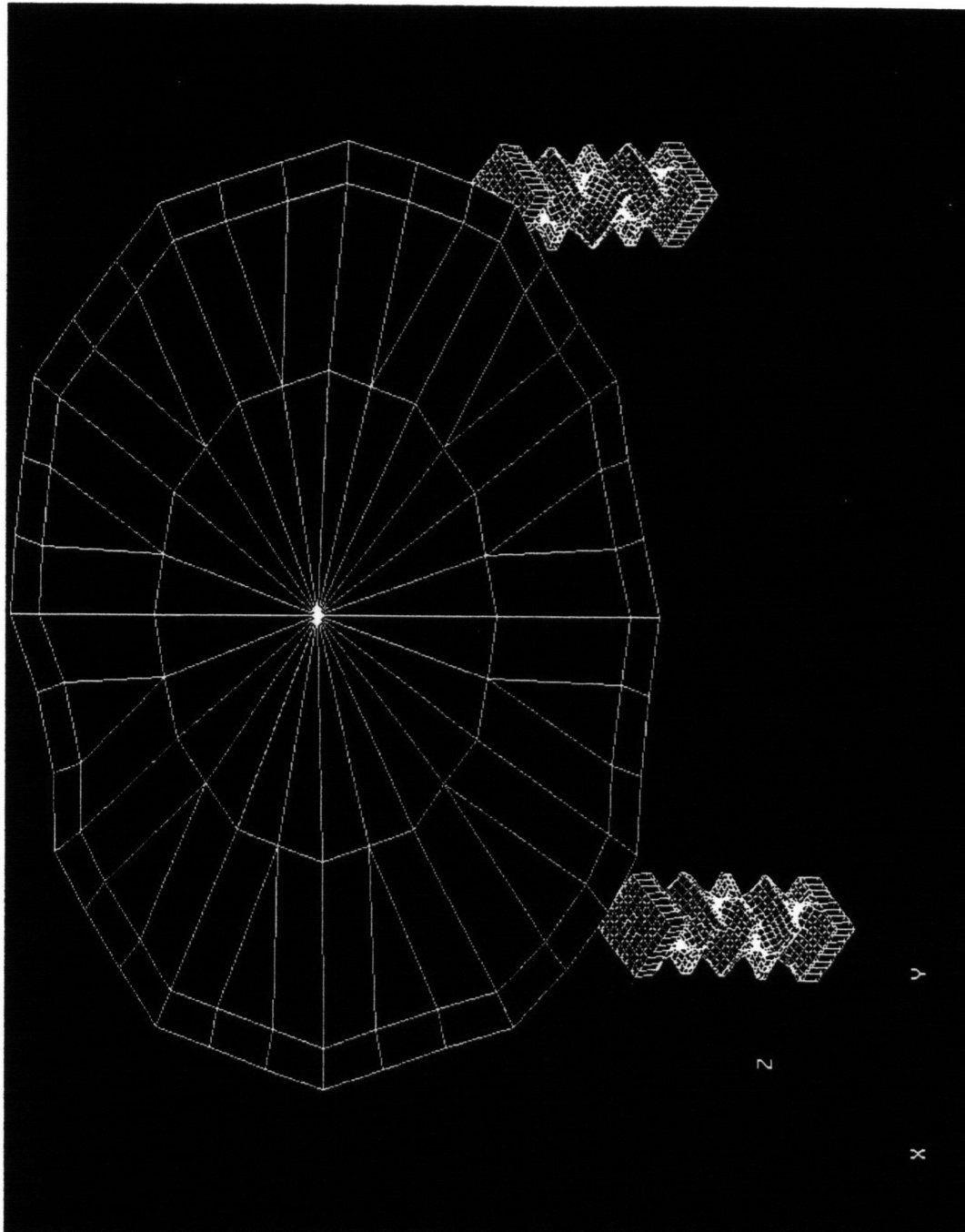
Figure 4-11: Mode 4 - 26.83 Hz

Figure 4-12: Mode 5 - 385.53 Hz

4.4.4 Experimental Performance

The frequency response of the system consisting of the platform, the three four-axis flexures, and the three shakers was determined experimentally using a Hewlett Packard 3562A dynamic analyzer. The system was operated open-loop without a controller. Furthermore, each degree-of-freedom was tested separately (single-input single-output testing). Figure 4-13 depicts the experimental setup. The dynamic analyzer was utilized to create a single sinusoidal voltage signal which, through the use of the coordinate transformation (beneath the dynamic analyzer), excited a single degree-of-freedom in the system.

The magnitude and phase for the transfer functions of θ_x, θ_y, and Z are shown in Figures 4-14, 4-15, 4-16, respectively. These transfer functions plot the ratio of output acceleration in m/s^2 or rad/s^2 and input voltage over a frequency range of 1 to 2000 Hz.

The 49.6 Hz natural frequency of a single bare shaker has moved to 17.8 Hz for the new system. This corresponds to a stiffness increase of a factor of 3 (three shakers) and a mass increase of a factor of 21 (mass of platform and flexures compared to mass of armature). The transfer functions in both θ_x and θ_y exhibit an antiresonance at approximately 12 Hz. The mode shape for this resonance is composed mainly of lateral motion (Y in the case of θ_x and X in the case of θ_y). This conclusion is supported by the finite element analysis which predicts a mode shape composed of primarily lateral motion at 8.20 and 8.96 Hz. This is not a shearing mode of a single-axis flexure (as calculated earlier), but rotation of the four-axis flexures with deflection of the shaker shear mounts, as shown in Figure 4-8. The higher resonances are the result of mode shapes of the platform itself and a piston mode of the flexures at 600 Hz. This piston mode is predicted by the finite element analysis at 385 Hz.

The torsional motion of the platform, rotation about the Z axis, is also important, since the payload should not be subjected to motion in this direction. The torsional motion was observed by using two accelerometers mounted 180 degrees apart on the platform facing in the X direction. The torsional mode of the system was observed to be approximately 30 Hz.
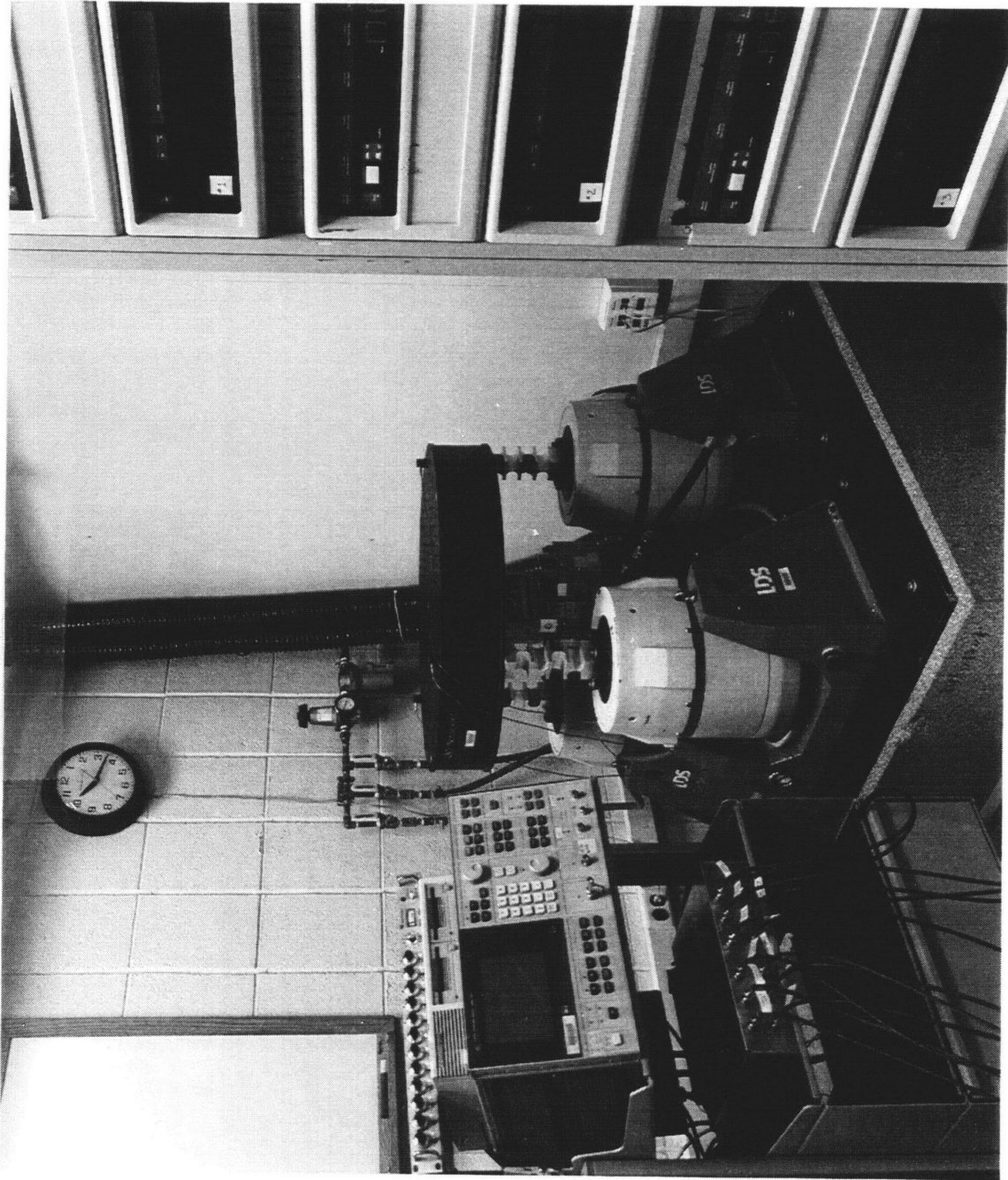
Figure 4-13: Experimental setup showing Signal Analyzer, Coordinate Transformation Circuit, Shaker System, and Power Amplifiers
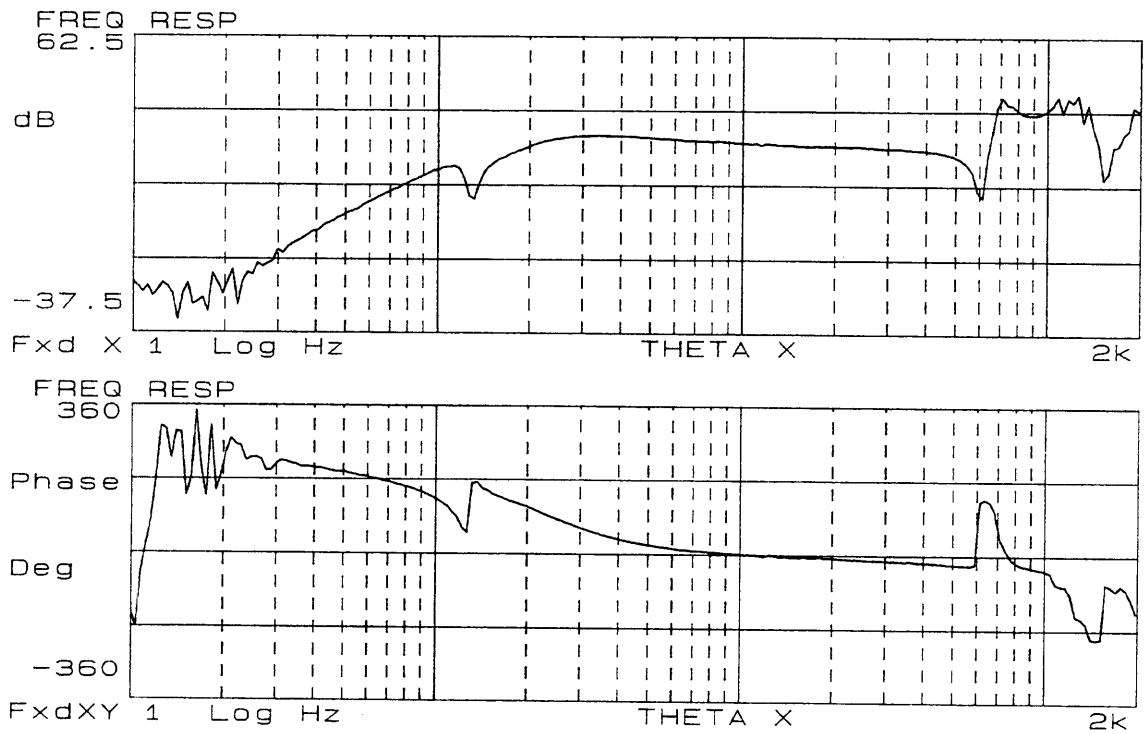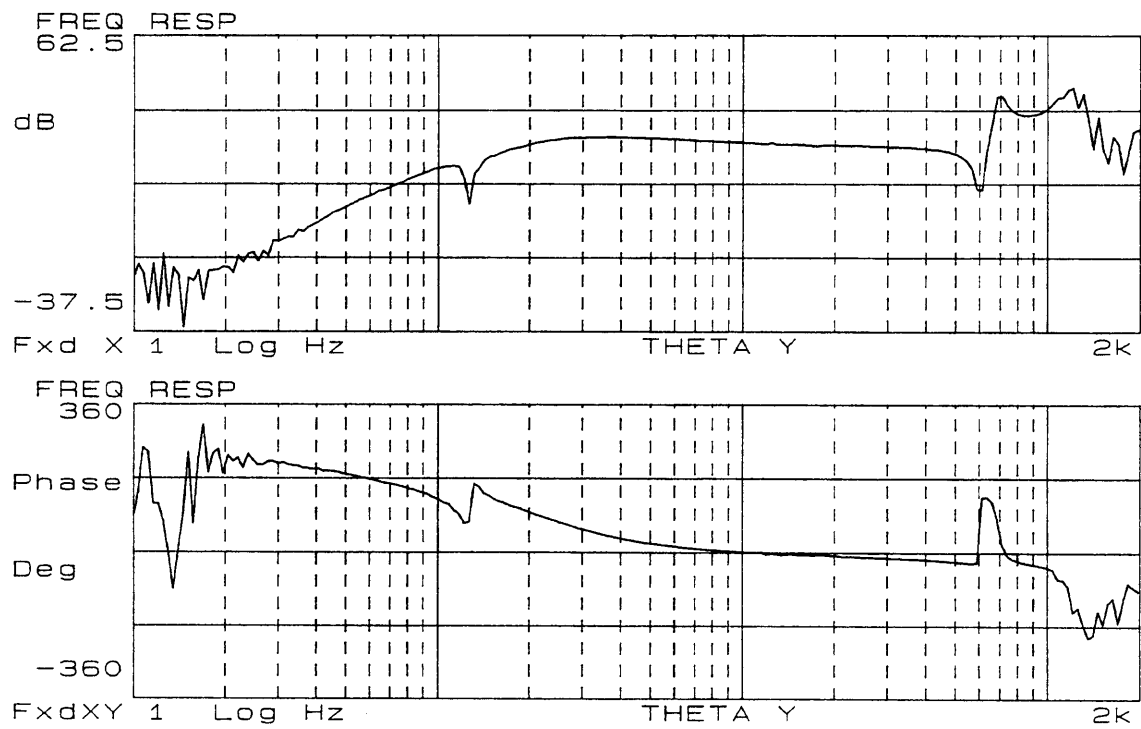
Figure 4-14: Magnitude and Phase of θ_x
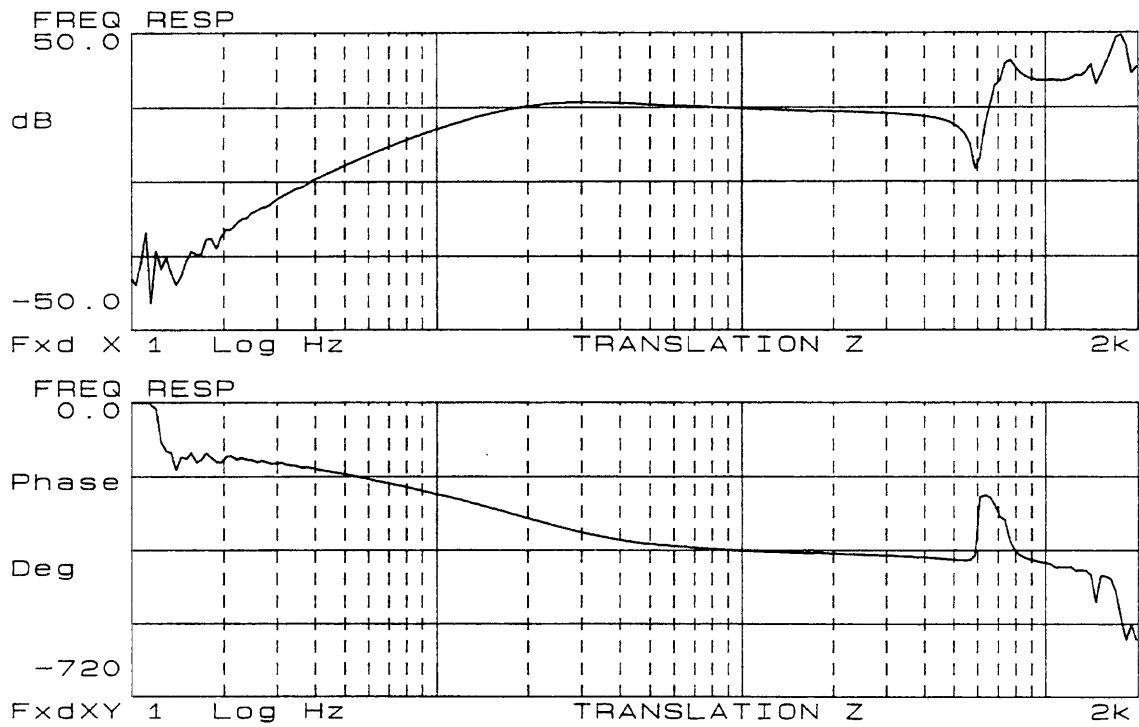

Figure 4-15: Magnitude and Phase of θ_y

Figure 4-16: Magnitude and Phase of Z

73

4.4.5   Alternative Solutions

Flexible Damped Struts

The flexible damped struts which were discussed in Chapter 2 introduced an important concept which provides an alternative approach to the shaker/platform coupling problem. The large steering mirror project utilized critically damped struts to attach the hydraulic actuators to the 2m mirror. This approach effectively damped the low-frequency lateral mode of the system. This approach could be used in the three degree-of-freedom vibration facility by adding damping to the system to produce a well-damped 12 Hz mode. This approach does not alter the location of the resonance. The goal of the vibration facility is to remove all undesired resonances from the frequency operation range. Consequently, a different approach which involves stiffening the system in the undesired degrees-of-freedom was taken.

Universal Joints (Flexures Produced by Ormond)

Ormond, Inc. of California offers an alternative to manufacturing the four-axis flexures. Ormond produces universal joints which allow rotation to occur in two orthogonal directions. The unique characteristic of these flexures can be seen in Figure 4-17: the rotation axes intersect. In the four-axis flexure design, the axes are separated by a vertical distance of 2.5 inches (see Appendix B). Two universal joints would be necessary to provide the four axes of rotation required for each shaker/platform coupling. These joints can be ordered with rotational stiffnesses varying from 0.2 in-lbf/degree to 13,500 in-lbf/degree with maximum angular displacements of ± 2 or ± 4 degrees. The deciding factor against the universal joints was the investment required, considering that six universal joints must be purchased each six month period due to fatigue life considerations. The manufactured flexures were much less expensive to produce.
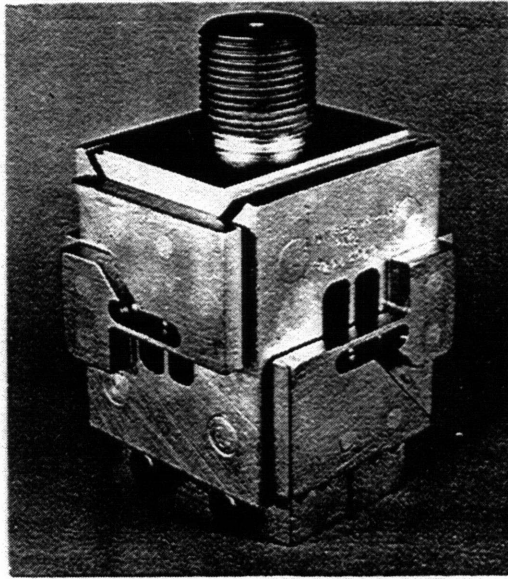
Figure 4-17: Universal Joints by Ormond

4.5 Center Post

4.5.1 Design Goals

As mentioned earlier, the system consisting of the three flexures and the mounting platform possesses a very low lateral stiffness due to the nature of the four-axis flexure design. This lateral stiffness results in a low frequency undamped resonance which appears in both the θ_x and θ_y transfer functions at approximately 12 Hz. The system also exhibits a torsional mode in θ_z at 30 Hz.

The center post was designed with two goals in mind. The first goal of the center post in general terms is to allow platform motion in the three controlled degrees-of-freedom (θ_x, θ_x, and Z) and constrain platform motion in the uncontrolled degrees-of-freedom (θ_z, X, and Y). The center post was designed to increase the lateral (X and Y) stiffness and torsional (θ_z) stiffness of the system in order to push the uncontrolled natural frequencies above the operating frequency range. The second goal of the center post is to constrain the point of rotation of the platform and place it as close as possible to the center of gravity of the payload.

4.5.2 Design of Center Post

The original concept of a center support developed because lateral stiffness could be added to the system at the center of the platform without increasing the rotational stiffness of the desired angular degrees-of-freedom. An attachment at the center of the platform would not require the same four-axis flexure design, which possesses low stiffness in X and Y. The center support will not need to allow for any lateral motion of the platform since it is defining the point of rotation for the system.

The design for the center post was borrowed from the suspension design of the electrodynamic shakers. The shakers meet all the required design characteristics but for the low rotational stiffness in θ_x and θ_y. The low rotational stiffness requirements were achieved with another flexure system. Each shaker allows vertical translation while retaining high lateral stiffness of 1300 lbf/in. The suspension system for a

single shaker consists of upper and lower guidance systems. The upper guidance system features four low-mass rollers mounted on polypropylene flexure strips and two shear mounts. The rollers and flexures allow the armature to translate in the Z direction and provide the high cross-axial stiffness. The lower guidance system features a linear bearing which constrains rotation in θ_x and θ_y.

This suspension system was duplicated by ordering spare rollers, polypropylene flexures, and shear mounts from Ling Dynamic Systems for the V556 shakers. The linear bearing from Ransom, Hoffman, and Pollard of England was replaced with a Nyliner nylon sleeve bearing from Thomson with a Case-hardened shaft. Finally, the armature and supporting structures were redesigned and fabricated at Lincoln Laboratory.

The center post suspension system supports a block of aluminum which has a .75 inch diameter Case-hardened steel shaft threaded into its base. The shaft slides through the nylon linear bearing. The entire suspension system is bolted to a 6 inch diameter, 24 inch tall cylinder of aluminum which is reamed to house the linear bearing.

In order to allow the platform to rotate in θ_x and θ_y, a new flexure configuration was designed. This flexure configuration couples the suspended aluminum block and the center of the platform. It is desirable place the center flexures as close as possible to the center of gravity of the payload, which will be some unknown distance above the upper surface of the platform. The point of rotation of the system, which should be at the center of gravity of the payload, is controlled by the placement of these flexures. If the point of rotation is below the center of gravity, the payload will be subjected to linear acceleration as well as angular acceleration with a pure angular acceleration input. However, due to time constraints, the flexures were attached beneath the lower surface of the platform. The point of rotation is 6.0 inches below the upper surface of the platform. If more time were available, the platform could be drilled to allow connection directly to the *upper* plate of the platform reducing the offset distance to 1.75 inches.

In addition, this flexure design features three separate flexures (one for θ_x and

two half-flexures for θ_y) which couple the suspended block to the platform via an intermediate member. This design allows the two rotation axes to intersect. The front view of the final design, which shows the suspension rollers, is shown in Figure 4-18. The side view of the final design, featuring the shear mounts, is shown in Figure 4-19. A photograph of the center post assembly appears in Figure 4-20. The complete drawings for each mechanical component of the system are collected in Appendix C.

The suspension rollers were designed to be preloaded so that all four rollers would be in contact with the roller support block and the armature. The preloading configuration, featuring the preload brackets, adjusting screws, and gage adjusting block is shown in Figure 4-21. The rollers must be preloaded prior to attachment of the flexure system. Preloading is accomplished by bolting the preload bracket to the armature and the roller support block. Tightening the preload adjusting screw forces the suspension block to move closer to the armature. A quarter turn was applied to the adjusting screws to achieve sufficient preloading.

Each flexure is machined from 17-4PH (H900) heat treated stainless steel and has a very narrow section which is .050 inches at the thinnest section. The two half flexures were designed to have the same rotational stiffness as the center flexure when added. The complete flexure assembly allows rotation about two orthogonal angular degrees-of-freedom with intersecting axes. A two-axis design was sufficient to allow the platform to rotate. Again, this flexure design was chosen because it eliminates friction entirely; the thin strip of steel acts as a torsional spring within its linear range of elasticity.
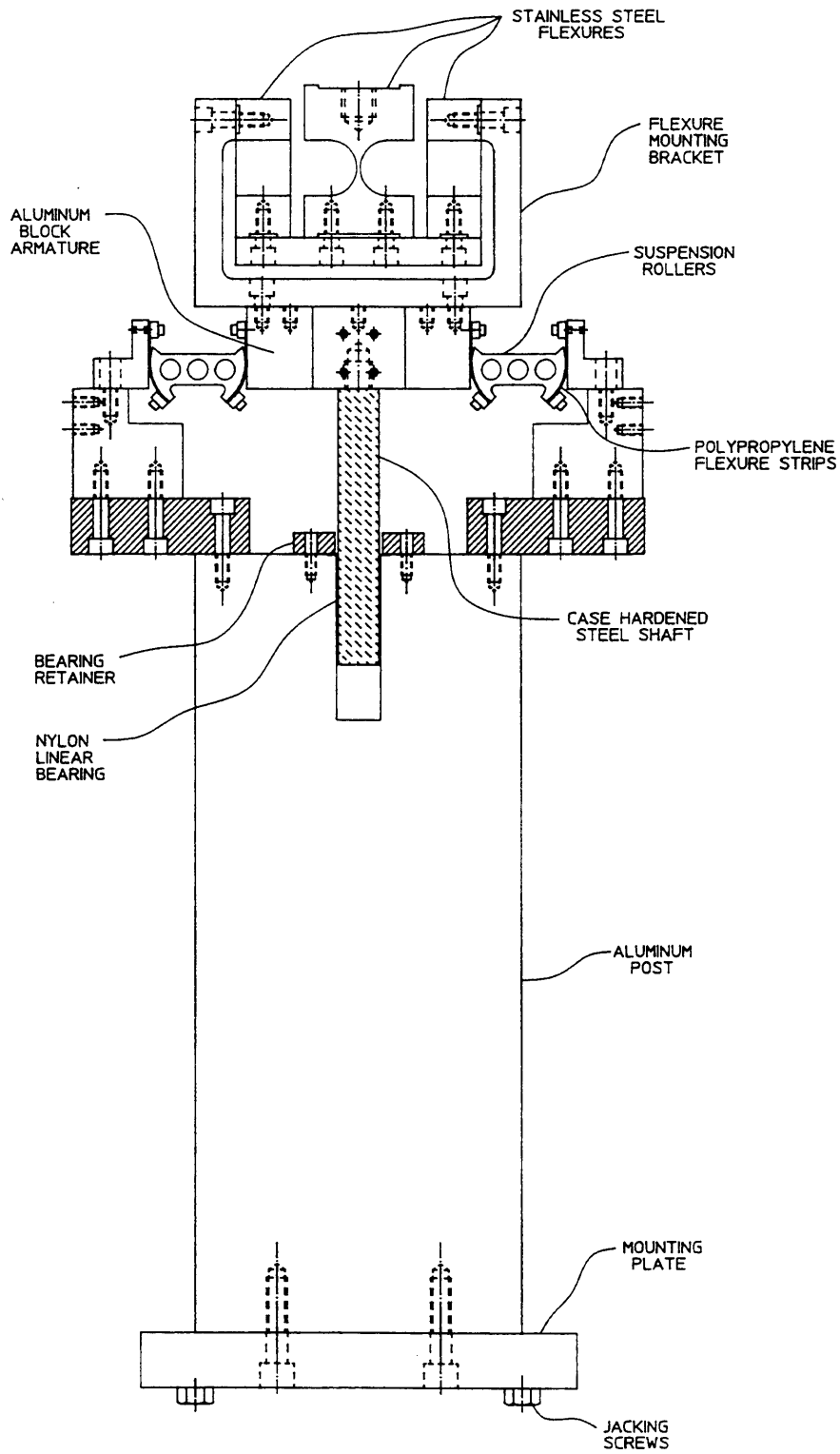
STAINLESS STEEL
FLEXURES

FLEXURE
MOUNTING
BRACKET

ALUMINUM
BLOCK
ARMATURE

SUSPENSION
ROLLERS

POLYPROPYLENE
FLEXURE STRIPS

CASE HARDENED
STEEL SHAFT

BEARING
RETAINER

NYLON
LINEAR
BEARING

ALUMINUM
POST

MOUNTING
PLATE

JACKING
SCREWS

Figure 4-18: Assembly Drawing of Center Post - Front View

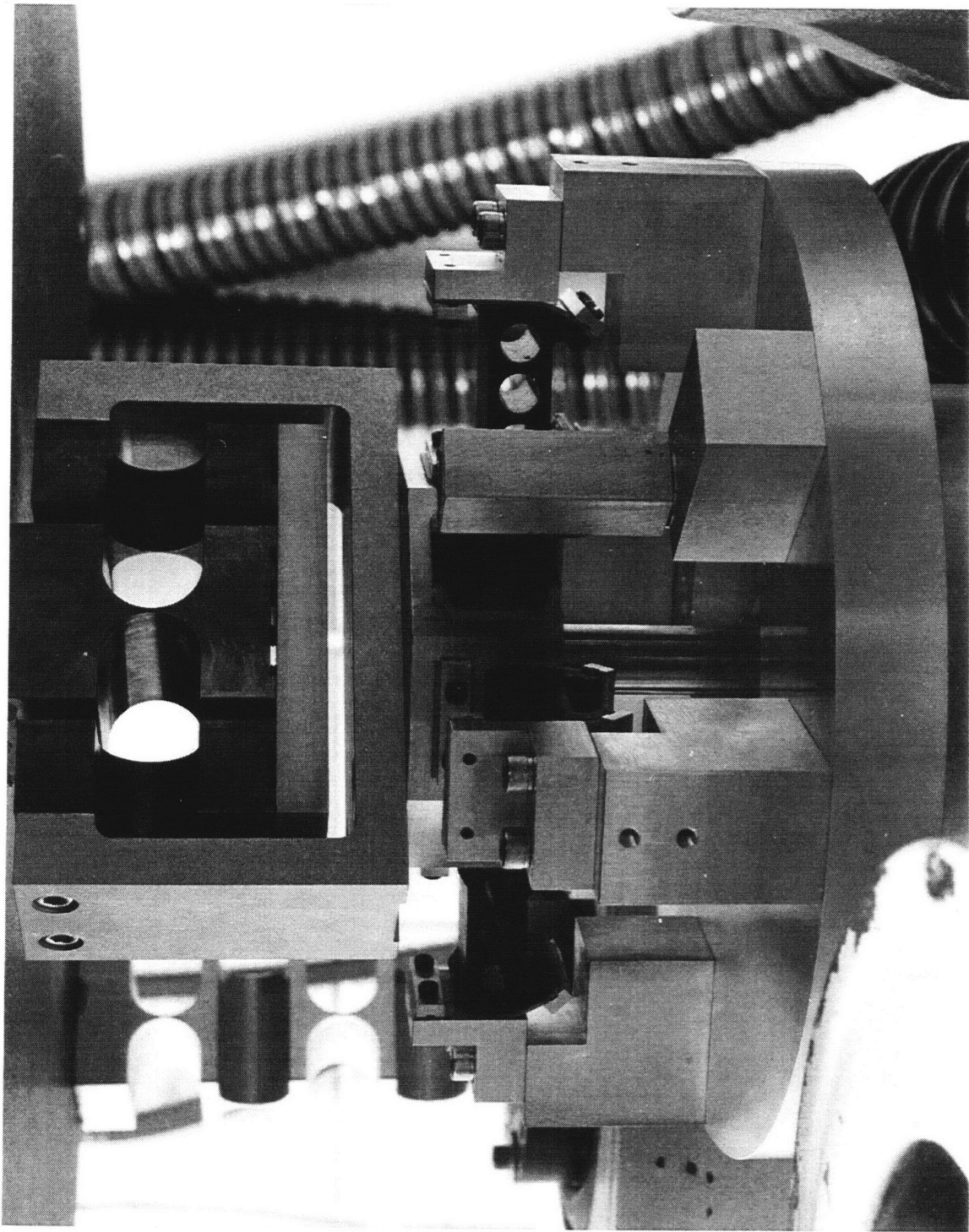79
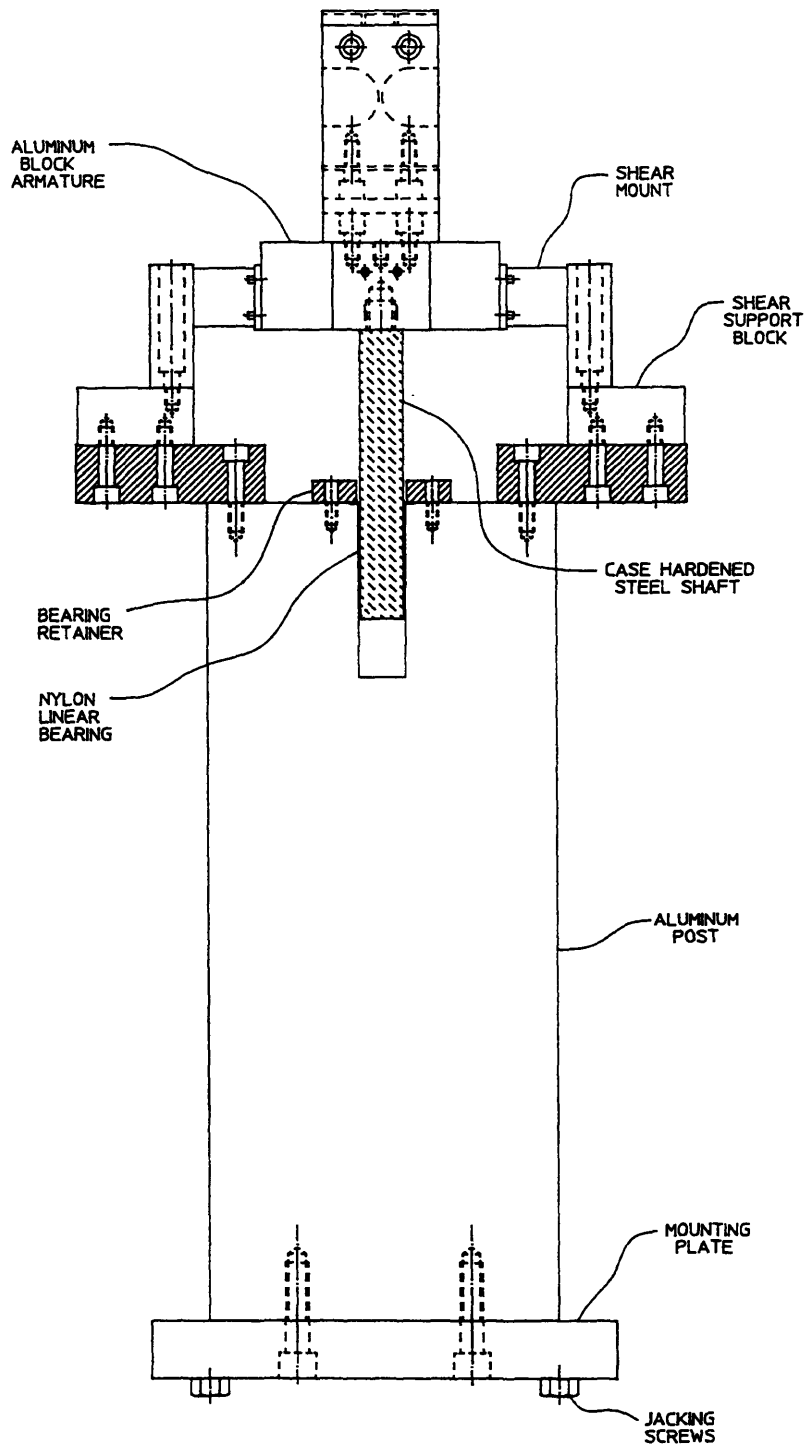
Figure 4-19: Assembly Drawing of Center Post - Side View

ALUMINUM
BLOCK
ARMATURE

SHEAR
MOUNT

SHEAR
SUPPORT
BLOCK

CASE HARDENED
STEEL SHAFT

BEARING
RETAINER

NYLON
LINEAR
BEARING

ALUMINUM
POST

MOUNTING
PLATE

JACKING
SCREWS

Figure 4-20: Photograph of Center Post Assembly

PRELOAD
BRACKET

GAGE
ADJUSTING
BLOCK

PRELOAD
ADJUSTING
SCREW
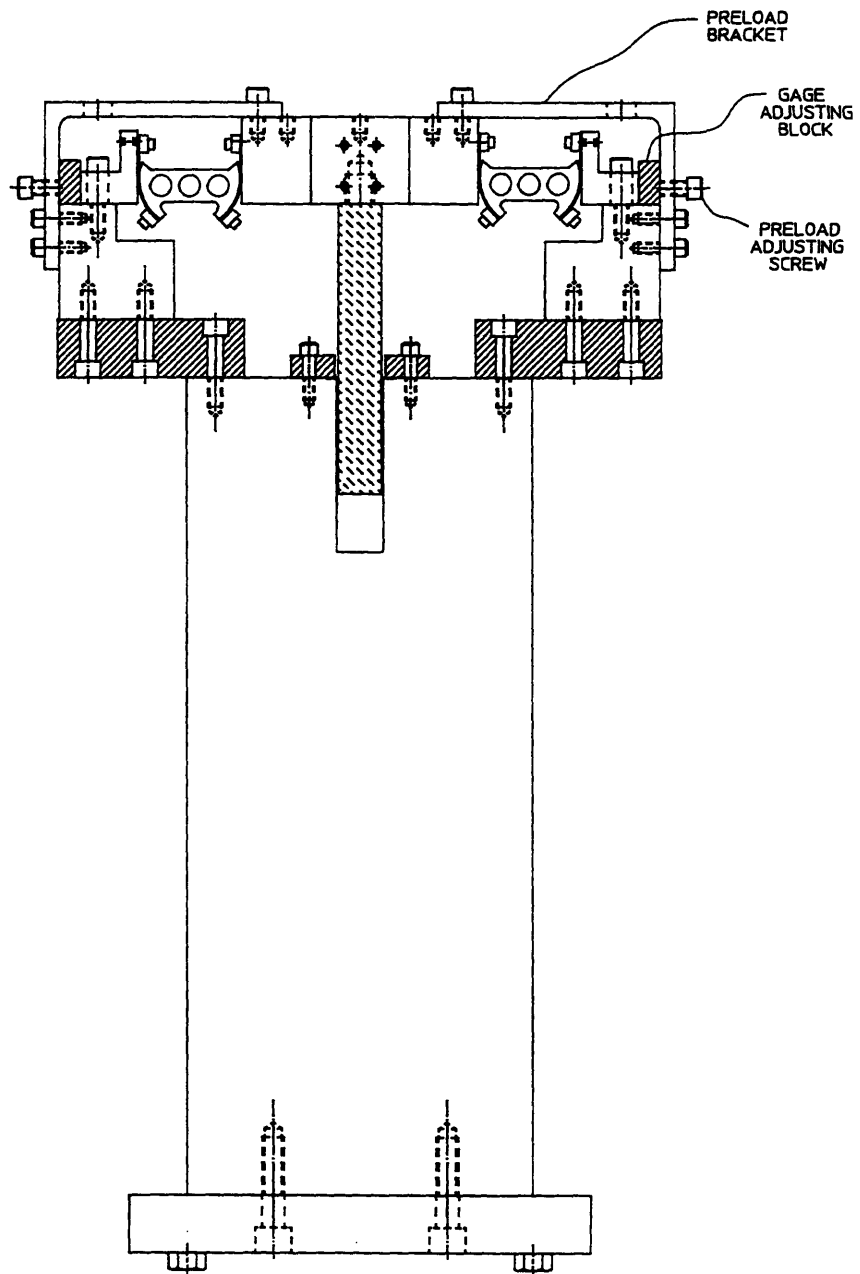
Figure 4-21: Preloading Configuration of Center Post Suspension

Fundamental Rocking Modes

The rotational stiffness of flexures for the center post follows Equation 4.4. The center single-axis flexure composed of stainless steel with R of 0.5 inches, b of 2 inches, and t of 0.05 inches was designed to have rotational stiffnesses of 58.5 in-lbf/degree. Each half flexure has the same dimensions of the center flexure except for half the depth. These dimensions correspond to a rotational stiffness of 29.3 in-lbf/degree. Again, in order to determine the rough location of the natural frequencies of the combined platform/flexure/center post system, this rotational stiffness was used in a simple model consisting of the rotational inertia of the platform, J, on a torsional spring, $3k_{aluminumflexures} + k_{steelflexure}$ (for four flexures in parallel). The corresponding natural frequency for this system follows Equation 4.9. The natural frequency for the rocking mode of this system is 6.43 Hz. The mode shape of the actual system which is dominated by motion in θ_x

will appear at approximately this frequency. This analysis will also hold for the mode shape dominated by motion in θ_y. The mode shapes do not consist entirely of pure rotation as this simple mass/spring model suggests, but are comprised of motion in many degrees-of-freedom, as shown by the more detailed model in Chapter 3.

The natural frequencies for these simplified rocking modes are consequently extremely low frequency and were designed to appear below the desirable frequency operation range (10-100 Hz).

Fundamental Piston Mode

An expression for the fundamental piston mode (displacement purely in Z) for a single-axis steel flexure follows Equation 4.8. The axial stiffness of a single-axis flexure with the same dimensions as the last case is $8.1 X 10^6$ lbf/in. The corresponding piston mode natural frequency for a simple model consisting of three four-axis aluminum flexures and two steel single-axis flexures (in parallel) $3k_{aluminumflexures}/4 + 2k_{steelflexure}$ attached to a weight representing the mounting platform follows Equation 4.9. $f_n = 2207$ Hz. This piston mode natural frequency is well above the desired frequency operation range.

83

Fundamental Shearing Mode

The fundamental shearing mode for a single-axis steel flexure can be determined from the shear stiffness, Equation 4.10. The Shear Modulus for 17-4PH (H900) steel $10.6X10^6$ psi. A single flexure possesses a shearing stiffness of $2.88X10^6$ lbf/in. The fundamental shearing mode in both X and Y for a system consisting of three four-axis aluminum flexures and two single-axis steel flexures (in parallel) $3k_{aluminumflexures}/4$ $+ 2k_{steelflexure}$ and a lumped mass representing the platform appears at 1321.2 Hz. The system should exhibit a mode which will be dominated by shearing motion at this frequency. This natural frequency lies well outside the desired operation range.

Maximum Stress

The maximum stress developed in the steel flexures occurs as the platform rotates through an angle of ±12 mrad. The calculation for the maximum stress follows Equation 4.11 and was found to be 45,000 psi (a factor of three more than the aluminum flexures).

Fatigue Life Data

The main reason for fabricating the new flexure configuration from stainless steel is to improve the fatigue life. It has been proven empirically that 17-4PH (H900) stainless steel can undergo an infinite number cycles of this stress level before yielding occurs (runout on the S/N curve) [9]. The method for determining the fatigue life of the aluminum flexures was followed again for this calculation. The steel flexures can operate ideally for an unlimited time at full stroke before failure will occur.

4.5.3 Experimental Performance

The frequency response of the system consisting of the platform, the three four-axis flexures, the center post, and the three shakers was determined experimentally using a Hewlett Packard 3562A dynamic analyzer. The system was again operated open-loop with no controller. The magnitude and phase for the transfer functions of θ_x, θ_y, and Z are shown in Figures 4-22, 4-23, 4-24, respectively. These transfer functions represent the ratio of output acceleration in m/s^2 or rad/s^2 and input voltage.
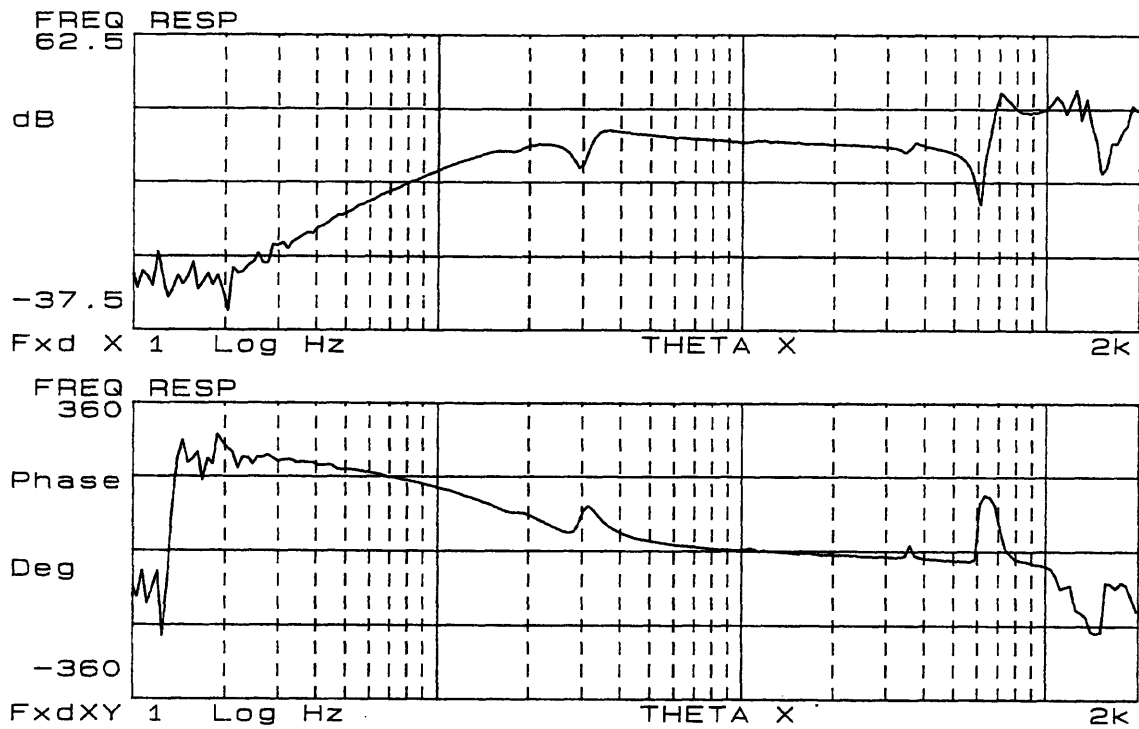
84

Figure 4-22: Magnitude and Phase of θ_x with Center Post
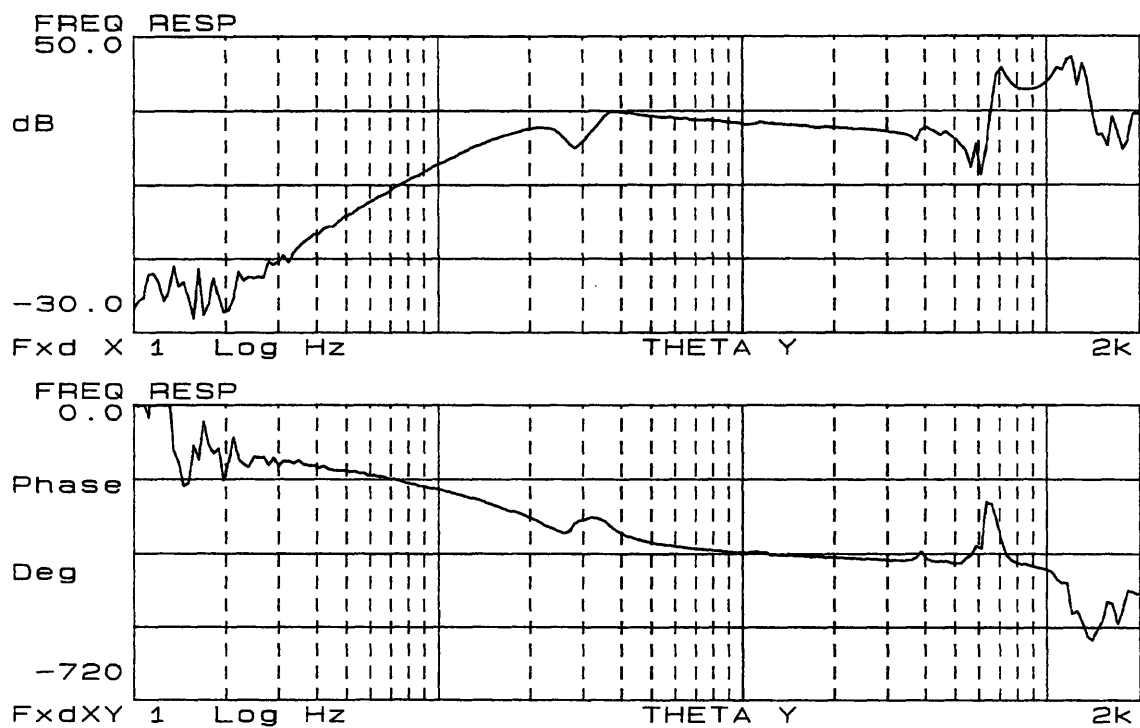

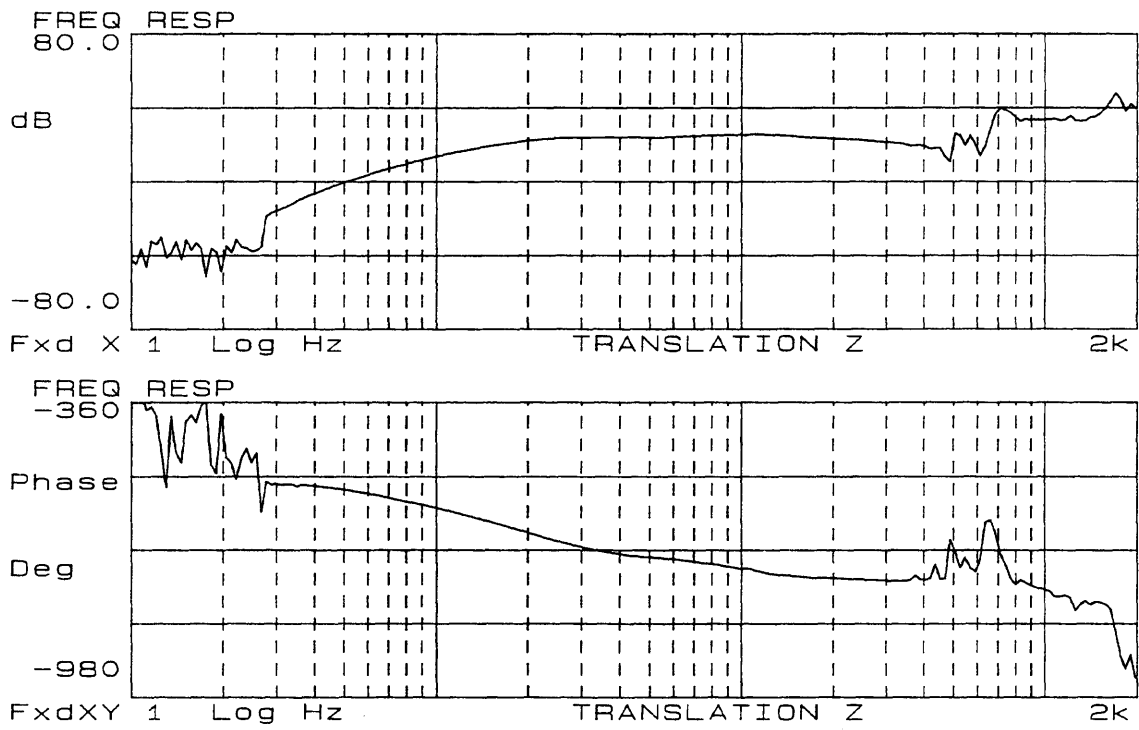Figure 4-23: Magnitude and Phase of θ_y with Center Post

85

Figure 4-24: Magnitude and Phase of Z with Center Post

The transfer functions with the post are very similar to the previous transfer functions. The major difference can be clearly seen: the 12 Hz resonance has been replaced by a 24 Hz resonance. This 24 Hz resonance was not predicted by the hand calculations or by the finite element model. Great care was taken to determine the mode shape for this resonance; accelerometers were mounted in different locations and orientations to determine the ratio of lateral to vertical acceleration. This 24 Hz resonance was experimentally determined to be a mode shape consisted of mainly angular displacements (θ_x for the θ_x transfer function and θ_y for the θ_y transfer function).

This led to the conclusion that the center flexure system actually possesses a much higher rotational stiffness than was originally predicted, since the rocking mode natural frequency was predicted at 6.43 Hz. The stiffness of the center flexures was then determined experimentally. The three four-axis flexures were removed from the system, leaving the platform supported solely by the center post. Wooden blocks were used to prevent the center suspension from bearing the weight of the platform (preventing damage to the shear supports of the center suspension). The platform was essentially constrained to rotation about the X and Y axes with the rotational stiffnesses provided by the center flexures. Static loads were placed on the platform a distance away from the center and the resulting displacement of the platform was measured with a micrometer mounted on a spring platform. The experimental setup is shown in Figure 4-25.

The rotational stiffness, k_θ was determined from the relation:

$$k_\theta = \frac{\tau}{\theta} = \frac{mgr}{sin^{-1}\left(\frac{x}{R}\right)} \qquad (4.12)$$

Where mg is the weight of the applied mass, r is the radius at which the mass is placed, x is the measured vertical displacement of the platform, and R is the radius of the platform. From this technique, the rotational stiffness, k_{θ_x} was found to be 44.3 inlbf/degree, and k_{θ_y} was found to be 42.4 inlbf/degree. This stiffness corresponds to fundamental rocking modes at 3.96 Hz for θ_x and 3.87 Hz for θ_y.
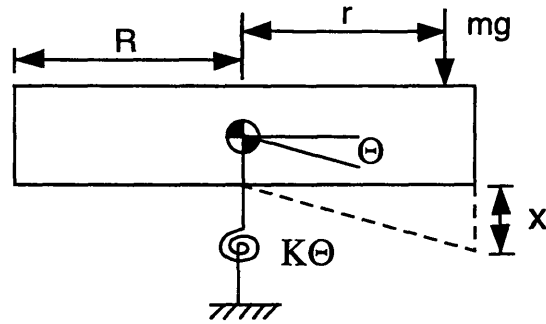
Figure 4-25: Experimental Determination of the Center Flexure Rotational Stiffnesses

This result was verified using a different technique involving exciting the mode shape with a modal hammer and using an accelerometer, determine the resulting natural frequency. This method resulted in fundamental rocking modes at 3.28 Hz for θ_x and 3.43 Hz for θ_y. These results closely match the expected rocking mode natural frequencies of 4.55 Hz (k of 58.5 lbf/in) and confirm the predicted rotational stiffnesses of the center flexures was accurate.

However, these results do not coincide with the experimental results of the previous system which included the shakers and the four-axis flexures. Either the shakers or the four-axis flexures are providing significant additional rotational stiffness to the system. The flexures undoubtedly add to the rotational stiffness of the system, but their contribution will roughly double the stiffness. The answer lies in looking at a simple model of a rotational inertia J which is allowed to rotate about a fixed point which has an associated rotational stiffness k_t (the center flexures) and has a spring k located a distance a from the point of rotation (see Figure 4-26).

The corresponding natural frequency for this system is:

$$f_n = \frac{1}{2\pi}[\frac{ka^2 + k_t}{J}]$$ (4.13)

The spring k models the axial stiffness of the shear supports of the shakers, which

88
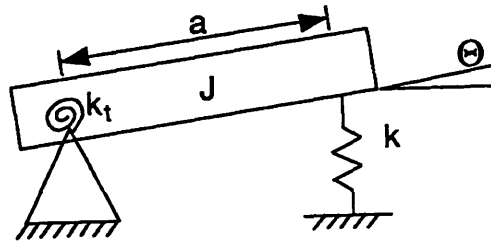
Figure 4-26: Rocking Mode Model

is listed as 90 lbf/in [4]. The experimental value for this stiffness was found to be 562 lbf/in. This stiffness was calculated from the bare table transfer function, by solving for the stiffness of the shaker using the mass of the armature and the experimental natural frequency. The rocking mode natural frequency predicted by this model using the experimentally determined shear support stiffness is 27.7 Hz, which is near the experimental result of 24 Hz.

This rocking mode was designed to be below the desired frequency operation range (below 10 Hz). From Equation 4.13 it is clear that the equivalent stiffness term is dominated by the stiffness provided by the shear mounts. In order to place this natural frequency in the desired location, it is necessary to replace the shear supports of the shakers with shear supports of lower stiffness values (approximately 20 lbf/in).

The center post was also intended to increase the rotational stiffness $k_{\theta z}$. However, due to the design constraints of the center post, rotational stiffness could not be added. The torsional mode of the system was observed to be relatively unchanged at approximately 30 Hz. A design which will stiffen $k_{\theta z}$ is offered in the Chapter 6.

4.5.4 Alternative Solutions

Magnetic Bearings

The problems which the center post was designed to solve mainly focus upon adding stiffness to the system to alter the location of the uncontrolled modes and placing the point of rotation of the system. Another possible approach involves in-
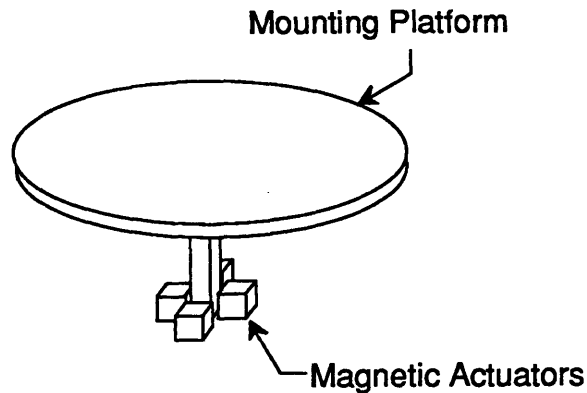
Figure 4-27: Magnetic Bearing Actuator Design

corporating more actuators into the system to control the previously uncontrolled resonances. This approach can be accomplished by applying magnetic bearing research. Two sets of two magnetic actuators working in opposition could be added to the system to control motion of the platform in the X and Y directions. A possible design is shown in Figure 4-27.

This configuration would allow the operator to adjust the point of rotation of the system, thus ensuring it matches the center of gravity of any payload.

A good source of magnetic bearing research can be found in [Trumper].

Bipod Leg Design

The research conducted by Gregory Loney on the High Bandwidth Steering Mirror mentioned in Chapter 2 presents another approach of adding stiffness to the system: bipod legs [6]. The bipod legs possess a high axial stiffness, but low bending stiffness. They were used to constrain the small mirror in all directions except for two orthogonal angular degrees-of-freedom. This design could be applied to the vibration test facility if the system were limited to two angular degrees-of-freedom. A possible design is shown in Figure 4-28. The bipod legs cannot allow the vertical travel in the Z direction to occur; considerable force would be required to stretch the bipod legs as the platform translates. Furthermore, this design would be difficult to implement
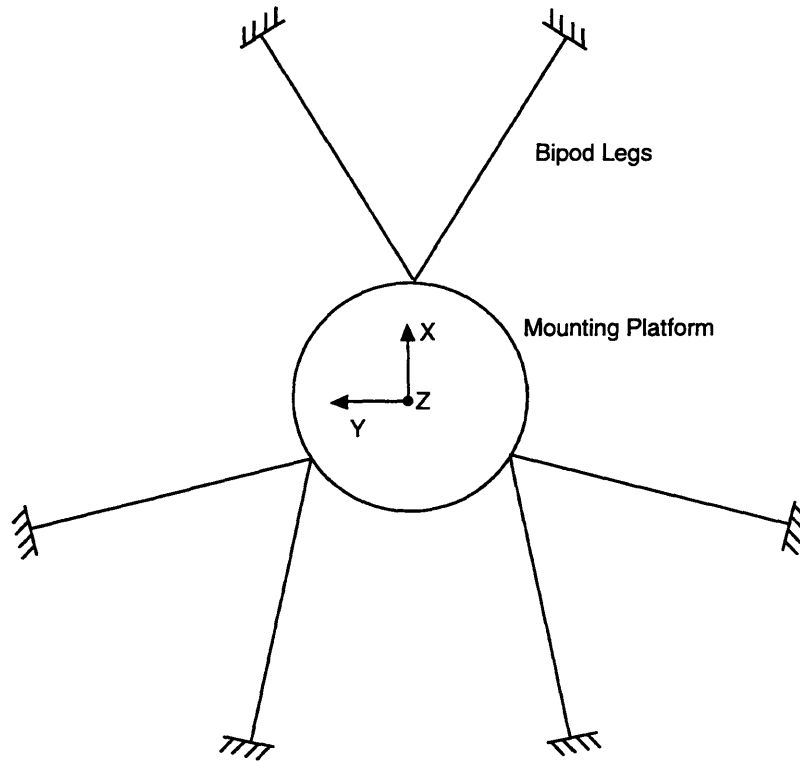
Figure 4-28: Bipod Leg Design

with the current constraints upon lab space. This design retains one major advantage: high torsional θ_z stiffness.

Air Bearings

Ideally, the linear bearing in the center post should have no friction. The best possible linear bearing for this application is a linear air bearing. The low viscosity of air leads to low friction losses and essentially zero wear over time. An excellent guide to gas bearings can be found in [Stout]. The new design would replace the current nylon linear bearing with the air bearing.

This approach was not followed for two reasons (both very practical): the large investment in time and money necessary; and the nylon sleeve bearing produced very

good results with small expense. The nylon sleeve bearing must be replaced fairly often, but at under 2 dollars per bearing, this design proved to be very economical.

Shaker Design

The suspension system of a smaller shaker from Ling Dynamic Systems (Model 400) provides another interesting possibility. The suspension system, like the one for model V556, features upper and lower guidance system. However, in this model, the low mass rollers and linear bearing are replaced by lower and upper flexure systems which are bonded to the moving coil assembly [5]. The flexures, as shown in Figure 4-29 as 3, allow the armature to translate vertically and constrain the armature from rotation and translating laterally.

This approach was not considered feasible for the system because of the greater travel allowed by the V556 shakers. The system can translate $\pm$ .125 inches. The suspension system of the smaller shakers were not designed for that extensive travel. Further, I believe modifying the design to allow greater travel would sacrifice lateral stiffness.

4.6   Accelerometers

As mentioned earlier, three linear, single axis accelerometers were used in the development of the vibration test facility. The accelerometers, Model 336B04 from PCB Piezotronics provide 100mV/g over a frequency range of 10 to 2000 Hz (I have found these limits to be very coneservative) with the first natural frequency at 9 KHz. The accelerometers can detect $\pm$50 g.
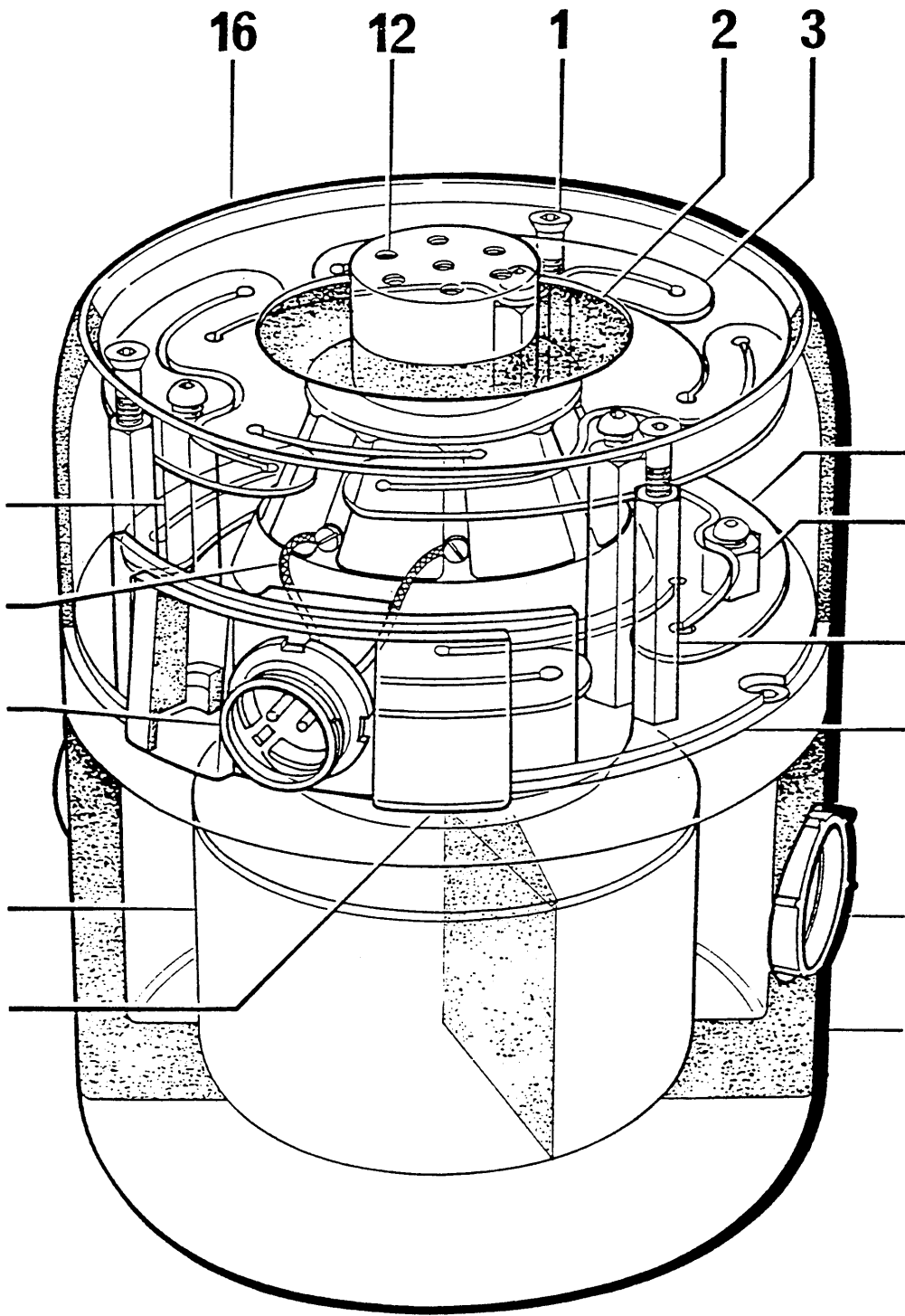
Figure 4-29: L.D.S. Model 400 Series Shaker

Chapter 5

Controller Results

This chapter describes the results obtained when utilizing the I*star controller in the loop. The ultimate goal of the mechanical designs earlier described is twofold: 1) allow a payload to be subjected to the desired accelerations in θ_x, θ_y and Z; and 2) ensure the system can be controlled using only three actuators (the shakers). The I*star computer was incorporated into the loop to determine if these goals could be met with the current mechanical setup. In the following tests, the three actuated degrees-of-freedom were tested simultaneously, as three single-input single-output decoupled plants.

5.1 I*star Performance with the Center Post

The following results were recorded with the center post design in operation. A photograph of the I*star computer used in the experiment is shown in Figure 5-1. The I*star computer uses estimates of the plant transfer function to shape the input to the plant to achieve the desired power spectral density output curves. A plot of the transfer function of θ_y as seen by the I*star controller is shown in Figure 5-2. When compared to Figure 4-23 we can see that the I*star controller steeply rolls off the transfer function at approximately 190 Hz. Since the controller uses this transfer function shape the input, the true output P.S.D. will be affected, as will be shown shortly. The tests were conducted over a frequency range of 10 to 200 Hz, a larger

range than the desired (10 to 100 Hz). A desired output P.S.D. curve for each degree-of-freedom was defined over this frequency range (as shown in the following response plots).

Plots of the output power spectral density curves from the I*star controller for θ_x, θ_y and Z are shown in Figures 5-3, 5-4, and 5-5 respectively. The data are plotted in g^2/Hz versus a frequency range on a log scale of 10 to 200 Hz. The three lines in each plot represent the +1 dB upper bound, the desired P.S.D. level, and the -1 dB lower bound.

The PSD curves for θ_x and θ_y exhibit irregular spikes near the new 24 Hz rocking mode resonances. The I*star controller, using the inverted plant transfer function, must cancel the effect of this resonance, but it cannot exactly match the location of the resonance, thus causing irregular spikes in the output. These spikes, however, are within ± 1 dB of the desired level.

The I*star computer requires approximately 5 minutes of operation time to accurately track all three input P.S.D. curves. The I*star computer controls the $\theta_x$ and θ_y transfer functions well initially, but does not control the Z transfer function well for approximately 5 minutes. The data was recorded after approximately 10 minutes of three-axis operation.

In order to determine the true output P.S.D., a Hewlett Packard 3562A dynamic analyzer was used to record the output P.S.D. controlled by the I*star computer. Figures 5-6, 5-7, and 5-8 show the data recorded on the dynamic signal analyzer during the previous test.

Some of the noise of the previous data recorded on the I*star computer has been eliminated by using the dynamic signal analyzer. More importantly, however, the P.S.D. response deviates from the desired response greatly beginning at 190 Hz. This is due to the inaccurate transfer functions captured by the I*star computer, as shown in Figure 5-2. The I*star computer increases the input in the range 190-200 Hz to counteract the steep rolloff which it sees. The data from the dynamic analyzer shows the corresponding true P.S.D. response.

The PSD curves for θ_x and θ_y exhibit irregular spikes near the new 24 Hz rocking

mode resonances. The I*star controller, using the inverted plant transfer function, must cancel the effect of this resonance, but it cannot exactly match the location of the resonance, thus causing irregular spikes in the output. These spikes, however, are within $\pm$ 1 dB of the desired level.

The I*star computer requires approximately 5 minutes of operation time to accurately track all three input P.S.D. curves.
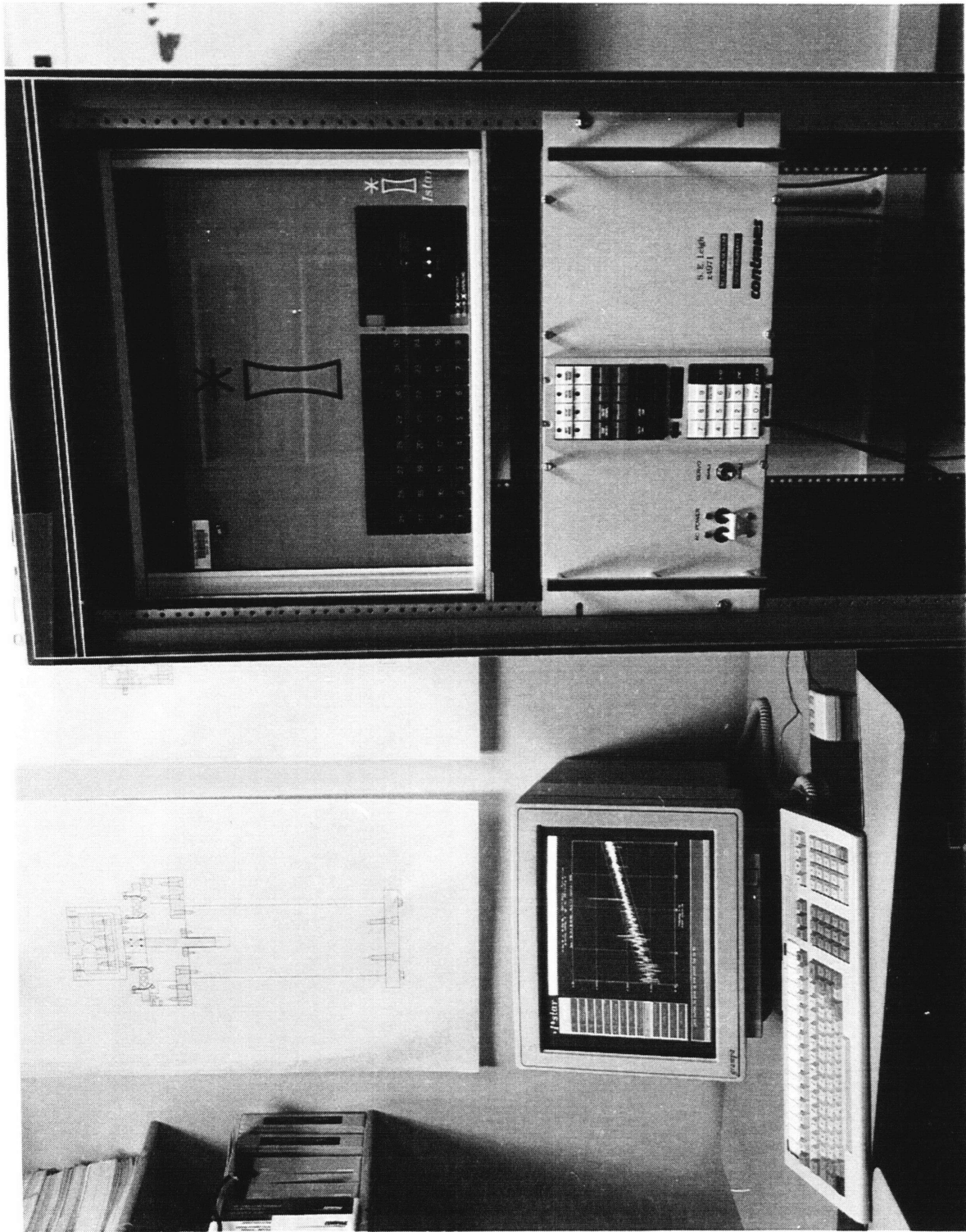
Figure 5-1: Photograph of I*star Computer
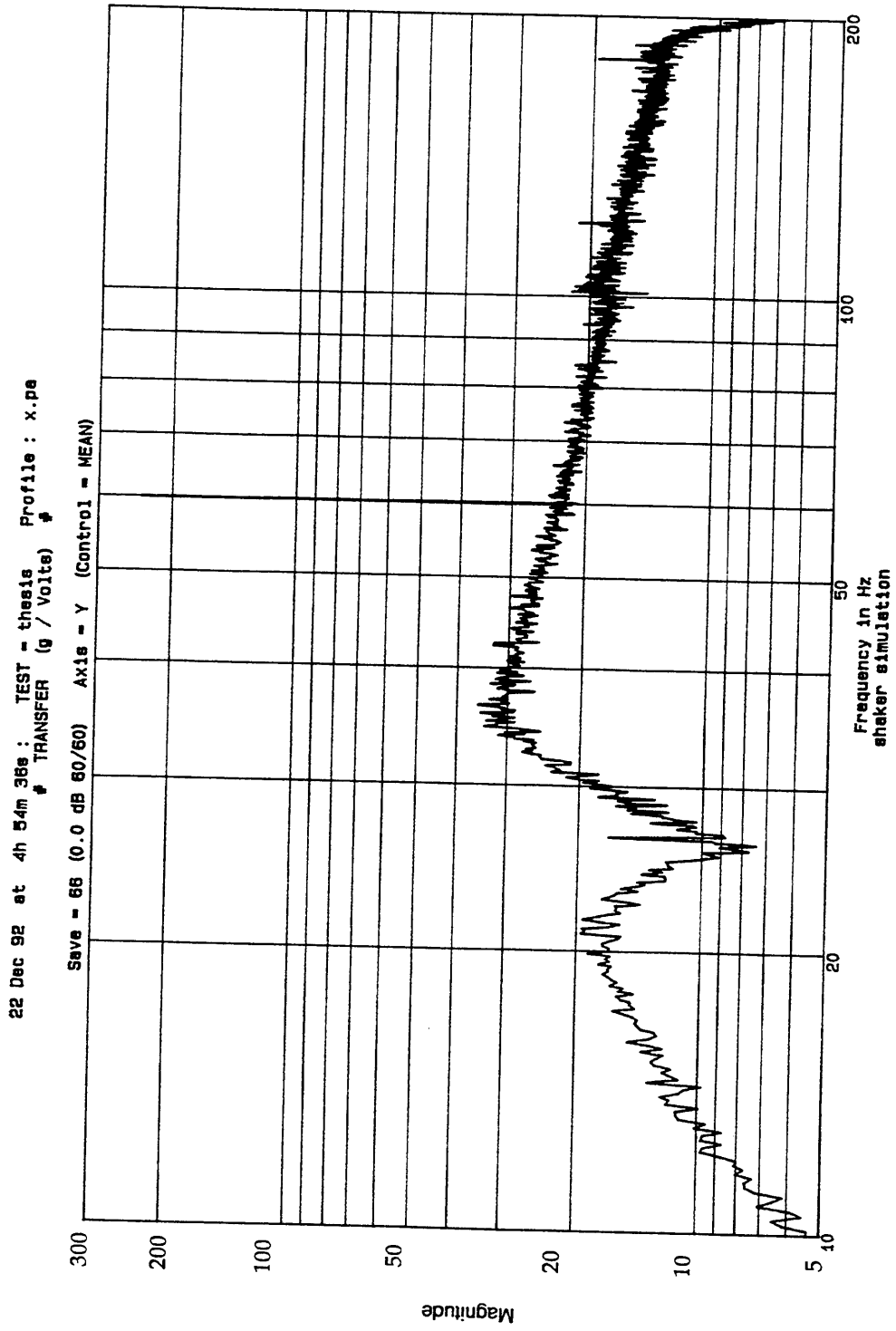
Figure 5-2: θ_y Transfer Function as Seen by I*star Controller
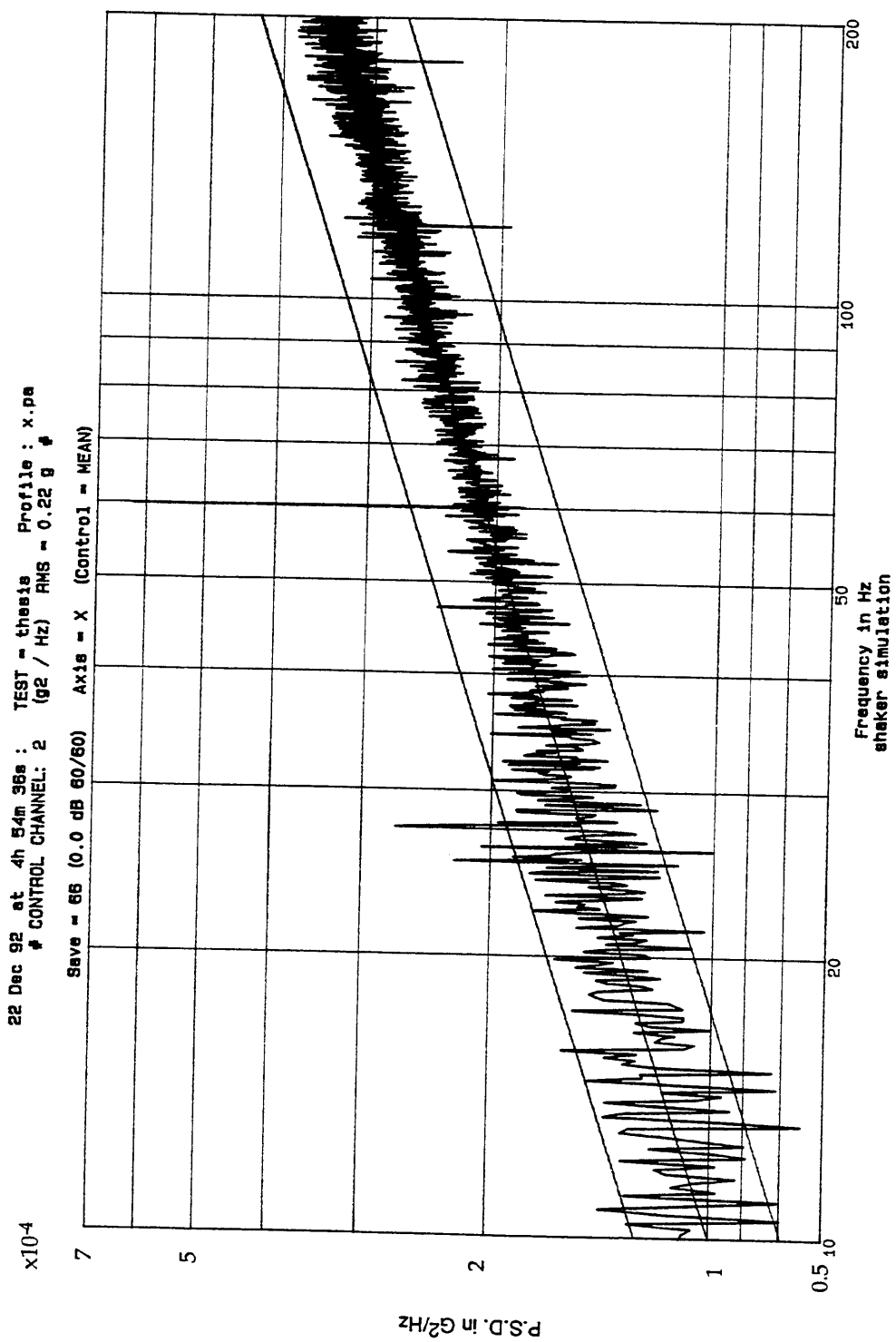
Figure 5-3: P.S.D. Response of θ_x (System with Center Post)

x10⁻⁴

P.S.D. in G2/Hz

Frequency in Hz
shaker simulation
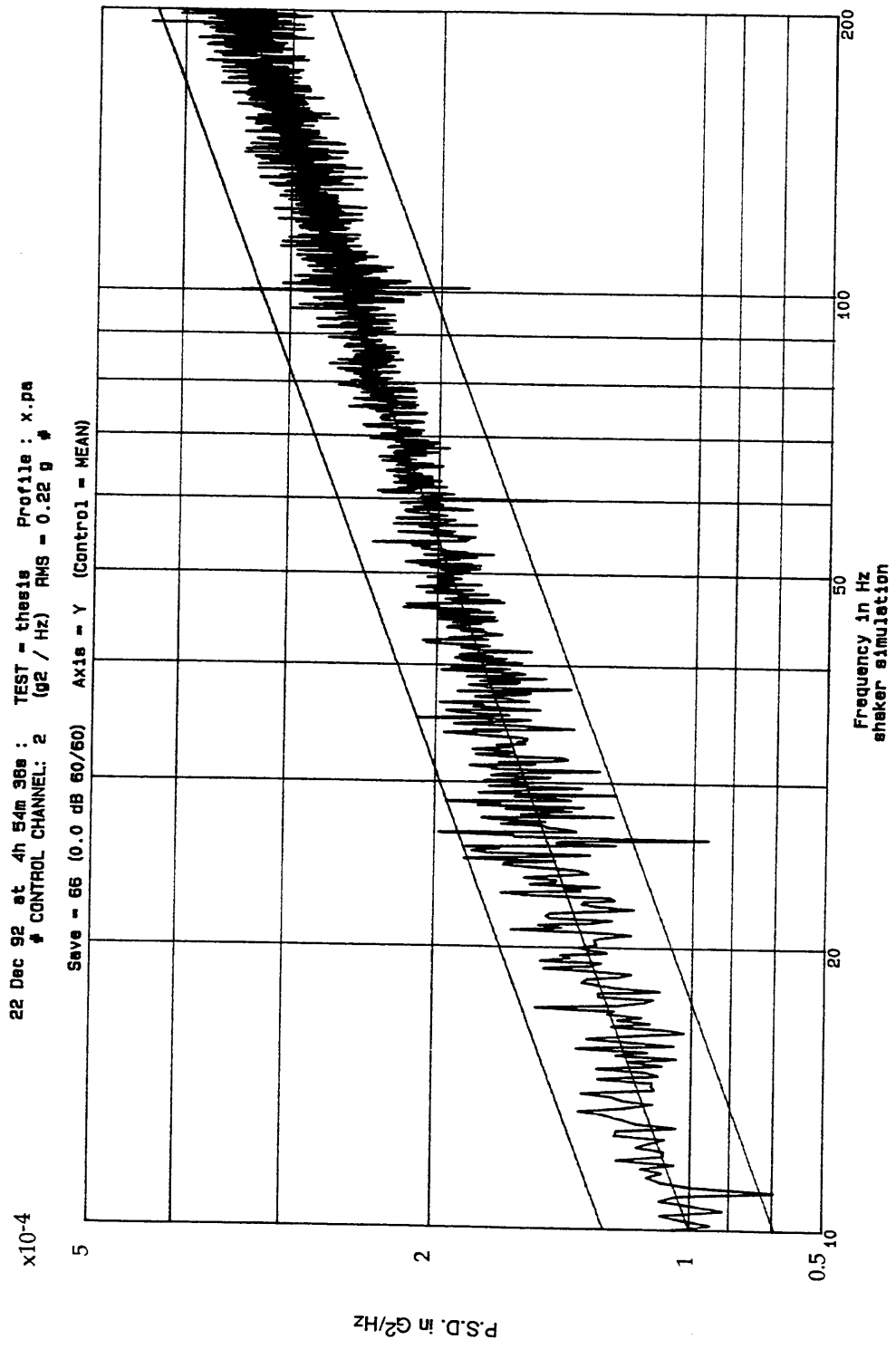
Figure 5-4: P.S.D. Response of θ_y (System with Center Post)

100
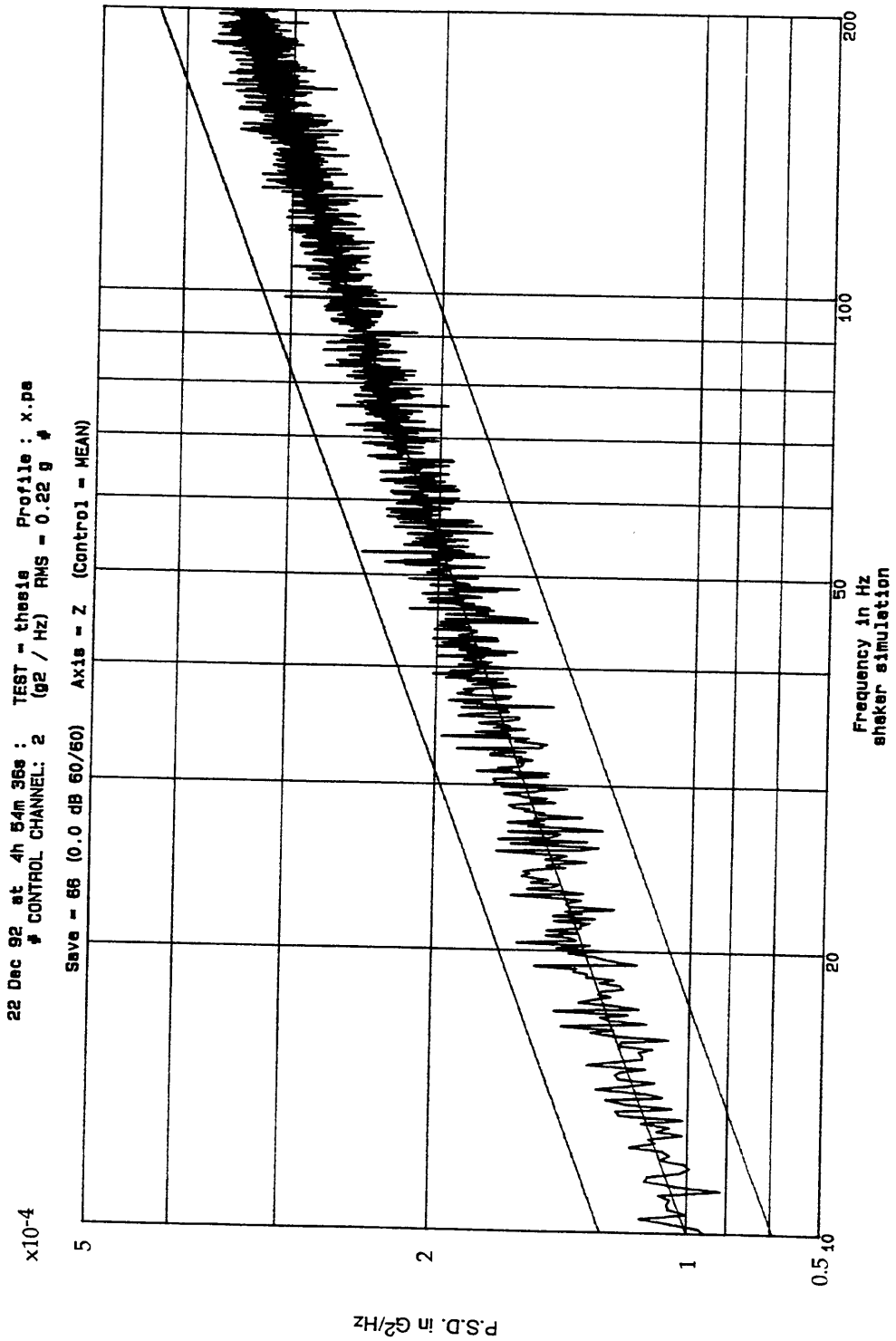
Figure 5-5: P.S.D. Response of Z (System with Center Post)
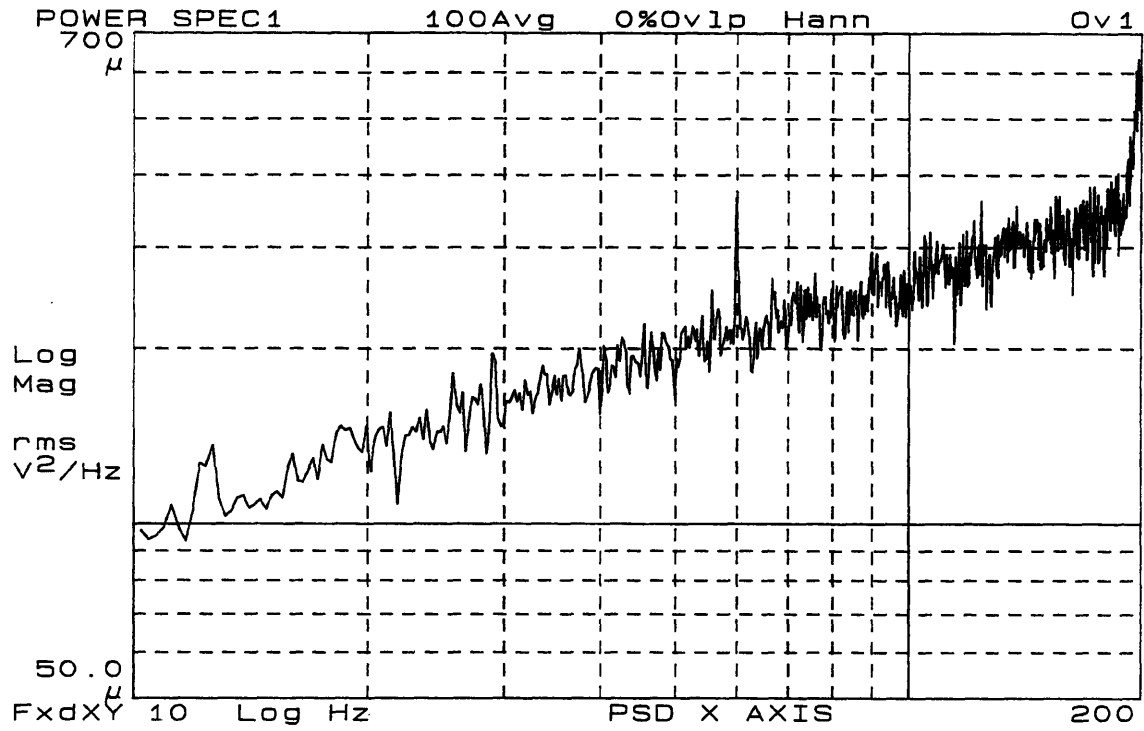
Figure 5-6: P.S.D. Response of θ_x (System with Center Post) as Seen by Dynamic Signal Analyzer

POWER SPEC2   100Avg   0%Ovlp Hann   Ov2
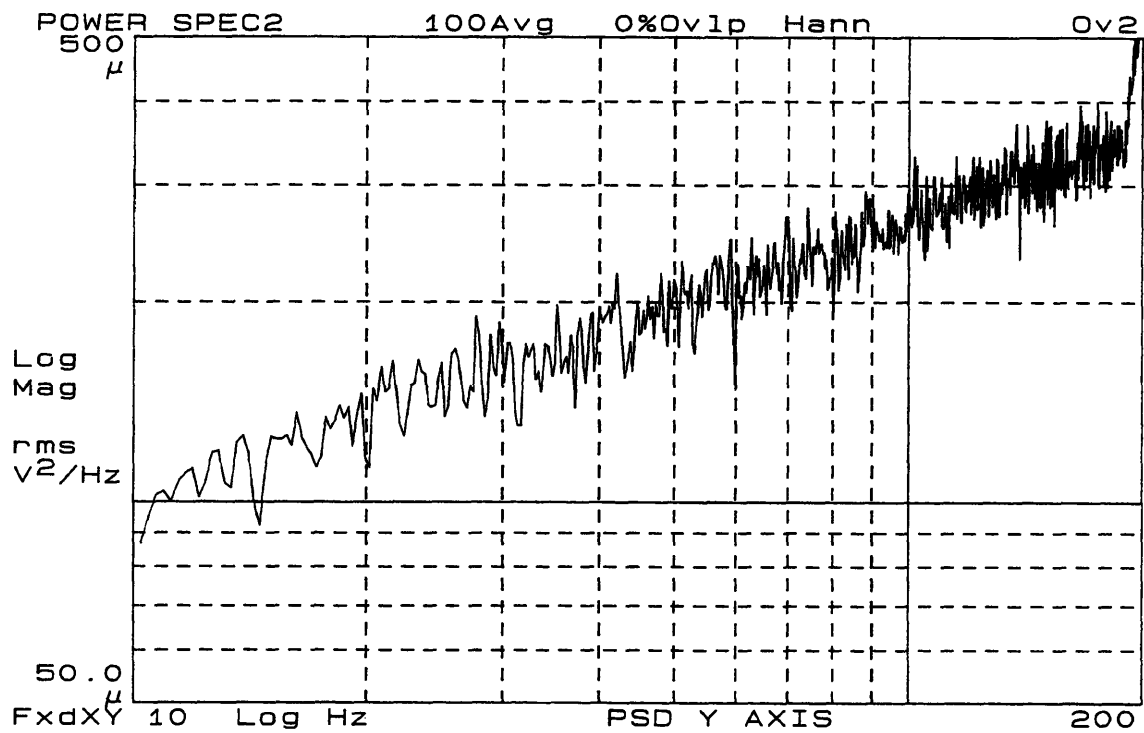
Figure 5-7: P.S.D. Response of θ_y (System with Center Post) as Seen by Dynamic Signal Analyzer
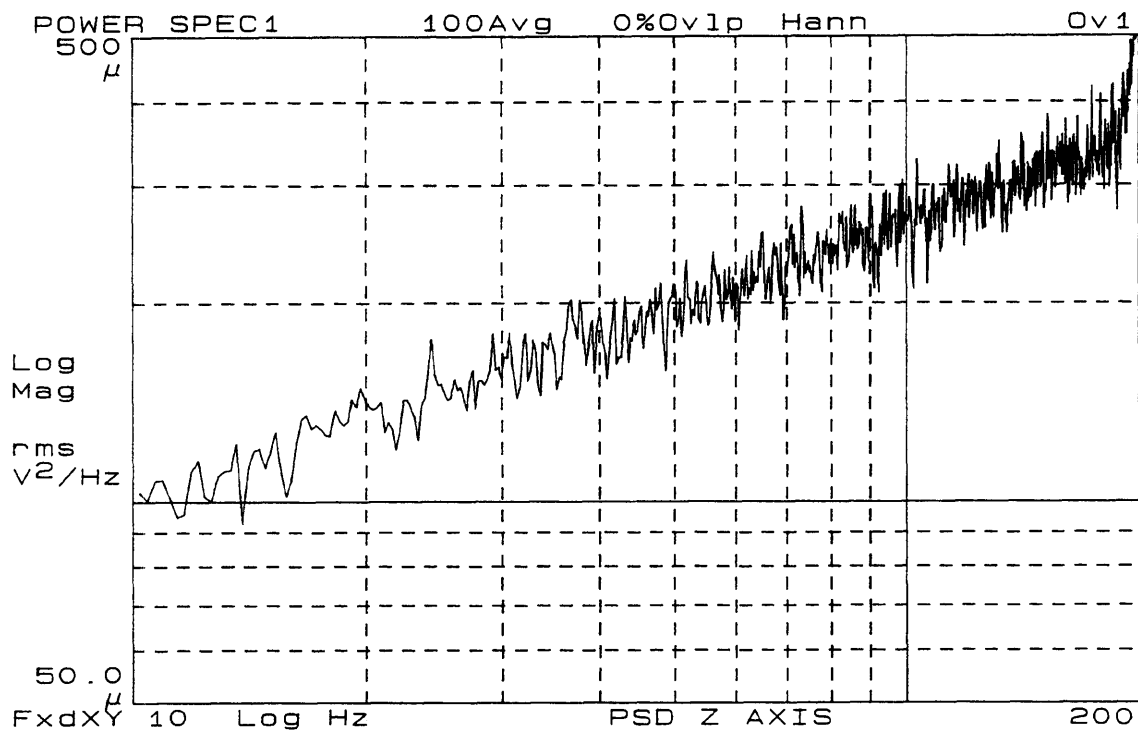
Figure 5-8: P.S.D. Response of Z (System with Center Post) as Seen by Dynamic Signal Analyzer

Chapter 6

Conclusions

The I*star controller results demonstrate the validity of the assumption of the decoupled actuated degrees-of-freedom. The system can be considered as three single-input single-output plants. Also, the I*star controller is able to control the three actuated degrees-of-freedom to within ± 1 dB of the desired power spectral density output, except in the vicinity of the undamped frequencies of the system. However, there remain three areas of concern: the θ_z mode which occurs at 30 Hz; the θ_x and θ_y rocking modes at 24 Hz; and the performance of the I*star controller. This chapter will address these concerns as well as provide recommendations for those interested in developing similar test facilities.

6.1   Torsional Mode of System

The torsional stiffness of the system can be improved through the design of an additional torsional support. Future research will be necessary to determine a suitable design which would couple the mounting platform to ground and increase the torsional stiffness of the system. This torsional support has many other design goals as well: allow motion in θ_x, θ_y, and Z. This torsional support design process proved to be beyond the scope of this project. However, it is important to note that if the payload may be subjected to torsional motion, the test facility will provide a suitable disturbance environment as it is designed currently.

6.2 Rocking Modes of System

The center post was designed to eliminate the 12 Hz lateral modes of the system. The final system retains two low frequency modes at 24 Hz, but since these modes are rocking modes in θ_x and θ_y, they are controlled by the actuators. The I*star controller has difficulty controlling the system near the 24 Hz modes, but no changes are necessary unless additional accuracy is required (beyond $\pm$ 1 dB). If greater accuracy is demanded, there are two possible solutions. The first involves lowering the natural frequency, the other involves damping it.

As mentioned in Chapter 4, the stiffness terms of rocking modes are dominated by the axial stiffness of the shear mounts in each shaker. In order to place this natural frequency below the desired range, I recommend replacing the two shear mounts in each shaker with mounts of lower stiffness values. The I*star controller will be able to control the three actuated degrees-of-freedom to within ±1 dB over the entire desired frequency operation range if the rocking modes are moved below 10 Hz.

The other possible solution lies in increasing the damping of the rocking modes. This would allow the I*star controller to track the desired output P.S.D. curve more accurate in the range of the resonance.

6.3 Recommendations for Improving I*star Performance

Figure 5-2 points to the most significant limitation of the I*star controller. The I*star system does not acquire an accurate transfer functions of the system. Figure 5-2 should match the transfer function depicted in Figure 4-23, but the I*star transfer function has a much higher level of high-frequency noise (Figure 4-23 is much smoother) as well as rolling of steeply near the upper frequency limit. The latter problem is easily remedied. Simply define the disturbance environment over a slightly larger range to ensure the output P.S.D. curve will match the desired curve over the desired range. I recommend future efforts to focus upon the former area, im-

proving the accuracy of the I*star computer in the acquisition of the system transfer functions.

6.4 Recommendations for Development of a Similar Test Facility

In overview, this test facility was limited by two important choices made two years prior to my efforts: the actuators and controller. The complex flexure systems developed were necessary to allow the platform to rotate through an angle since the shakers will not allow lateral motion. The design could be simplified greatly through the use of voice coil actuators which would allow the required lateral motion to occur. There would be no need for a center post system in such a facility because there would be no low-frequency uncontrolled resonance (no lateral mode). Additional torsional supports as shown in Figure 6.4 could be easily designed, although special consideration must be given to the spatial constraints of the laboratory (long supports leading from the platform are necessary).

In addition, I would strongly urge that the control system be developed in conjunction with the mechanical system as opposed to purchasing an off-the-shelf controller. The performance of ACCEL is limited mainly by the I*star controller. The I*star controller does not provide the flexibility which I desired. Also, I found that troubleshooting control-related problems was extremely difficult because the I*star controller is, in essence, a black box. I could not alter or adjust the I*star controller to improve performance.
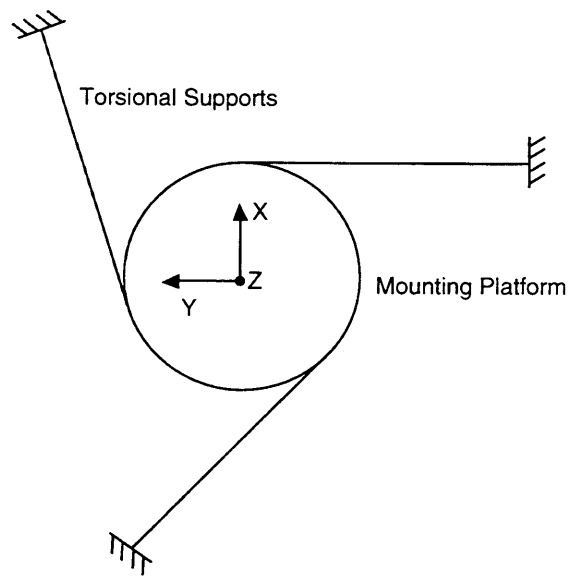
Figure 6-1: Torsional Supports

Appendix A

Decoupling Process

The coordinate transformation was determined using a decoupling process shown in Figure A.
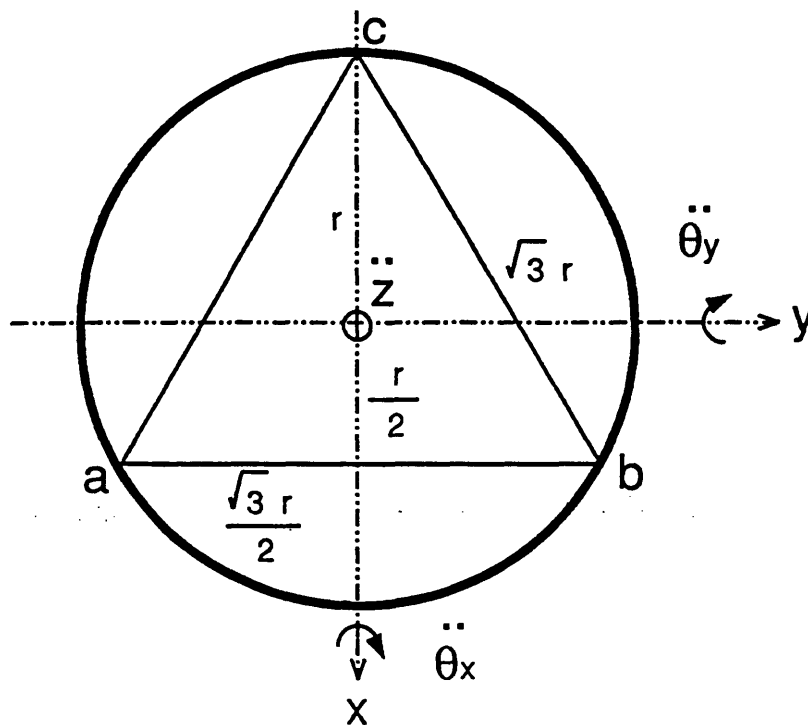
Figure A-1: Diagram of decoupling process

From mechanics of solid bodies,

$$\ddot{\theta} = \frac{\ddot{Z}}{r} \tag{A.1}$$

where $\ddot{\theta}$ is the jerk, the angular acceleration, $\ddot{Z}$ is the linear acceleration, and r is the moment arm. The decoupling equations become:

$$\ddot{\theta}_x = \frac{\ddot{Z}_a - \ddot{Z}_b}{\sqrt{3}r} \tag{A.2}$$

$$\ddot{\theta}_y = \frac{\frac{\ddot{Z}_a + \ddot{Z}_b}{2} - Z_c}{\frac{3r}{2}} \tag{A.3}$$

$$\ddot{Z} = \frac{Z_a + Z_b + Z_c}{3} \tag{A.4}$$

By replacing r with the radius of the platform (0.3048 m), the equations uniquely define the decoupling matrix:

$$\begin{bmatrix} \ddot{Z}_1 \\ \ddot{Z}_2 \\ \ddot{Z}_3 \end{bmatrix} = \begin{bmatrix} \mathbf{M} \end{bmatrix} \begin{bmatrix} \ddot{\theta}_x \\ \ddot{\theta}_y \\ \ddot{Z} \end{bmatrix} = \begin{bmatrix} 0.264 & 0.152 & 1.0 \\ -0.264 & 0.152 & 1.0 \\ 0.0 & -0.305 & 1.0 \end{bmatrix} \begin{bmatrix} \ddot{\theta}_x \\ \ddot{\theta}_y \\ \ddot{Z} \end{bmatrix} \tag{A.5}$$

The inverse matrix is given by:

$$\begin{bmatrix} \ddot{\theta}_x \\ \ddot{\theta}_y \\ \ddot{Z} \end{bmatrix} = \begin{bmatrix} \mathbf{M}^{-1} \end{bmatrix} \begin{bmatrix} \ddot{Z}_1 \\ \ddot{Z}_2 \\ \ddot{Z}_3 \end{bmatrix} = \begin{bmatrix} 1.894 & -1.894 & 0.0 \\ 1.094 & 1.094 & -2.187 \\ 0.333 & 0.333 & 0.333 \end{bmatrix} \begin{bmatrix} \ddot{Z}_1 \\ \ddot{Z}_2 \\ \ddot{Z}_3 \end{bmatrix} \tag{A.6}$$

Appendix B

Drawing of Four-Axis Flexure

The following drawing was used in the fabrication of the four-axis flexures.

2.00
TYP

1.00
TYP

5/8-18 BOTTOM TAP
TO 1/2 DEEP

.475
TYP

6.25

2.500

2.500

.50R TYP

2.500

2.500

1.250

.50
TYP
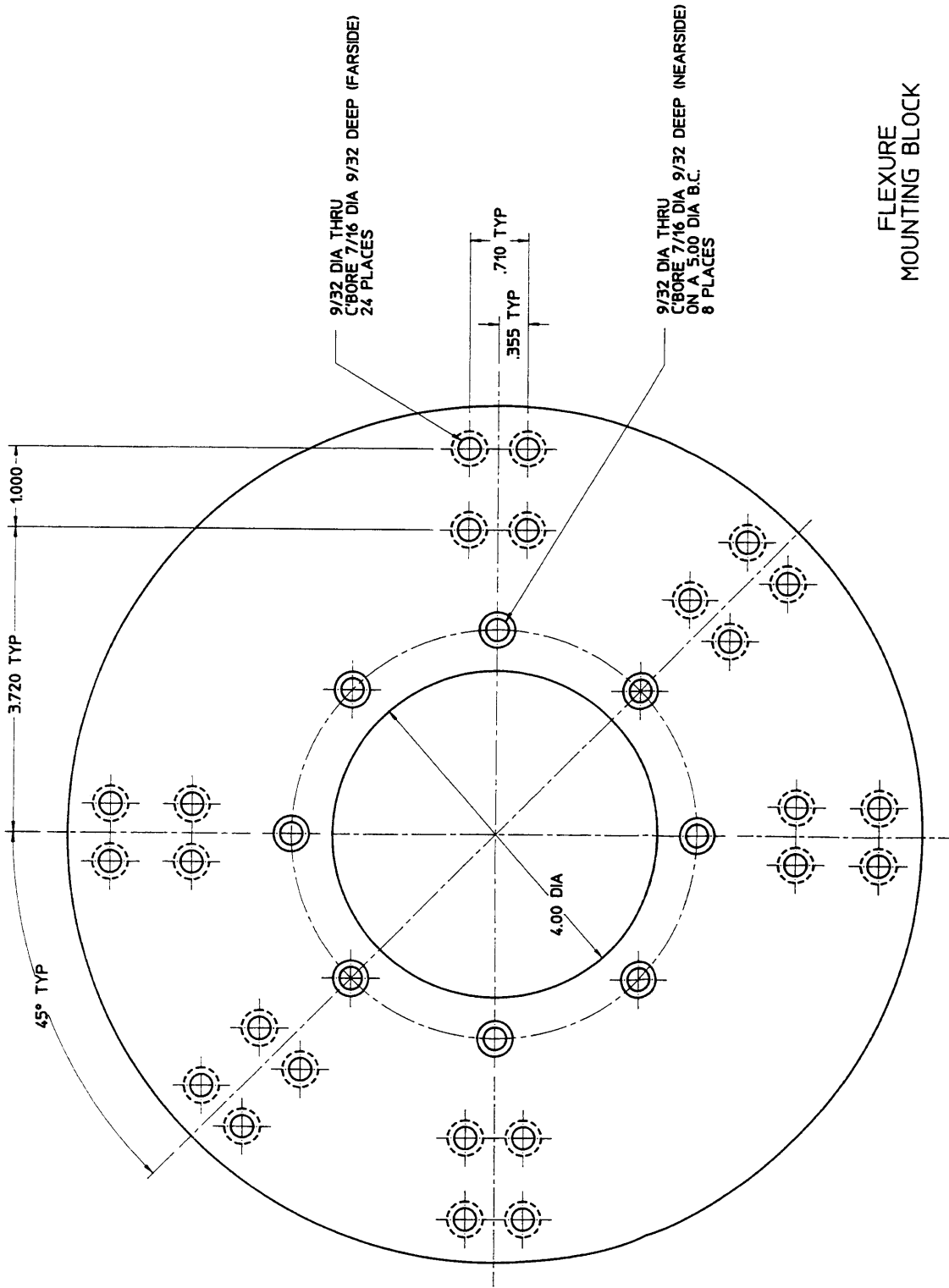
1.000
TYP

1/4-28 BOTTOM TAP
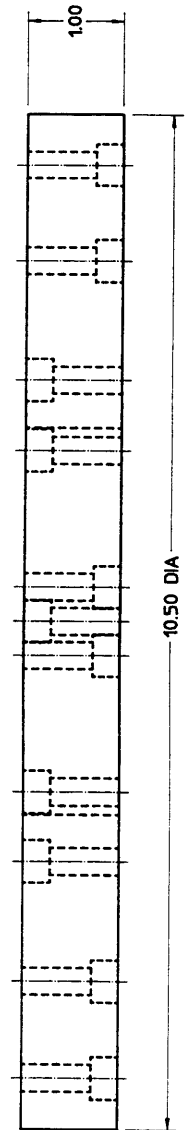TO 1/2 DEEP
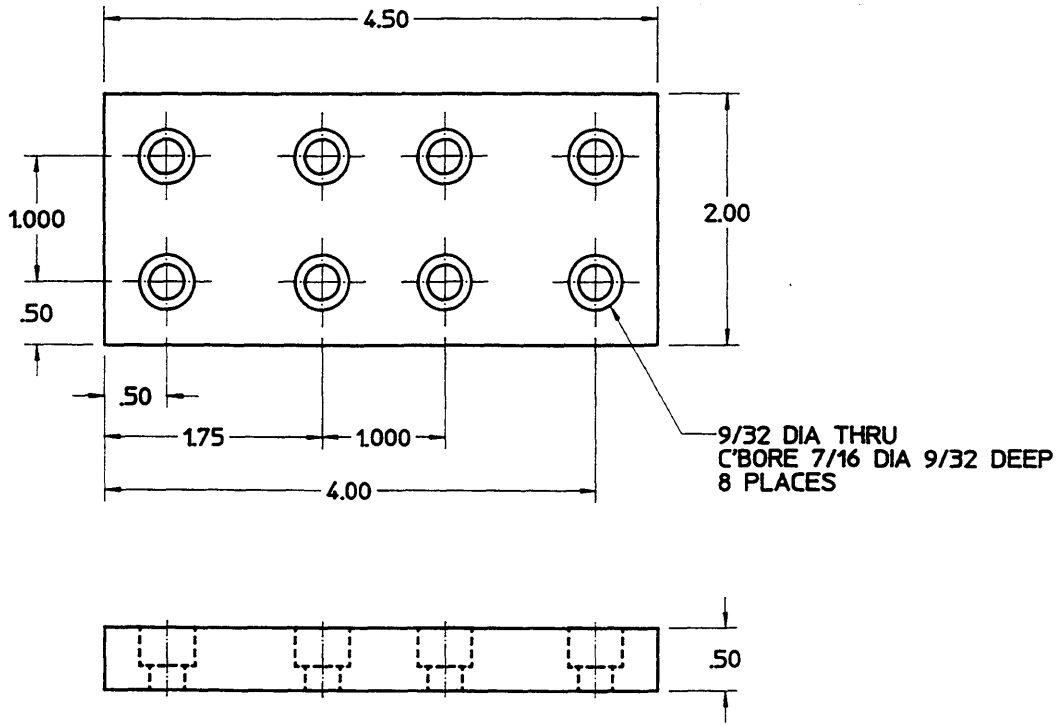4 PLACES
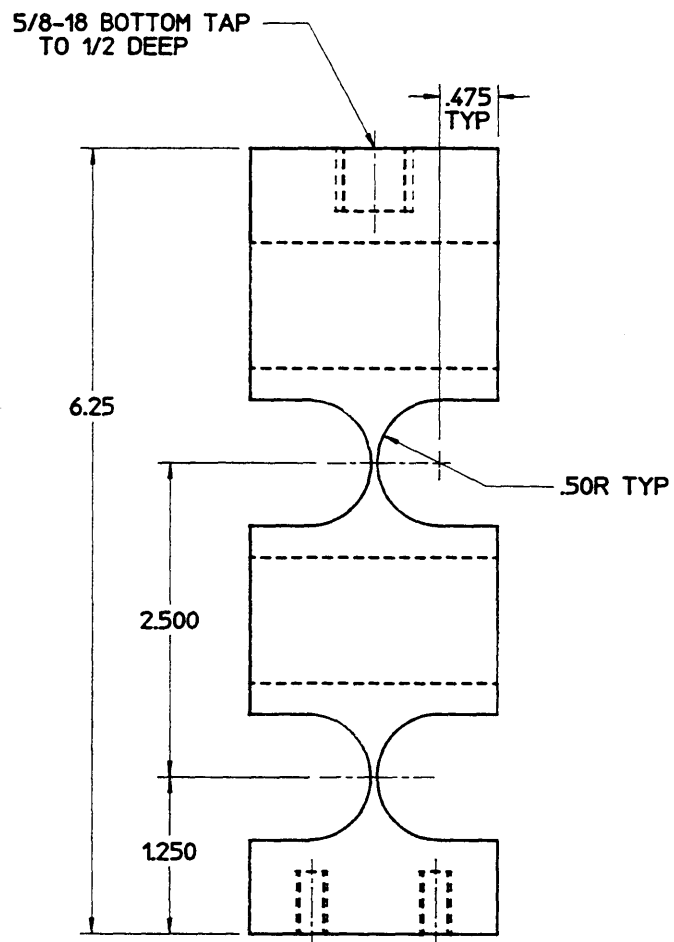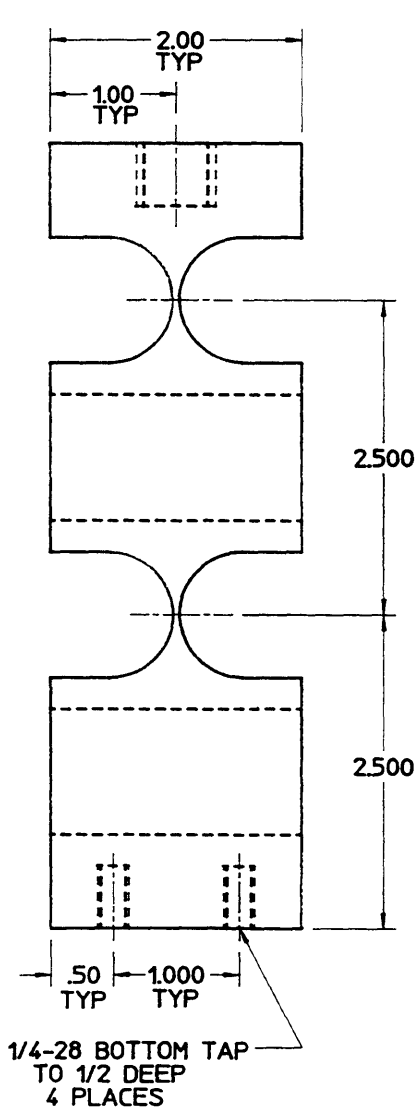
SHAKER FLEXURE

Appendix C

Drawings of Center Post Design

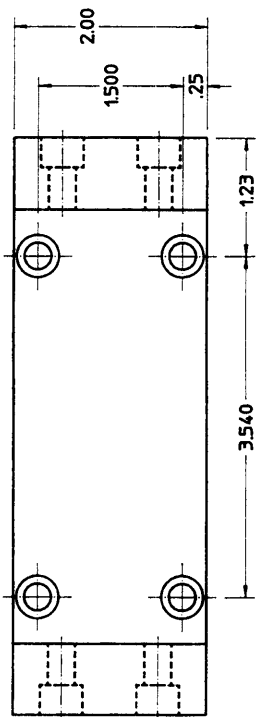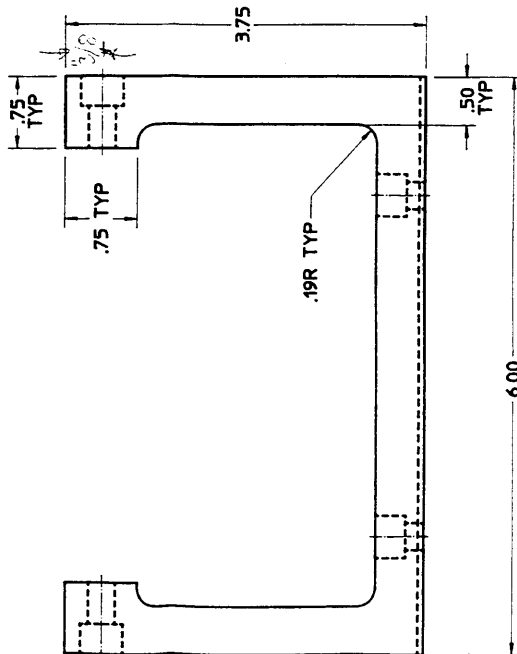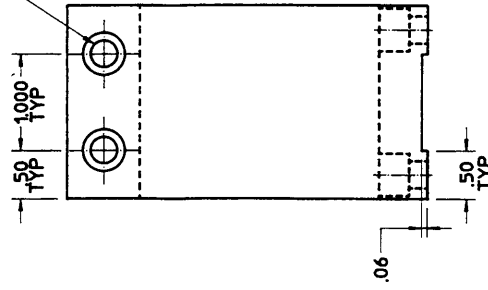The following drawings were used in the fabrication of the mechanical components which compose the center post described in Chapter 4.

M3 x 1/2 DEEP
8 PLACES

.355 TYP

.710 TYP

1.07 TYP

4.090 TYP

1/4-28UNF x 1/2 DEEP
ON 3.540 DIA B.C.
PLACES

.750

1.500

45° TYP

1/4-28UNF x 1/2 DEEP
5 PLACES

1.770 REF

1.50

.700 TYP

.30 TYP

1/2-20UNF x 3/4 DEEP

M4 x 1/2 DEEP
8 PLACES

.430 TYP

.860 TYP

114

9/32 DIA THRU
C'BORE 7/16 DIA 9/32 DEEP (FARSIDE)
24 PLACES

9/32 DIA THRU
C'BORE 7/16 DIA 9/32 DEEP (NEARSIDE)
ON A 5.00 DIA B.C.
8 PLACES

.710 TYP
.355 TYP

1.000

3.720 TYP

45° TYP

4.00 DIA

FLEXURE
MOUNTING BLOCK

1.00

10.50 DIA

115

4.50

2.00

1.000

.50

.50

1.75

1.000

4.00

9/32 DIA THRU
C'BORE 7/16 DIA 9/32 DEEP
8 PLACES

.50

FLEXURE
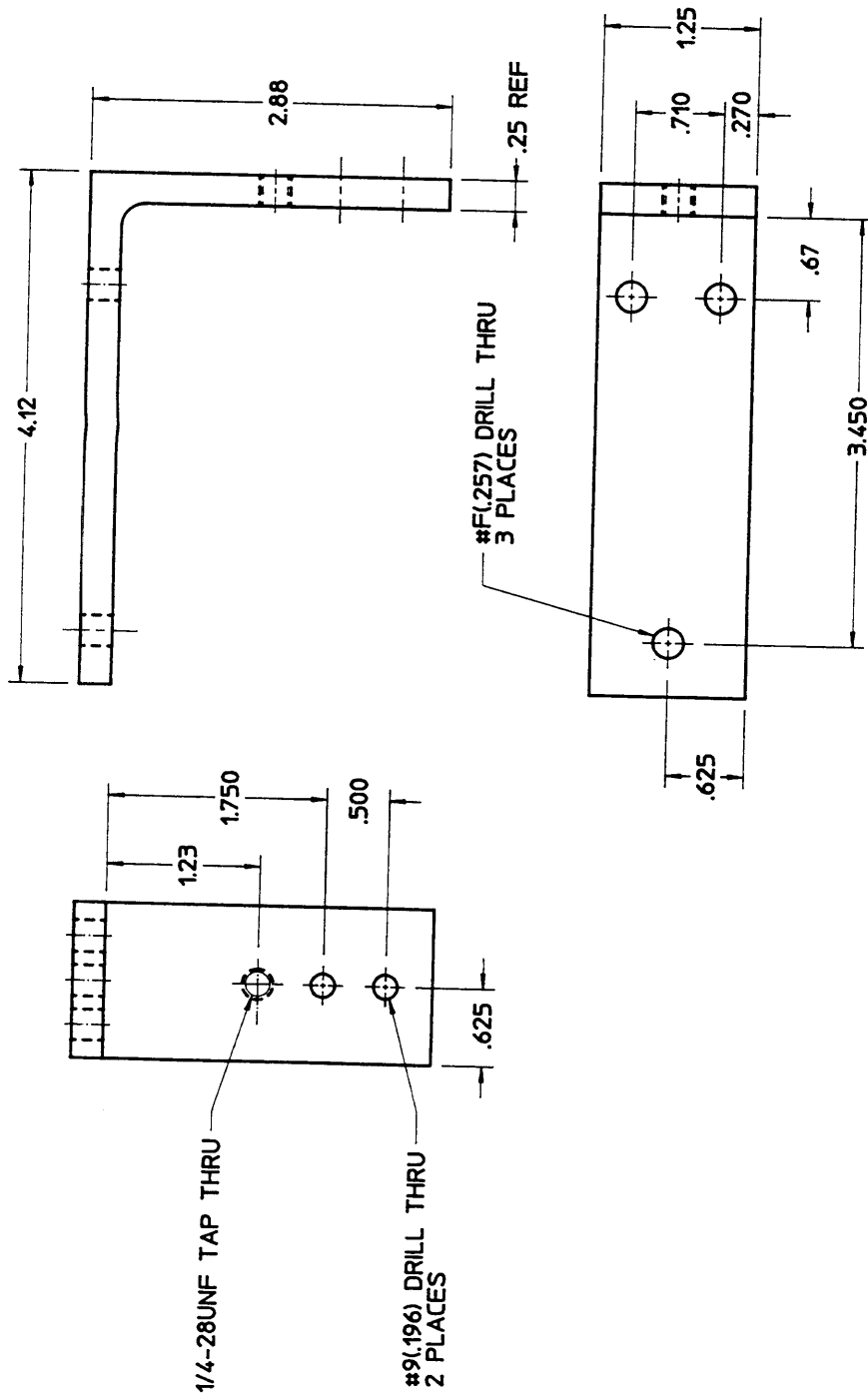MOUNTING PLATE

116

9/32 DIA THRU
C'BORE 7/16 DIA 9/32 DEEP
8 PLACES

.50
TYP
1.000
TYP
.50
TYP
.06

FLEXURE
SUPPORT

2.00
1.500
.25
1.23
3.540

3.75
3/8
.75
TYP
.50
TYP
.75 TYP
.19R TYP
6.00

117

.50R TYP
1.00 REF

1.00

2.75

.475 REF
TYP

.06 TYP

.25 TYP

.050

2.00

1.000

.50

1/4-28 UNF x 1/2 DEEP MAX
4 PLACES
DO NOT BREAK THRU

.50

2.00

1.000

1.00

1.00

5/8-18UNF x 1/2 DEEP

FLEXURE
MIDDLE

1/4-28 UNF x 1/2 DEEP MAX
4 PLACES
DO NOT BREAK THRU

1.000   .50

.380

.75

.50R TYP

1.00 REF

.475 TYP
REF

.050

.12

.06

.50

2.50

.25

.50

.06

2.00

1.000   .50

.50

1.00

FLEXURE
RIGHT & LEFT

119

2.88

4.12

.25 REF

#F(.257) DRILL THRU
3 PLACES

1.25

.710

.270

.67

3.450

.625

1.750

1.23

.500

1/4-28UNF TAP THRU

#9(.196) DRILL THRU
2 PLACES

.625

FLEXURE
ALIGNMENT

120

.340

.75

1.25

GAGE BLOCK

1/4-28 UNF TO 1/2 DEEP
8 PLACES ON 5.0" DIA
BOLT CIRCLE

#10-32 UNF
TO 3/8 DEEP
4 PLACES
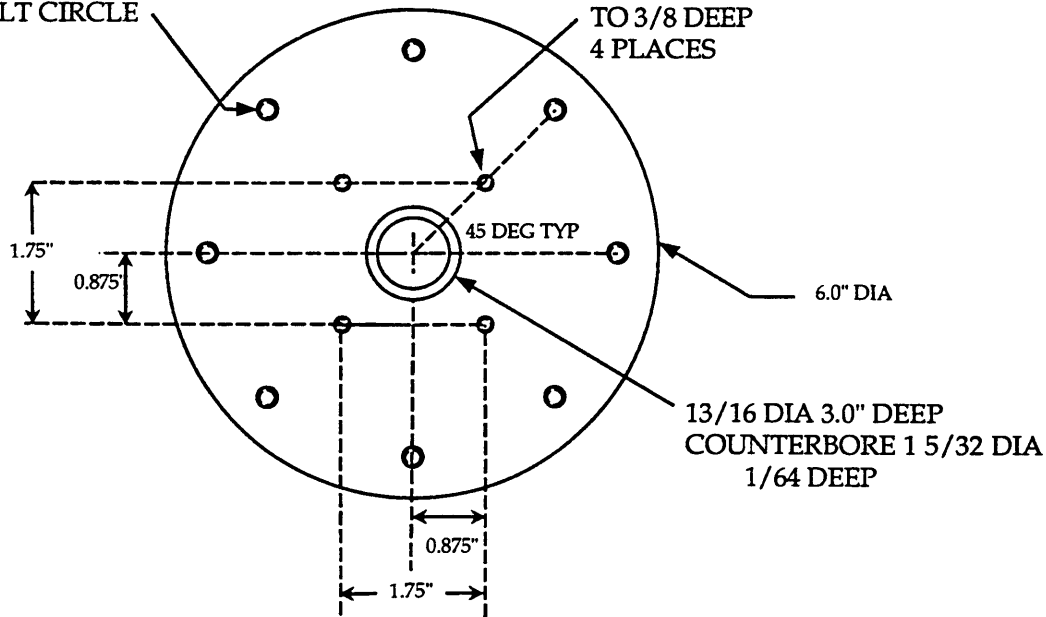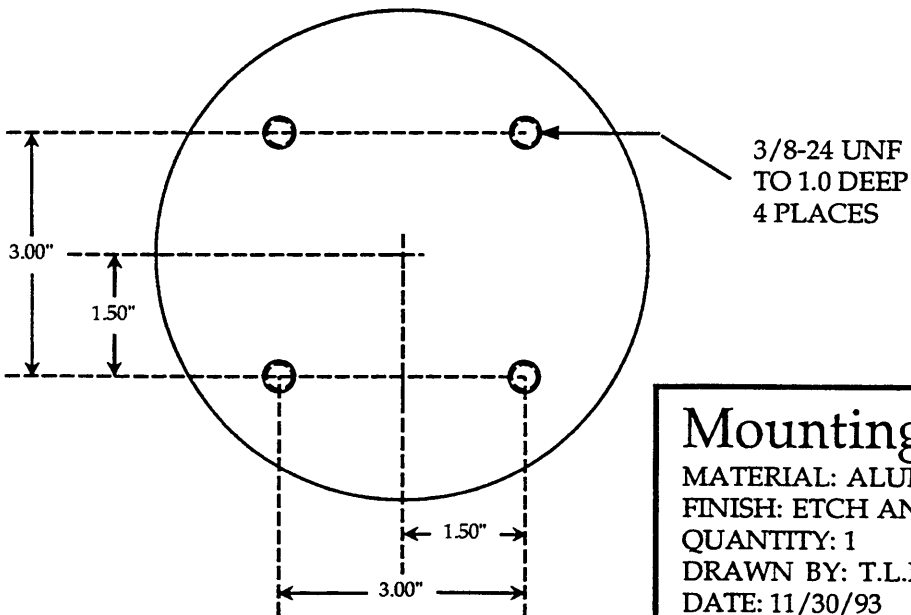
1.75"

0.875"

45 DEG TYP

6.0" DIA

13/16 DIA 3.0" DEEP
COUNTERBORE 1 5/32 DIA
1/64 DEEP

0.875"

1.75"

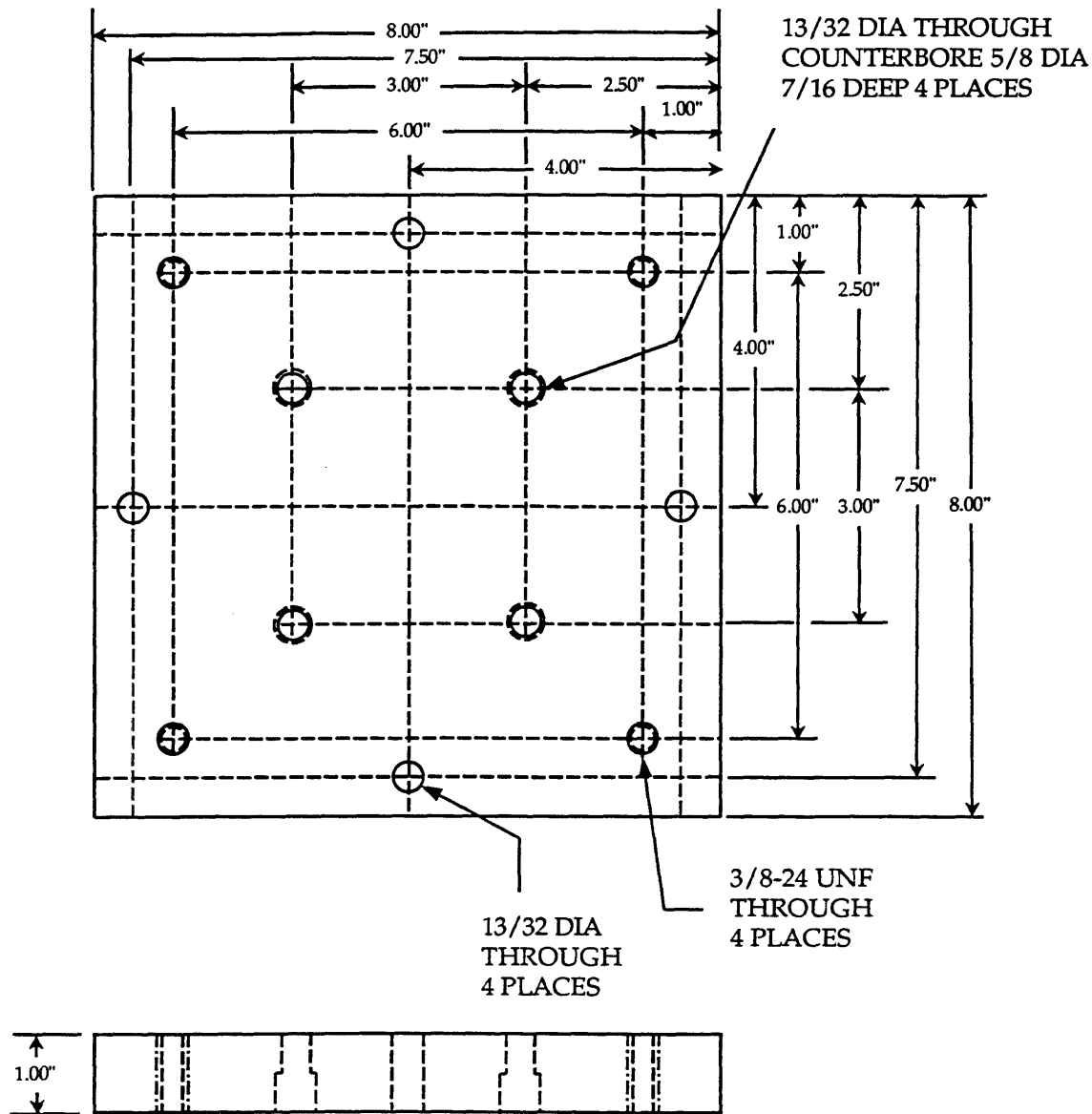TOP VIEW

3/8-24 UNF
TO 1.0 DEEP
4 PLACES

3.00"

1.50"

1.50"

3.00"

Mounting Post
MATERIAL: ALUM 6061-T6511
FINISH: ETCH AND CLEAN
QUANTITY: 1   SCALE: 1/2
DRAWN BY: T.L.HEIN
DATE: 11/30/93

BOTTOM VIEW

FOR SIDE VIEW SEE PAGE 2

14.12"

6.00"
DIA
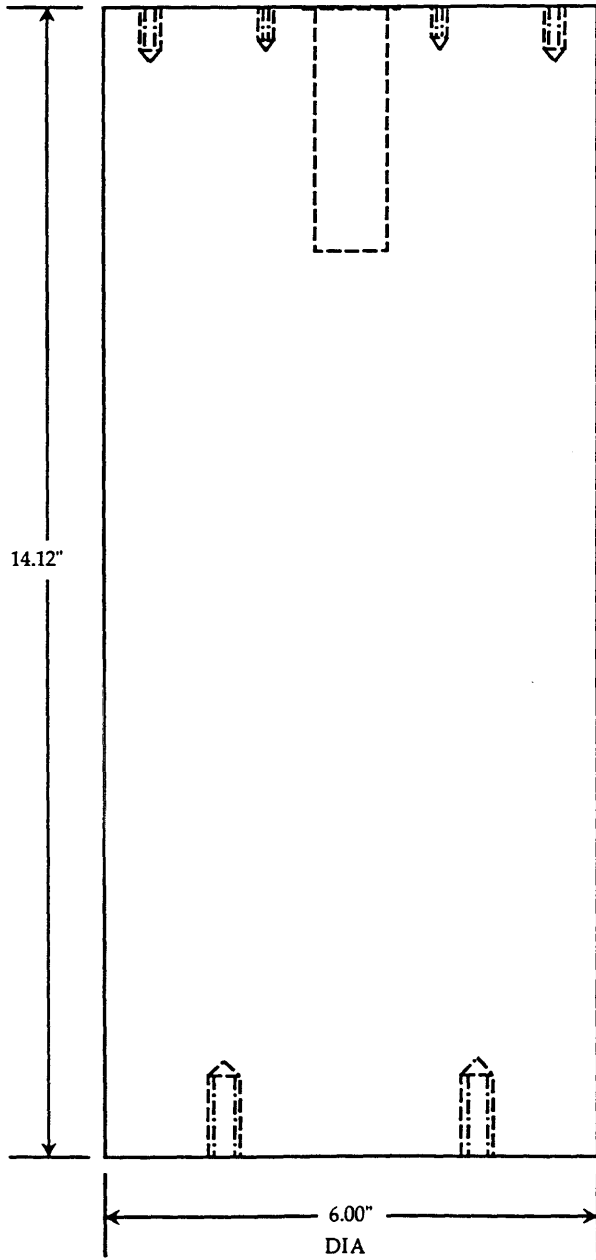
**Mounting Post**
MATERIAL: ALUM 6061-T6511
FINISH: ETCH AND CLEAN
QUANTITY: 1   SCALE: 1/2
DRAWN BY: T.L.HEIN
DATE: 11/30/93

FOR TOP AND BOTTOM VIEWS SEE PAGE 1   PAGE 2 of 2

13/32 DIA THROUGH
COUNTERBORE 5/8 DIA
7/16 DEEP 4 PLACES

8.00"
7.50"
3.00"
2.50"
1.00"
6.00"
4.00"

1.00"
2.50"
4.00"
6.00"
3.00"
7.50"
8.00"

13/32 DIA
THROUGH
4 PLACES

3/8-24 UNF
THROUGH
4 PLACES

1.00"

Mounting Plate
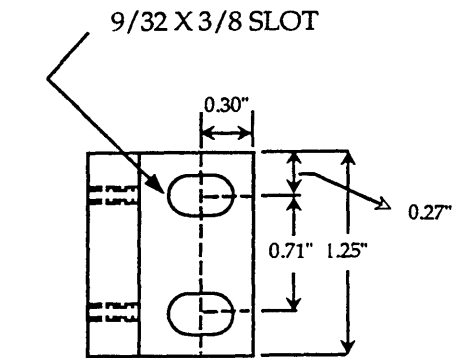MATERIAL: ALUM 6061-T651
FINISH: ETCH AND CLEAN
QUANTITY: 1   SCALE: 1/2
DRAWN BY: T.L.HEIN
DATE: 11/30/93

9/32 X 3/8 SLOT

0.30"

0.27"

0.71" 1.25"

Suspension Block
MATERIAL: ALUM 6061-T651
FINISH: ETCH AND CLEAN
QUANTITY: 4   SCALE: 1/1
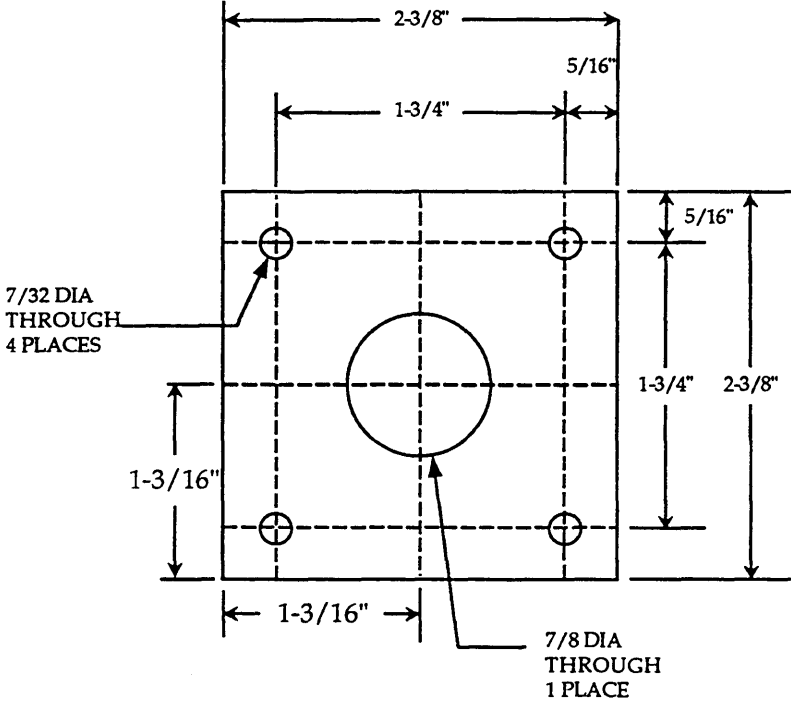DRAWN BY: T.L.HEIN
DATE: 11/30/93

1.00"

0.30"

0.70"

1.25"

0.27"

1.25"

0.71"

0.18"

M3 THROUGH
2 PLACES
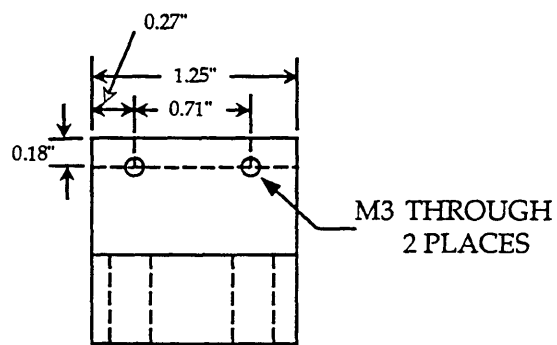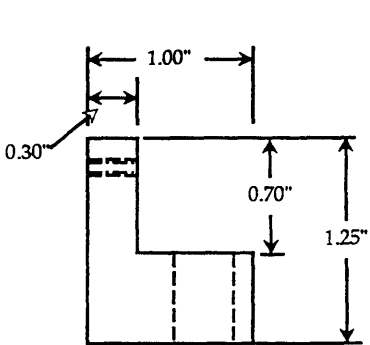
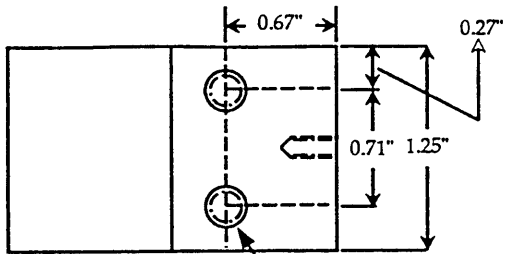**Bearing Retainer**
MATERIAL: ALUM 6061-T651
FINISH: ETCH AND CLEAN
QUANTITY: 1   SCALE: 1/1
DRAWN BY: T.L.HEIN
DATE: 11/30/93

2-3/8"

5/16"

1-3/4"

7/32 DIA
THROUGH
4 PLACES

5/16"

1-3/4"   2-3/8"

1-3/16"

1-3/16"

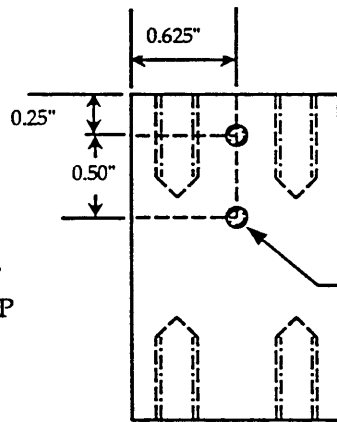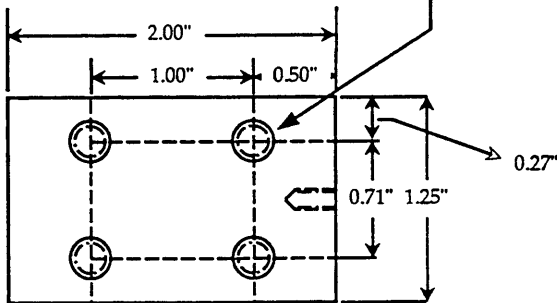7/8 DIA
THROUGH
1 PLACE

3/8"

0.67"

0.27"

0.71" 1.25"

TOP VIEW

Roller Support Block
MATERIAL: ALUM 6061-T651
FINISH: ETCH AND CLEAN
QUANTITY: 4   SCALE: 1/1
DRAWN BY: T.L.HEIN
DATE: 11/30/93

2.00"

1.00"

0.64"

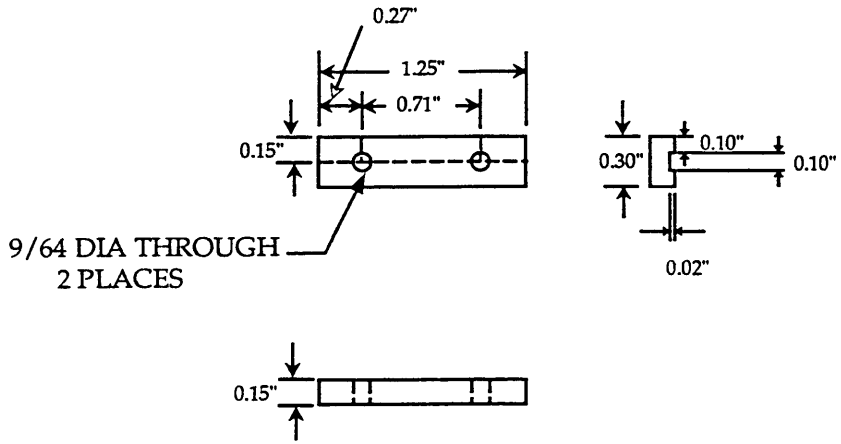2.00"
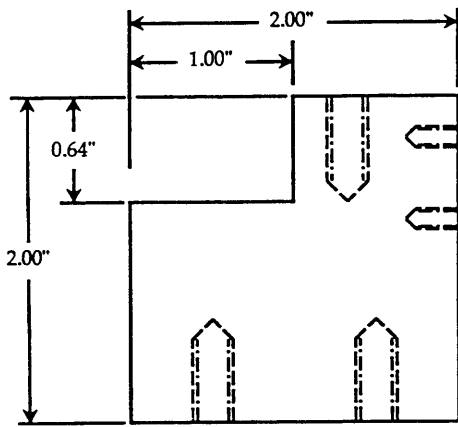
1/4-28 UNF
TO 1/2 DEEP
6 PLACES

0.625"

0.25"

0.50"

#10-32 UNF
TO 3/8 DEEP
2 PLACES

2.00"

1.00"   0.50"

0.27"

0.71" 1.25"

BOTTOM VIEW

Flexure Clamp
MATERIAL: ALUM 6061-T6
FINISH: ETCH AND CLEAN
QUANTITY: 16   SCALE 1/1
DRAWN BY: T.L.HEIN
DATE: 11/30/93

0.27"
1.25"
0.71"
0.15"

9/64 DIA THROUGH
2 PLACES

0.30"   0.10"   0.10"

0.02"

0.15"

Bibliography

[1] Blevins, R.D. *Formulas for Natural Frequencies and Mode Shape*, Robert E. Kreiger Publishing Company, Malabar, Florida, 1984.

[2] Davaine, J. *Multi-Axis Vibration Environment Simulation for a Helicopter-Borne Equipment*, TEST Engineering and Management Magazine.

[3] Forman, S.E., Sultana, J.A., and LeClair, R.A. *Laser Radar Beam Steering Mirrors*, MIT Lincoln Laboratory Project Report ODT-24, February 9, 1990.

[4] Ling Dynamic Systems *User Manual: Installation Commisioning and Operating: Vibrator - Model V550 Series*, May, 1987.

[5] Ling Dynamic Systems *Instruction Manual: Vibrator Model 400 Series* April, 1984.

[6] Loney, G.C. *Design of a Small-Aperture Steering Mirror for High Bandwidth Acquisition and Tracking*, Optical Engineering, Vol. 29, No. 11, 1360-1365, November, 1990.

[7] Ludwig, T.J. *Inertial Line-of-Sight Stabilization for Space-based Optical Communications Systems*, S.M. Thesis, Massachusetts Institute of Technology, May, 1993.

[8] *MIL - STD 810E, Military Standard Environmental Test Methods and Engineering Guidelines* U.S. Department of Defense, July 1989.

[9] *MIL - HDBK 5F, Military Handbook Metallic Materials and Elements for Aerospace Vehicle Structures, Volume 1* U.S. Department of Defense, November 1990.

[10] Paros, J.M. and Weisbord, L. *How to Design Flexure Hinges*, Machine Design, 151-156, November 25, 1965

[11] Roberge, J.K. *Operational Amplifiers: Theory and Practice*, John Wiley and Sons, Inc., New York, 1975.

[12] Shahian, B. and Hassul, M. *Control System Design Using Matlab* Prentice Hall, Englewood Cliffs, New Jersey, 1993.

[13] Stout, Ken *The Design of Externally Pressurized Gas Bearings*

[14] Touzeau, C. and Antalovsky, S. *Vibration Environment Simulation for Helicopter-Borne Equipment*, Proceedings - Institute of Environmental Sciences, 273-278, 1993.

[15] Tung, R. *The Advanced Control Concepts Evaluation Laboratory* S.B. Thesis, Massachusetts Institute of Technology, May, 1992.

[16] Trumper, D.L. *Magnetic Suspension Techniques for Precision Motion Control* PhD. Thesis, Massachusetts Institute of Technology, September, 1990.

[17] Vukabratovich, D. and Richard, R.D. *Flexure Mounts for High-Resolution Optical Elements*, SPIE Vol. 959 Optomechanical and Electro-Optical Design of Industrial Systems, 1988.

[18] Weinstein, W. *Flexure Pivot Bearings*, Machine Design, June 10, 1965, pp. 150-157.